Dissertation zur Erlangung des Doktorgrades

der Fakultät für Chemie und Pharmazie

der Ludwig-Maximilians-Universtität München

Characterization of two novel myelin proteins

Karin Schaefer
aus
Nordenham

2009

Contents

1 SUMMARY

Myelination is a key step in vertebrate evolution: oligodendrocytes in the central nervous system (CNS) and Schwann cells in the peripheral nervous system (PNS) tightly wrap their cytoplasmic processes around axons. This allows rapid, saltatory nerve impulse conduction while keeping axon diameters small, thus permitting compact, powerful nervous systems at relatively small metabolic cost. In addition, signalling pathways between myelinating cells and axons mediate mutual trophic support, axonal growth and morphology.

Although myelination has been studied intensely, many questions remain regarding the differentiation of myelinating glial cells, regulation of myelin specific gene expression, and neuro-glial interactions. To identify novel factors involved in myelin formation and function we performed a microarray screen, comparing gene expression levels in wild type zebrafish (zf) with those in the myelin-deficient *colourless^{t3}/sox10* mutant. In my PhD project I characterized two novel transcripts identified in this screen: *zwilling* and *claudin* k.

For the *zwilling* transcript, I reconstructed a full length cDNA, which contains two short open-reading-frames coding for protein sequences that are highly similar and conserved in teleosts. I demonstrated the presence of these proteins via mass spectrometry in myelin membrane fractions. Both Zwilling proteins are highly basic and have no predicted structural motives. In this they are similar to myelin basic protein, one of the major myelin constituents. Myelin basic protein possesses an N-terminal myristyl anchor (an N-terminal myristoylation site is also predicted and conserved for the Zwilling proteins) and associates tightly to the myelin membrane and mediates compaction of individual lamellae.

Zebrafish Claudin k is a teleost-specific protein and is expressed exclusively in Schwann cells and oligodendrocytes. Claudins are essential components of tight junctions, which form selective permeability barriers across paracellular pathways and function as a "fence" between apical and basolateral membrane domains in

Summary

epithelia. In myelin of mammals, Claudins are expressed in autotypic tight junctions of oligodendrocytes (Claudin 11/OSP) and Schwann cells (Claudin 19). They contribute to electrical insulation, presumably by regulating ion flow between interstitium and intramyelinic space. The fence function of Claudins may also contribute to compartmentalization of the myelin membrane into different domains. Using monoclonal and polyclonal antibodies, which I raised against peptides, I showed that Claudin k localizes to the Schmidt-Lantermann incisures, the paranodal loops, and the inner and outer mesaxons – similar to mammalian Claudin 11 and 19. While mammalian Claudin 11 and 19 are restricted to the CNS and PNS respectively, zebrafish possess not only Claudin k but also Claudin 11 and 19, all of which we find to be expressed in both CNS and PNS. That raises the question whether myelin Claudins in teleosts are redundant or evolved divergent functions. To address this question, I analyzed the phylogenetic relationship of Claudins and performed knock down experiments in zebrafish larvae.

To further establish zebrafish as a model organism for myelination, we have identified and cloned the *claudin k* promoter. It drives strong, specific expression of transgenic reporters in myelinating glia, in both the CNS and the PNS. Using the flexible Tol2 mediated Gal4-UAS system (Paquet, Bhat et al. 2009) with independent driver and responder constructs and optional fluorescent reporters, this promoter can be used to express proteins specifically in myelinating glia. We generated transgenic lines expressing membrane-bound eGFP, eGFP-Claudin k and Cherry-Claudin k fusion proteins. We selected two strong and specific membrane-bound eGFP lines labeling the oligodendrocyte and Schwann cell membrane. For eGFP-Claudin k fusion lines we verified the proper localization of the fusion protein to autotypic tight junctions. These lines will enable the monitoring of myelination and tight junction formation *in vivo* and can serve as a read out for screens affecting myelination and proper tight junction formation. For transgenic expression of Cherry-Claudin k fusion protein, we see partial localization to the tight junctions but a major proportion of the protein aggregates within the cell body and processes. Since myelin protein aggregation with subsequent ER stress, including the unfolded protein response, proteasomal degradation and autophagy, have been implicated in myelin disorders, such as Pelizaeus-Merzbacher, vanishing white matter, and Charcot-Marie-Tooth disease (Lin and Popko 2009), we propose this transgenic line to serve as a more

general model for diseases caused by ER stress due to misfolded proteins in myelinating glia.

2 INTRODUCTION

2.1 GLIAL CELLS

Glial cells accompany neurons in all vertebrate and some invertebrate nervous systems and outnumber neurons by far (Sherwood, Stimpson et al. 2006). The term glia originates from the Greek word meaning "glue" and reflects the nineteenth-century presumption that these cells held the nervous system together in some way. While the term persisted, the concept radically changed. In contrast to this simple term very diverse roles of the different gial cell types have since emerged (Barres 2008): Glial functions that are nowadays well-established include axonal guidance by Bergmann glia (Rakic 1972; Hatten and Mason 1990), modulation of neuronal activity, synaptic transmission and synaptic plasticity by astrocytes (Araque 2008; Perea, Navarrete et al. 2009), important roles in the immune defense for microglia (Griffiths, Gasque et al. 2009; Tambuyzer, Ponsaerts et al. 2009) and the insulation and support of axons (Simons and Trajkovic 2006; Hartline and Colman 2007; Nave and Trapp 2008) a complex role in regeneration and structural plasticity (Maier and Schwab 2006; Jessen and Mirsky 2008; Martini, Fischer et al. 2008) for myelinating glia.

2.2 EVOLUTION OF MYELIN

The velocity of conduction of the electrical nerve impulse along nerve fibers has been improved by two basic evolutionary adaptations: axon gigantism and myelin formation. While axon gigantism relies on a simple increase of the axon diameter to reduce the interior resistance, myelination involves the production of a specialized insulating cover around the axons and formation of electrically active nodes. Myelin, or myelin like structures, have evolved multiple times during evolution, in crustaceans, annelids and vertebrates (Figure 2.2-1) (Gunther 1976; Davis, Weatherby et al. 1999; Xu and Terakawa 1999; Hartline and Colman 2007). When myelin first appeared in the vertebrate lineage is not entirely clear: myelin is absent
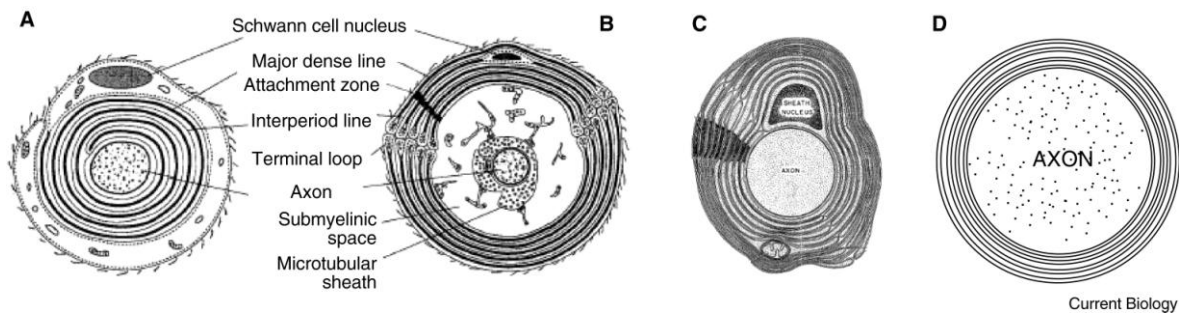
Figure 2.2-1: Schematics of myelin wraps in the different myelinated taxa.

Schematics of vertebrate (A), penaeid shrimp (B), palaemonid shrimp (C) and copepod (D) myelin. In all organisms multiple layers of lipid membrane surround the axon to achieve reduced electrical capacitance and increased resistance. In vertebrate the myelin membrane is arranged spirally around the axon (A). To prevent short-circuiting by current following along the spiral path between lamellae, membrane 'compaction' has evolved, in which electrically conductive cytoplasmic and extracytoplasmic spaces are minimized by the near-fusion of apposed internal and external leaflets of the lipid bilayer. Shrimp and copepod myelin are concentrically arranged (B-D). In shrimp (B,C) terminal loops of lamellae of a given layer are located in a specialized zone. There is also a so called attachment zone indicated in black. Fibers of penaeid shrimps (B) are unusual, in that the axon occupies only a part of the space within the sheath, leaving a large extracellular space termed the 'submyelinic space'. Copepod myelin (D) is compact in the outermost layers of the sheath, but often there is a substantial gap between rings. There is no evidence of terminal loops or seams within layers. Figure from (Hartline and Colman 2007).

in the most primitive members of the vertebrate clade such as hagfish and lampreys (Bullock, Moore et al. 1984). The first myelinated vertebrate is believed to have been a placoderm (Zalc 2006; Zalc, Goujet et al. 2008), the now extinct antecedent of contemporary sharks and bony fish and the most basal living species that possess myelin. The appearance of myelin has been temporally linked to the appearance of the hinged jaw (Zalc, Goujet et al. 2008). Characteristic structural features such as spiral wrapping, minor and major dense line and nodal organization are conserved from shark to human (Schweigreiter, Roots et al. 2006). Myelination leads to an increase in conduction velocity of 10-100 fold compared to an unmyelinated axon of the same diameter. Reversely, an unmyelinated 600-µm diameter squid axon and a myelinated 12-µm vertebrate axon both have conduction velocities of approximately 12 m/s. The unmyelinated squid giant axon, however, occupies several thousand times the space of the myelinated vertebrate axon and requires several thousand-

5

folds more energy (Lodish 2000). Thus myelination allowed vertebrates the evolution of exceedingly complex nervous systems, while minimizing size and metabolic costs.

2.3 MYELINATING GLIA

During vertebrate myelination oligodendrocytes in the CNS and Schwann cells in the PNS spirally wrap their processes around axons forming the myelin sheath (Figure 2.3-2). This is the basis for fast, saltatory nerve impulse conduction because myelin as an internodal insulator ensures, that membrane depolarization can only occur at special structures at the intersegmental gaps, the nodes of Ranvier. The myelin sheath is essential for proper neural function, and demyelination of nerve fibers is associated with convulsions, paralysis, and several severely debilitating or lethal diseases. In the CNS, oligodendrocytes typically myelinate several internodes of several axons and the nodes are contacted by processes of perinodal astrocytes, whereas Schwann cells in the PNS wrap only one and are covered by a basal lamina and extend microvilli contacting the nodes (Figure 2.3-1). Additionally, a subset of non-myelinating Schwann cells ensheathes multiple axons, sorting them into so called Remak bundles (Figure 2.3-2), which are important for neuronal function, axon maintenance, and neuronal survival.
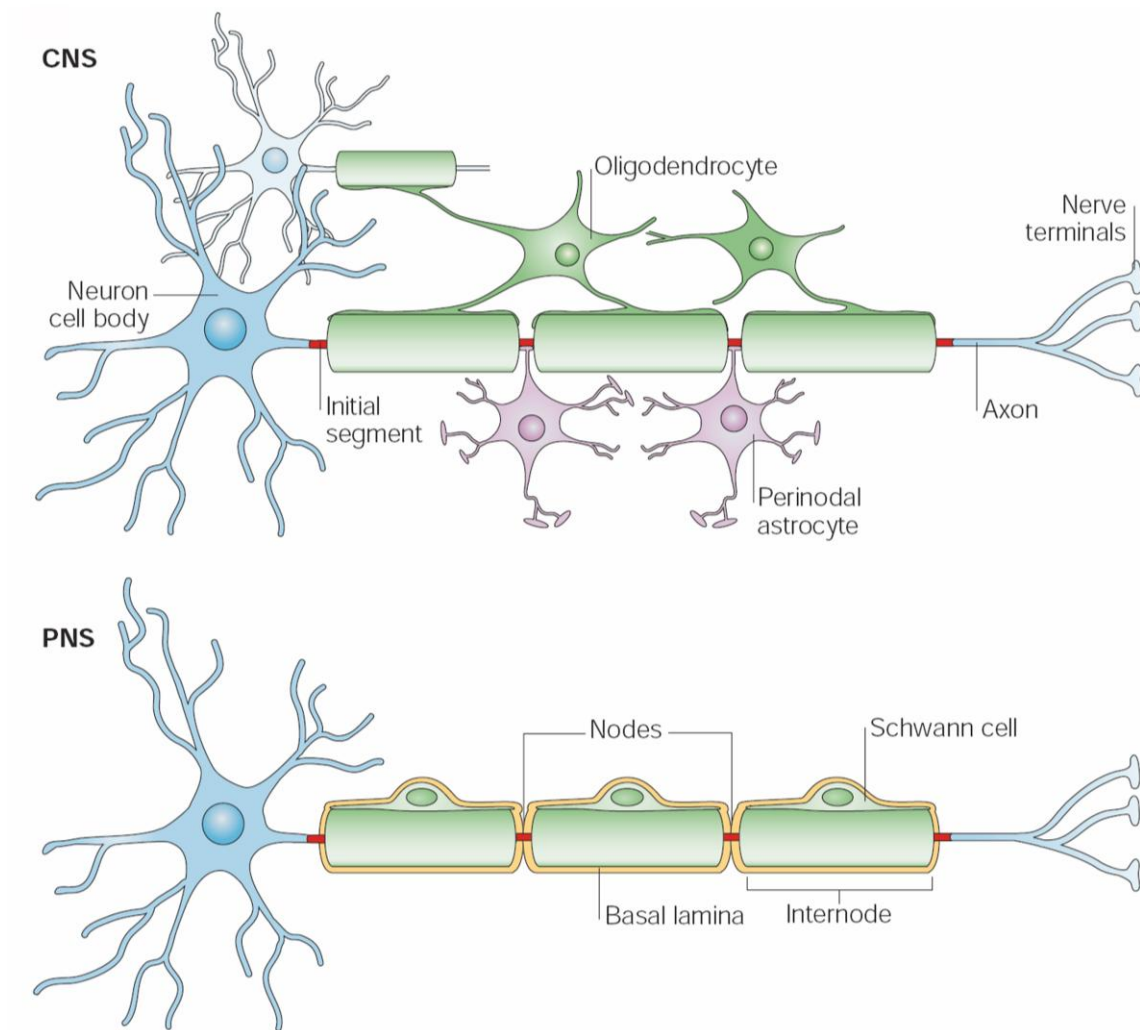
Figure 2.3-1: Myelinating glia in the CNS and PNS.

Oligodendrocytes in the CNS and Schwann cells in the PNS form the myelin sheath by wrapping their membranes several times around the axon. Myelin covers the axon at intervals (internodes), leaving bare gaps – the nodes of Ranvier. Oligodendrocytes can myelinate multiple axons and form several internodes per axon. Nodes in the CNS are contacted by perinodal astrocytes. Schwann cells myelinate a single internode of a single axon and Schwann cells and nodes are covered by a basal lamina. Figure modified from (Poliak and Peles 2003).

A

B
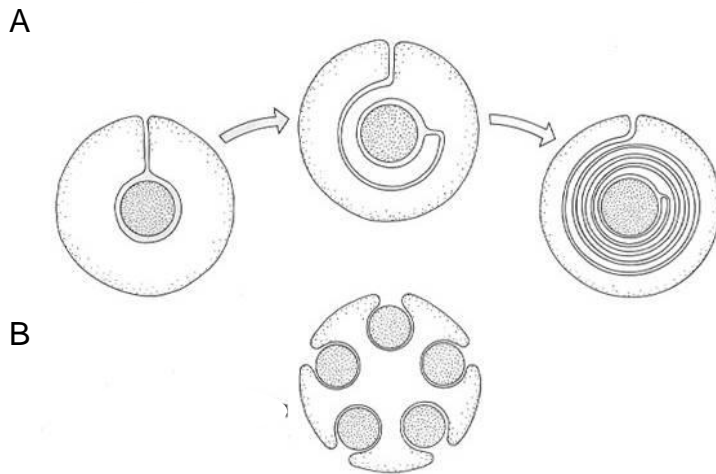
Figure 2.3-2: Formation of myelin and Remak bundles.

Oligodendrocyte or Schwann cell forming the myelin sheat, by spirally wrapping a process around an axon (A). Schwann cell forming a Remak bundle by surrounding several axons, thereby separating them with their cytoplasmic extensions (B). Figure modified from (Neurophysiology North Dakota State University).

2.3.1 MYELIN COMPOSITION AND STRUCTURE

Myelinating glia not only ensure by their passive insulating capacity, that membrane depolarization can only occur at the nodes of Ranvier, but also actively induce the formation of specialized domains within the myelinated axon (Salzer, Brophy et al. 2008; Susuki and Rasband 2008). Myelinated axons are compartmentalized into different microdomains with different functions and molecular compositions: nodes, paranodes, juxtaparanodes and internodes (Figure 2.3-3, A). The nodal segment is about 1 µm long and its axolemma contacted by Schwann cell microvilli in the PNS and processes of perinodal astrocytes in CNS. At the nodal axolemma a high density of voltage-gated Na^+ channels is responsible for the generation of the action potential. Several other transmembrane and cytoskeletal proteins have been identified at the nodal axolemma and function in recruiting nodal proteins, modulating channel gating and enhancing expression of Na^+ channels (Poliak and Peles 2003; Salzer, Brophy et al. 2008). At the paranodes flanking the nodes of Ranvier, the compact myelin membrane opens up and forms cytoplasm-filled loops, the paranodal loops, that wind helically around the axon. Septate-like junctions connect these

8
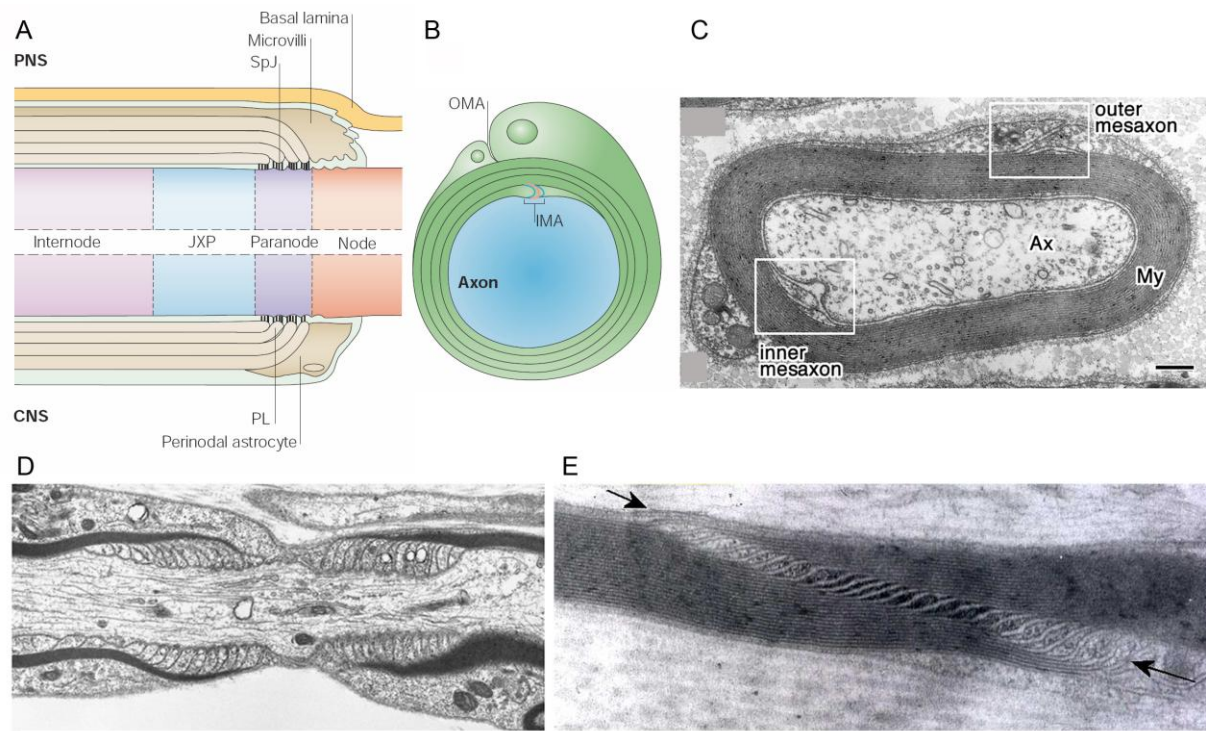
Figure 2.3-3: Structure and domains of a myelinated fiber

Schematic longitudinal cut of a myelinated fiber (A) around the node of Ranvier showing a heminode. The node, paranode, juxtaparanode (JXP) and internode are labeled. The node is contacted by Schwann cell microvilli in the PNS or by processes from perinodal astrocytes in the CNS. Myelinated fibers in the PNS are covered by a basal lamina. The paranodal loops form a septate-like junction (SpJ) with the axon. The juxtaparanodal region resides beneath the compact myelin next to the paranode (PN). The internode extends from the juxtaparanodes and lies under the compact myelin. Schematic cross-section of a myelinated nerve depicting the inner and outer mesaxons (IMA and OMA, respectively) (B). (C) Transmission electron micrograph of a myelinated nerve fiber, with inner and outer mesaxon (Ax: axon, my: myelin, scale bar: = 200 nm). Electron micrograph of longitudinal section at the region of a node of Ranvier in the PNS (D). Electron micrograph of a longitudinal section at the region of a Schmidt-Lantermann incisure (arrow) in the PNS (E). Schmidt-Lantermann incisures are cytoplasm filled channels in the myelin of the internode and facilitate transport of nutrients and molecules to the myelin sheath and the periaxonal region of the internode (Balice-Gordon, Bone et al. 1998; Arroyo and Scherer 2000). Diagrams (A) and (B) from (Poliak and Peles 2003), and electron micrographs (C) and (D) from (Miyamoto, Morita et al. 2005) and (E) from (Queiroz and Paes State University of Campinas).

directly with the axon helping to secure the paranodal loops to the axon at the axo-glial junction and restricting K^+ channels to the juxtaparanodal loops (Bhat, Rios et al. 2001; Boyle, Berglund et al. 2001; Xu and Shrager 2005). These K^+ channels

potentially prevent re-entrant excitation, help in maintaining the internodal resting potential and mediating axo-glial communication. The myelin of the internode is largely composed of compact myelin and few cytoplasmic filled channels – the inner and outer mesaxons and the Schmidt-Lantermann incisures (also referred to as radial component in the CNS) (Figure 2.3-3).

Electron micrographs reveal the characteristic structure of the compact myelin sheath: major dense lines alternate with thinner intraperiod lines to form the repeating units. The major dense line results from the apparent fusion of the thicker, inner leaflet of the plasma membrane, whereas the intraperiod line is formed by the apposition of the thinner, outer leaflet of this membrane (Figure 2.3-4) (Baumann and Pham-Dinh 2001). The myelin membrane is very rich in lipids, with its dry weight consisting of 70-80% lipids and 20-30% proteins. High lipid content corresponds to low water content and thus further improves the insulating properties. Myelin membranes of all species contain high amounts of cholesterol, phospholipids and glycolipids; particularly plasmalogens and glycosphingolipids. Deficiencies in biosynthesis or degradation of these lipids cause leukodytrophies, mainly associated with aggregation of toxic metabolites (Igisu and Suzuki 1984; Kalman and Leist 2004; Edvardson, Hama et al. 2008). Additionally, lipids contribute to myelin membrane stability and an excess or a deficit of lipids can result in instabilities (Min, Kristiansen et al. 2009).

While there are no lipids unique to myelin but rather a myelin-specific composition of lipids, there are many myelin-specific proteins, some of them specific for CNS myelin, some for the PNS and some for both (Figure 2.3-4). There are three major structural proteins important for close myelin apposition: Myelin basic protein (MBP), Myelin protein zero (MPZ, also called P_0) and Myelin proteolipid protein (PLP1, a tetrapod specific isoform of DM20). In phylogenetically older vertebrates such as cartilaginous fish and teleosts, the major protein constituent in both the CNS and PNS is MPZ. The membrane-spanning PLP in CNS myelin and MPZ in PNS myelin serve as spacers predominantly at the extracellular sides of the oligodendroglial and Schwann cell plasma membranes, respectively, whereas the peripheral MBP is localized at the cytoplasmic apposition in both CNS and PNS myelin membranes.
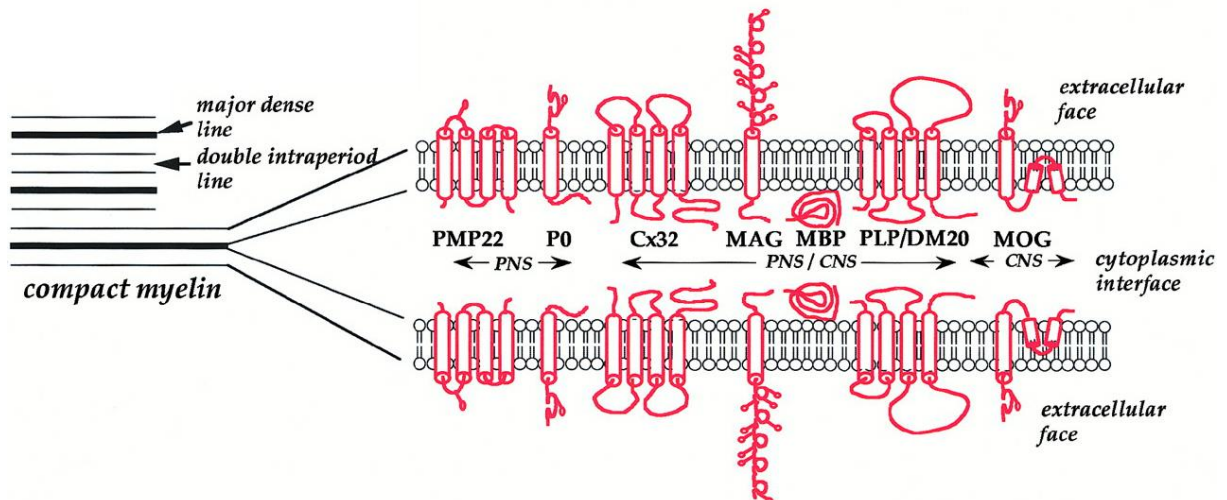
Figure 2.3-4: Compact myelin structure and composition

(A) depicts schematic drawing of major dense line and intraperiod lines as seen in high-resolution electron micrographs. Apparent fusion of the inner leaflets of the membrane gives rise to the major dense line while the double intraperiod line is the result of the close apposition of two outer leaflets. (B) shows structure and localization of selected myelin-specific proteins of the CNS and PNS. In the mammalian CNS, MBP and PLP, and the PNS, MBP and MPZ (P0) are the two major structural proteins. MAG and MOG are gylcoproteins, DM20, CX32 and PMP22 are distantly related tetraspanins. Diagram from (Baumann and Pham-Dinh 2001).

2.3.1.1 Myelin basic protein (MBP)

Myelin basic protein is a major component of both, the CNS and PNS myelin. MBP is intrinsically unstructured, very basic and binds electrostatically to negatively charged phospholipids on the cytosolic surfaces of the plasma-membrane. It localizes to the major dense line and is believed to glue the cytoplasmic membrane leaflets together. It also appears to have several other functions. It can interact with a number of polyanionic proteins including Actin, Tubulin, $Ca2^{+}$-Calmodulin, and Clathrin. The MBP found in myelin, also called classic MBP, is a product of a larger gene complex called Golli (Genes of Oligodendrocyte Lineage) and exists in many isoforms with masses from 14 – 22 kD (Boggs 2006; Harauz, Ladizhansky et al. 2009; Harauz and Libich 2009). While various Golli proteins are produced in developing myelin and also immune and hemopoietic cells (Givogri, Bongarzone et al. 2001; Marty, Alliot et al. 2002), classic MBP is present in myelinating glia only. The mRNAs are transported into the cell processes, where they are synthesized on free polyribosomes (Ainger, Avossa et al. 1993; Gould, Freund et al. 2000). Interestingly some isoforms of MBP

are also partially localized to the nucleus and might play a regulatory role in myelination (Pedraza, Fidler et al. 1997). The *shiverer* mouse mutant, which lacks MBP due to a mutation in the *MBP* gene, shows drastic myelin changes and deficits in the CNS – hypomyelination, myelin breakdown, absence of the major dense line – while changes in the PNS are more subtle (Kirschner and Ganser 1980; Hayashi, Nakashima et al. 2007). The reason that the PNS is not as severely affected in *shiverer* mice may be due to the basic cytoplasmic domain of MPZ, which may substitute for MBP to some degree (Martini, Mohajeri et al. 1995).

2.3.1.2 Proteolipid proteins DM20 and PLP

DM20 (also called DMalpha) and its longer splice variant PLP are tetraspan transmembrane proteins, very hydrophobic and PLP might play a role in fusion of the extracellular membrane leaflet (Boison, Bussow et al. 1995) and long-term integrity of axons (Griffiths et al., 1998). The insertion of a positively charged 35-amino-acid segment into cytosolic loop 3 of DM20 giving rise to PLP1, might have enabled the replacement of MPZ orthologues in the mammalian CNS (Mobius, Patzig et al. 2008). PLP/DM20 knockout mice show relatively normal myelin compaction with condensed intraperiod lines, but a late-onset axonopathy (Griffiths et al., 1998). Mutations, deletions or duplications of the human PLP gene cause Pelizaeus-Merzbacher disease (OMIM 312080 (OMIM® Johns Hopkins University)) which results in CNS dysmyelination, demonstrating again the importance of gene dosage for myelin composition (Duncan 2005; Woodward 2008). Although PLP is expressed at low levels by myelinating Schwann cells PNS abnormalities appear to be uncommon in patients and mice with PLP mutations (Anderson, Montague et al. 1997; Garbern, Cambi et al. 1997).

2.3.1.3 Myelin Protein Zero (MPZ)

MPZ comprises an extracellular IgG like domain, a transmembrane helix, and a small basic cytoplasmic domain (Eichberg 2002). It forms tetramers *in cis*, which interact *in trans* with each other, and is thus important for the tight apposition of myelin membrane (Martini, Mohajeri et al. 1995; Shapiro, Doyle et al. 1996; Plotkowski, Kim et al. 2007). MPZ was also shown to be essential for the formation of PNS Schmidt-Lantermann incisures and can induce the aberrant and detrimental formation of

Schmidt-Lantermann incisures in the CNS (Yin, Kidd et al. 2008). Mutations of the gene encoding MPZ result in a wide variety of peripheral nervous system diseases that are classified as Charcot-Marie-Tooth disease type 1B (OMIM 118200), Dejerine-Sottas syndrome (OMIM 145900), and congenital hypomyelination (OMIM 605253) (Hayasaka, Himoro et al. 1993; Patel and Lupski 1994; Warner, Hilz et al. 1996).

2.3.1.4 Myelin protein 22 (PMP22)

Myelin protein 22 (PMP22), is expressed in many tissues but is mainly present in the compact myelin of Schwann cells. It is a hydrophobic tetraspanin - like the evolutionarily related DM20/PLP - that interacts with MPZ (D'Urso, Ehrhardt et al. 1999) and its absence in mice results in a severe demyelinating neuropathy (Adlkofer, Martini et al. 1995). Mutations in genes encoding PMP22, especially duplications, are the most common cause for Charcot-Marie-Tooth type 1 cases (OMIM 118220 and OMIM 118200), thought to be caused by intracellular accumulation of PMP22, which in turn causes the apoptosis of Schwann cells (D'Antonio, Feltri et al. 2009; Lin and Popko 2009).

2.3.1.5 Claudins

Another member of the PMP22 superfamily is the Claudin family. Claudins are essential components of tight junctions and major determinants of paracellular solute flux across epithelia and endothelia. Several of the 24 mammalian family members have been detected in the myelin sheath. A prominent example is Claudin 11, formerly called oligodendrocyte specific protein (OSP), which is expressed in several tissues but particularly high amounts are present in CNS myelin (Bronstein et al., 1997) Claudin structure and function and their relation to myelinating glia will be introduced here in detail, since Claudin k, a novel myelin specific Claudin, will be presented in this thesis.

2.3.1.5.1 Tight junctions

Tight junctions are well known for epithelial cells, where they connect adjacent cells and form a paracellular diffusion barrier, as well as a barrier restricting intramembrane diffusion. These two functions are referred to as barrier and fence function, respectively (Figure 2.3-5). Tight junctions are a supramolecular organization of transmembrane proteins, and their adapter and scaffolding proteins. Depending on their composition, they vary considerably in their tightness and formation of selective pores. Typical components besides Claudins are junctional adhesion molecules (JAMs) and Occludin, which are connected to the cytoskeleton via adaptor proteins like the zonula occludens proteins 1-3 (ZO 1-3) and Cingulin (Harder and Margolis 2008). In transmission electron micrographs, tight junctions appear as fusion of the plasma membranes. In freeze fracture electron micrographs tight junctions present as networks of strands (Figure 2.3-6). Each tight junction strand associates laterally with another tight junction strand in the apposing membranes of adjacent cells to form ''paired'' tight junction strands (Staehelin 1973; Tsukita, Furuse et al. 2001).
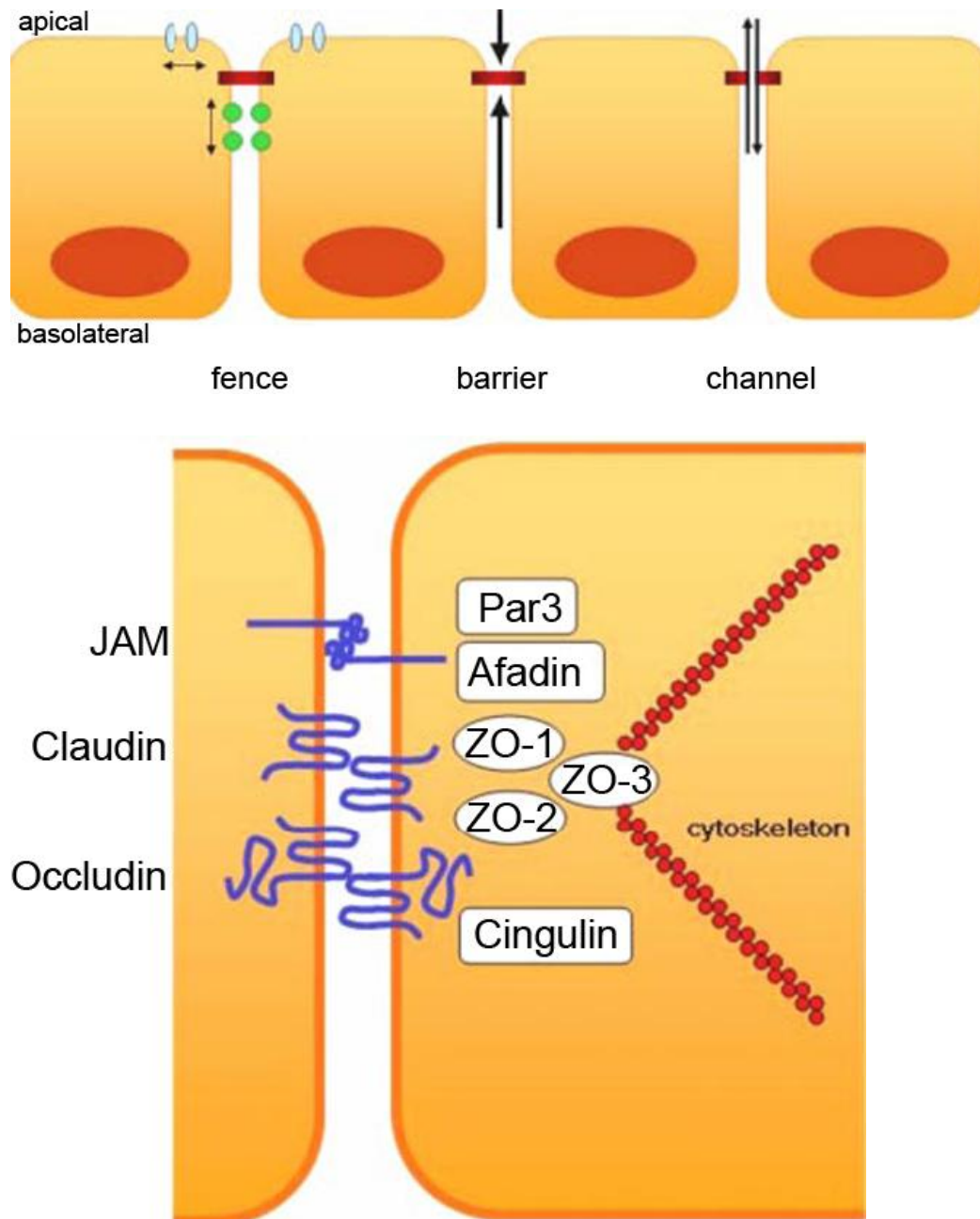
Figure 2.3-5: Principal characteristics of tight junctions.

Tight junctions form a diffusion barrier within the membrane, restricting proteins to certain membrane areas, which is referred to as "fence" function. They also form a paracellular diffusion barrier between adjacent cells, referred to as "barrier" function. This barrier can be size and charge selective, thus tight junctions can serve as channels (A). The interaction of typical transmembrane components, intracellular adaptor proteins, and actin cytoskeleton is presented in (B). Diagram modified from (Will, Fromm et al. 2008). For details on molecular structure and interaction, refer to (Harder and Margolis 2008).

2.3.1.5.2 Tight junctions of the myelin sheath

In the myelin sheath tight junction like structures can be found in the CNS as well as in the PNS connecting adjacent layers of the myelin sheath. Because these tight junctions connect adjacent membranes of the same cell, they are also called autotypic tight junctions. Like a classic epithelial tight junctions, they appear as fusion of the plasma membranes in transmission electron micrographs and present as networks of strands in freeze fracture electron micrographs. While classical tight junctions are comprised of continuous anastomosing strands, strands in the myelin are parallel, a feature characteristic for only few tissues (Gow, Southwood et al. 1999). Autotypic tight junctions have been found in fish, amphibians and mammals and are located along the inner and outer mesaxons, Schmidt-Lantermann incisures and paranodal loops (Mugnaini and Schnapp 1974; Sandri, Van Buren et al. 1977; Tetzlaff 1978; Shinowara, Beutel et al. 1980; Salzer 2003). Figure 2.3-7 A depicts tight junction strands in the folded and unfolded Schwann cell, while figure Figure 2.3-7 B indicates localization of tight junctions in a section at the node of a myelinated nerve. In the PNS several tight junction components including Claudin 1, 5 and 19 and ZO-1 and -2 and JAM-C have been identified (Poliak, Matlis et al. 2002; Scheiermann, Meda et al. 2007), though some of them are under debate, while in the CNS Claudin 11 is the only established tight junction component, and Occludin and ZO proteins seem to be absent (Gow, Southwood et al. 1999). Claudin 11 and 19 – expressed strongly in the CNS and PNS, respectively – were identified as key players since the respective knockout micelack the according tight junction strands. How close tight junctions of the CNS and PNS resemble 'classical' tight junctions or whether they evolved rather distinct features and functions is under debate (Miyamoto, Morita et al. 2005; Devaux and Gow 2008). Speculations about Claudin function ranges from sequestering antigens, to compartmentalization via their fence function (Mugnaini and Schnapp 1974; Tabira, Cullen et al. 1978; Gow, Southwood et al. 1999).There is some evidence from knockout mice, that they might play a role in structural stability (Chow, Mottahedeh et al. 2005) and good evidence for a function in electrical sealing (Miyamoto, Morita et al. 2005; Devaux and Gow 2008), as described in the following chapter.
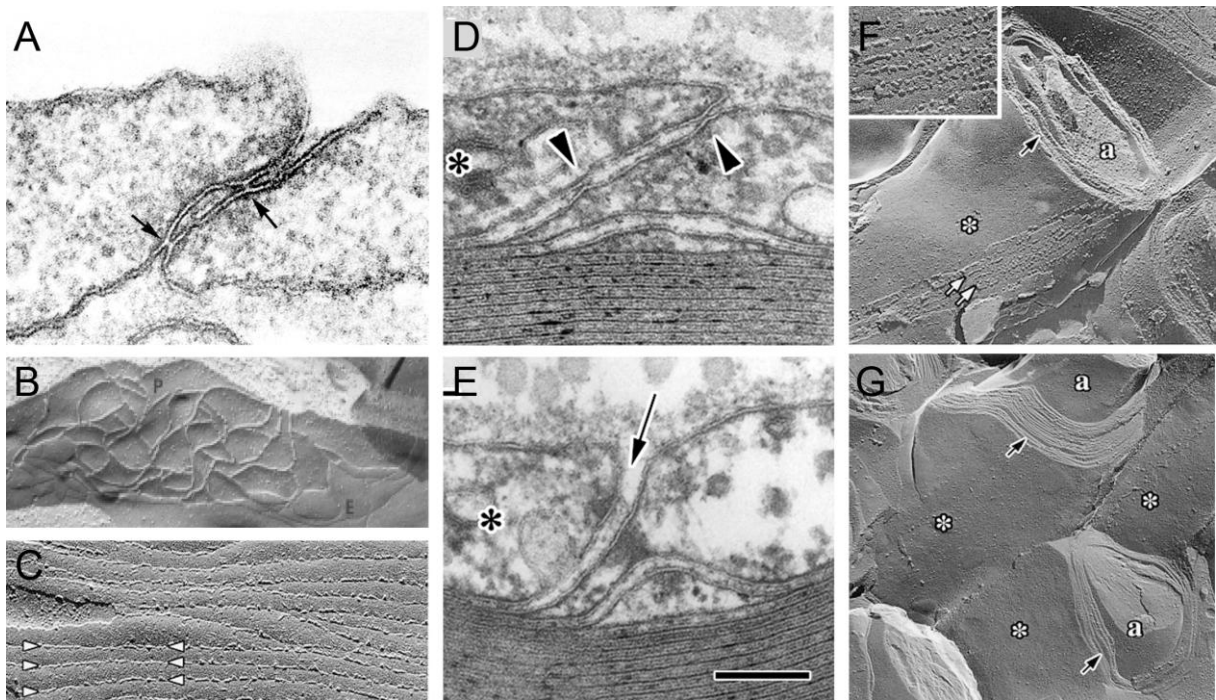
Figure 2.3-6: Tight junctions in myelinating glia

The transmission electron micrographs of tight junctions in endothelia (A, blood vessel) appear as close apposition of membranes (arrows), so called 'kissing points'. In freeze fracture electron microscopic images tight junctions appear as continous anastomosing bands in most ephithelial cells (B), while tight junction strands in the testis (C, arrwoheads) and few other tissues are parallel. In a mouse Schwann (D) tight junctions (arrowheads) at the outer mesaxon (asterisk) similar to (A) are present, while in the Claudin 19 -/- mouse these tight junctions are absent (E, arrow). In mouse oligodendrocytes parallel strands of tight junctions similar to (C) are present (F, white arrows), while in the Claudin 11 -/- mouse (G) they are absent (a, axon; asterisk, outer wrapping of the myelin sheath; black arrow, internodal myelin). Inset in (F) shows magnification of parallel tight junction strands. Scale bar = 100 nm in D, E. Electron micrograph (A) from (Wagner and Hossler University of Delaware); (B) from (Gonzalez-Mariscal, Betanzos et al. 2003); C, F and G from (Gow, Southwood et al. 1999); D,E from (Miyamoto, Morita et al. 2005).

17
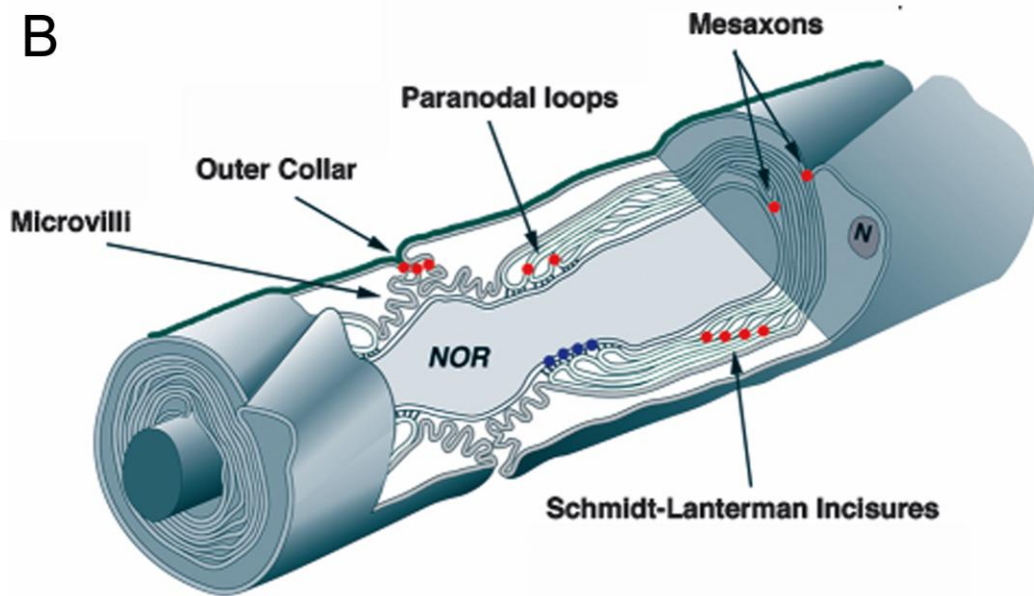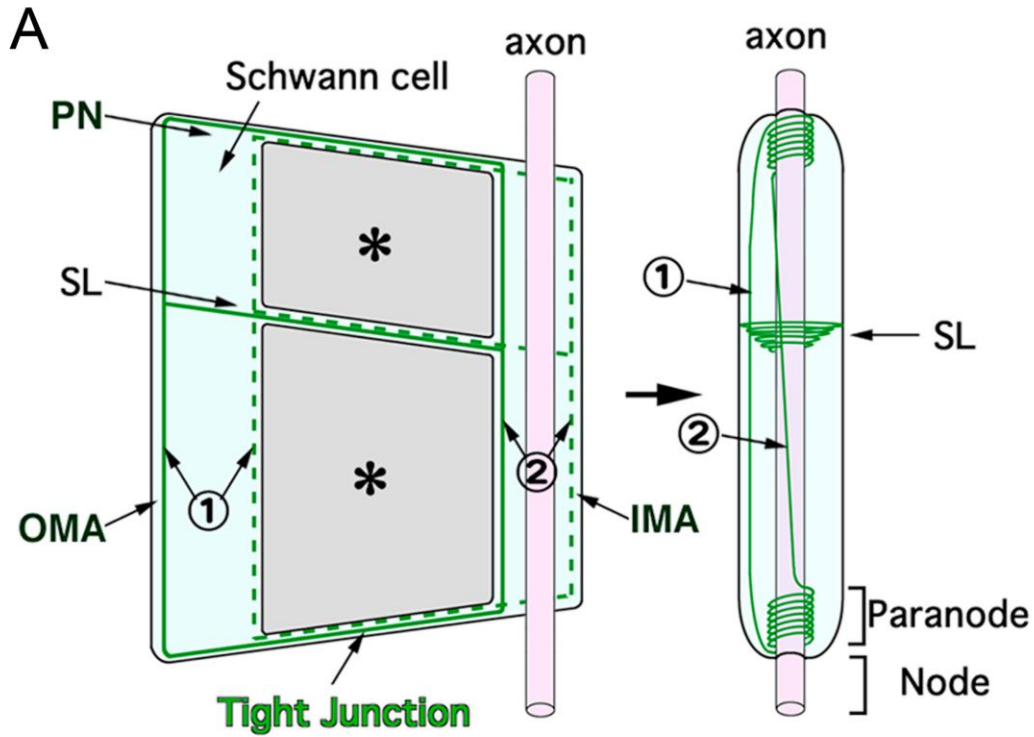
Figure 2.3-7: Localization of autotypic tight junctions in the myelin sheath.

Green line and dashed green line in (A) depict localization of autotypic tight junctions in the conceptually unfolded myelin sheath, which meet upon folding. Tight junctions are present along the outer and inner mesaxon (OMA, IMA), Schmidt-Lantermann incisures (SL) and paranodal loops (PN). Asterisks indicate compact myelin. (B) presents a schematic section of myelinated nerve at the node and red dots point out tight junctions, while blue dots indicate septate-like junctions. Diagram (A) from (Miyamoto, Morita et al. 2005), (B) modified from (Poliak, Matlis et al. 2002).

2.3.1.5.3 Claudin structure and function

Claudins are tetraspan transmembrane proteins of the PMP22-Claudin superfamily (Figure 2.3-8). It is a large family with at least 24 members in mammals and more than twice as many in teleosts. Different Claudins are expressed in tissue-specific combinations resulting in tissue-specific barrier characteristics. The larger first extracellular loop (ECL1) appears to be critical for determining the paracellular tightness and the selective ion permeability, while the shorter second extracellular loop (ECL2) may be involved in narrowing of the paracellular cleft and adhesion between the opposing cell membranes (Krause, Winkler et al. 2009). The cytoplasmic C-terminus is the least conserved part with respect to sequence, but in most family members holds a conserved PDZ-binding motif. For a number of Claudins it was shown to mediate interactions to scaffolding and adaptor proteins like the ZO proteins (Itoh, Furuse et al. 1999). Claudins can cooperate via homophilic and heterophilic *cis* and *trans*-interactions to form tight junction strands. Sequence analysis of claudins has led to differentiation into two groups, designated as classic Claudins (1–10, 14, 15, 17, 19) and non-classic Claudins (11–13, 16, 18, 20–24), according to their degree of sequence similarity (Krause, Winkler et al. 2008). Figure 2.3-8 summarizes structural features and possible interaction motifs of the Claudin protein family.

Two important, myelin-related Claudins are mammalian Claudin 11 and 19. Claudin 11, also called oligodendrocyte specific protein (OSP), is expressed in several tissues. However, specifically high amounts are present in CNS myelin, were Claudin 11 is the third most abundant protein, contributing 7% to total myelin protein (Bronstein et al., 1997). It is absent from PNS myelin. Immunostainings for Claudin 11 show localization to inner and outer mesaxons, paranodal loops and Schmidt-Lantermann incisures (Gow, Southwood et al. 1999). In the CNS myelin sheath of mice deficient for Claudin 11 tight junction strands are absent, but myelin structure and compaction appears otherwise normal. Knockout mice present with a mild tremor and reduced signal conduction speeds, which is especially pronounced in middle diameter axons (Devaux and Gow 2008). Claudin 11 and PLP/DM20 double knockout mice show severe neurological deficits, disrupted myelin compaction and smaller axon diameters. These phenotypes are not seen in either, PLP/DM20 or Claudin 11 knockout mice alone, suggesting overlapping functions.
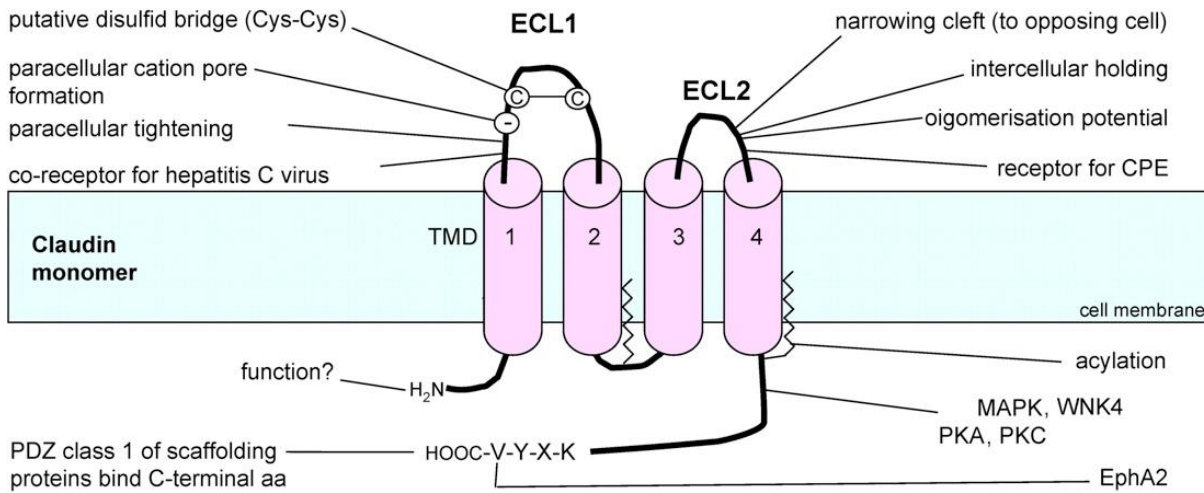
Figure 2.3-8: Structural features and possible interaction motifs of the Claudin protein family.

Claudins are tetraspan transmembrane proteins and all family members carry two cysteins in their first ECL, which supposedly form a disulfide bond. The first ECL is implicated in paracellular tightening and pore formation and can function as co-receptor for hepatitis C virus. The second ECL might play a role in intercellular holding and narrowing the cleft to the opposing cell and has the potential to oligomerize. Clostridium perfringens enterotoxin (CPE) was shown to bind to it. C-terminal acylation was shown to play a role in Claudin localization and several kinases (MAPK, WNK4, PKA, PKC, EphA2) have been reported to phosphorlylate Claudin family members and regulate tight junction permeability. Most Claudins carry a PDZ binding motive and for a number of Claudins it was shown to mediate interactions to scaffolding and adaptor proteins. Figure modified from (Krause, Winkler et al. 2008).

This is further supported by the fact, that either of these genes was up-regulated when the other one was deleted (Chow, Mottahedeh et al. 2005). Claudin 19, which is expressed strongly in Schwann cells but not in the CNS, also localizes to inner and outer mesaxons, paranodal loops and Schmidt-Lantermann incisures. In the PNS myelin sheath of mice deficient for Claudin 19 tight junction strands are absent, but myelin structure and compaction appeared otherwise unchanged. Knockout mice show behavioral abnormalities that can be attributed to peripheral nervous system deficits and electrophysiological analyses indicated altered nerve conduction of peripheral myelinated fibers (Miyamoto, Morita et al. 2005).

2.3.2 Axo-glia support

An important function of myelinating glia is the formation of the myelin sheath enabling fast and efficient saltatory nerve impulse conduction as discussed in chapter 3.3.1. In recent years, more and more evidence about the importance of myelinating glia for axonal integrity, function and survival has accumulated. Long term demyelination is associated with axonal loss (Raine and Cross 1989; Trapp, Peterson et al. 1998), while the presence of a myelin sheath can lead to an increase in axon diameter (Windebank, Wood et al. 1985). Axons with compromised myelin sheaths have altered axonal transport rates and changes in microtubule number or stability, or are swollen and show signs of degeneration (Kirkpatrick, Witt et al. 2001). Some of the supporting functions accomplished by oligodendrocytes and Schwann cells are associated with the presence of a structurally intact, insulating myelin sheath. Others however, appear independent of the insulating function and include trophic and metabolic support (Nave and Trapp 2008; Lassmann 2009).

2.3.3 Metabolism of myelinating glia as risk factor for disease

During development, myelinating glia produce an enormous amount of myelin membrane and a mature myelinating cell must support a membrane up to 1000 times larger than that of a typical mammalian cell (Pfeiffer, Warrington et al. 1993). This renders myelinating cells vulnerable in several respects: they are under increased oxidative stress due to extremely high metabolic rates and activity of synthetic enzymes, which use iron as a co-factor (Connor and Menzies 1996; McTigue and Tripathi 2008). Additionally, all membrane proteins, cholesterol and membrane lipids must pass through the secretory pathway. The membrane proteins are translocated into the ER lumen where they are properly modified and folded. Terminally misfolded proteins are usually retrotranslocated to the cytosol for ER-associated degradation (ERAD) by the proteasome or transported to the lysosome. An imbalance between the unfolded protein load and the ability to process that load, causes ER stress (Figure 2.3-9). Even slight variations in the amount of a single protein can perturb the entire system and result in the retention, misfolding, and accumulation of many other proteins (Bradl, Bauer et al. 1999; Colby, Nicholson et al. 2000; Bauer, Bradl et al. 2002; Dickson, Bergeron et al. 2002). This ER stress is met by the cell via an adaptive, coordinated response, the unfolded protein response (UPR). If the cellular
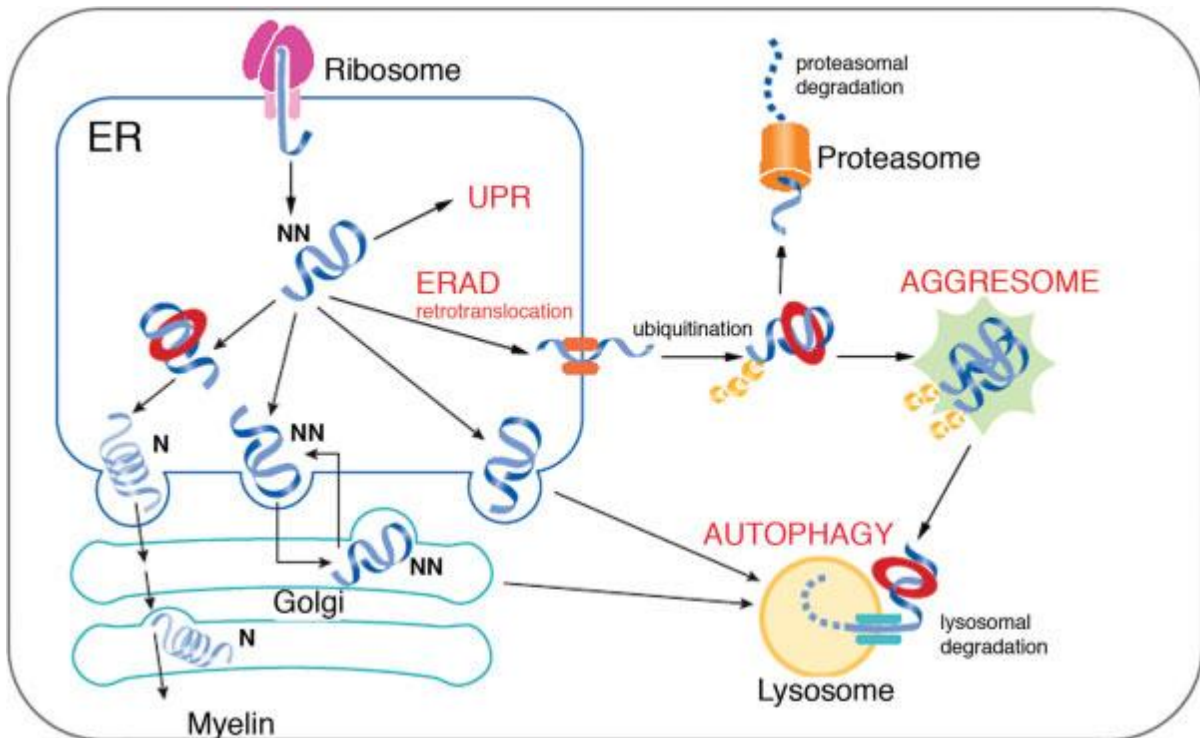
Figure 2.3-9: The possible outcomes of protein misfolding in the endoplasmic reticulum (ER) of glial cells.

In the ER newly synthesized proteins and other non-native proteins (NN) are folded with the help of chaperones (indicated as red ring). ER–Golgi cycling may occur at this stage. Once proteins are folded correctly (N), they can transit through the Golgi and are transported to the myelin sheath. Terminally missfolded proteins are usually retrotranslocated to the cytosol for ER-associated degradation (ERAD) by the proteasome. An imbalance between the unfolded protein load and the ability to process that load can elicit an unfolded protein response (UPR). If the cell cannot cope with the unfolded protein overload, UPR can ultimately lead to programmed cell death. In some cases misfolded proteins are retrotranslocated, but accumulate in the cytoplasm, forming the so-called aggresomes. This accumulation can in turn lead to the activation of autophagy and lysosomal degradation. Diagram from (D'Antonio, Feltri et al. 2009).

stress surpasses the cell's ability to cope with it, it may ultimately lead to apoptosis (Southwood, Garbern et al. 2002; Lin and Popko 2009). A number of myelin disorders, like Charcot-Marie-Tooth disease, Pelizaeus-Merzbacher disease, vanishing White Matter disease (OMIM 603896) and immune mediated demyelinating disorders have recently been linked to increased susceptibility of myelinating glia for ER stress. This might explain why elevated or mutated PLP, MPZ and PMP22 cause Pelizaeus-Merzbacher or Charcot-Marie-Tooth disease.

2.3.4 MYELINATION IN ZEBRAFISH

The myelin sheath of teleost exhibits the same structural characteristics as the mammalian myelin sheath and has a similar myelin-specific protein composition (Jeserich and Waehneldt 1986; Brösamle and Halpern 2002; Schweigreiter, Roots et al. 2006; Jeserich, Klempahn et al. 2008). While myelin proteins are highly conserved in mammals, some of them are much less conserved in lower vertebrates. Resulting from genome duplication after the divergence of the tetrapods (Amores, Force et al. 1998; Prince, Joly et al. 1998; Hurley, Mueller et al. 2007), there are often two orthologous teleost genes for each mammalian gene, as in the case for PLP/DM20 (Schweitzer et al., 2006, Brösamle 2009) and MPZ.

The major biochemical difference between teleost and mammalian myelin is the presence of MPZ as a major CNS myelin protein (Waehneldt, Stoklas et al. 1986; Jeserich, Klempahn et al. 2008). The closest orthologue of PLP/DM20 in zebrafish (DMalpha2) is expressed in myelinating glia (Brösamle and Halpern 2002), while the exon specific to PLP, a longer splice form of DM20, is absent from the zebrafish genome. Mammalian MPZ is found in the PNS only, while the two zebrafish orthologues are expressed in both PNS and CNS (Brösamle and Halpern 2002; Avila, Tevlin et al. 2006). Accumulating evidence suggests that PLP replaced MPZ as major myelin component in the mammalian CNS during evolution (Yin, Baek et al. 2006; Mobius, Patzig et al. 2008). In contrast, MBP is expressed throughout phylogeny in the CNS and PNS at high levels. While sequence similarity between orthologues of teleost and mammalian PLP/DM20 and MPZ is high, it is lower for MBP (Brösamle and Halpern 2002). Expression of the zebrafish myelin genes is first detected at 2 dpf in the oligodendrocytes of the hindbrain. During development, expression spreads rostrally to the midbrain and optic nerve, and caudally to the spinal cord (Figure 2.3-10). Expression of myelin genes precedes myelin formation observed by electron micrographs: first axons loosely wrapped by processes of myelinating glia were detected at 4 dpf in the ventral hindbrain. By 7 dpf, bundles of heavily myelinated axons were observed in the same region. Myelination was particularly prominent around the Mauthner axons. At this stage, compact myelin was also present around axons in the lateral line and optic nerves.

General advantages of zebrafish as a model organism include its very rapid embryogenesis and embryonic transparency. Moreover it produces high numbers of

offspring and offers relatively inexpensive upkeep, both important factors for large-scale screens. Together with the conservation of gene structure and expression patterns and the early appearance of myelinated axons described in this chapter, this supports using the zebrafish as model organism for myelination and myelin related disease.

_____

Figure 2.3-10: Expression of myelin genes in zebrafish larvae.

Myelin gene expression in the developing CNS and PNS was detected by whole-mount *in situ* hybridization. A–C: transcripts for DM20, P0 and MBP were detected at 2 dpf in the ventral hindbrain, close to the midline (arrows). In addition, MBP mRNA was detected in Schwann cells of the trunk lateral line (arrowhead). D–F, J-L: By 4 dpf many more expressing cells were found in the hind and midbrain, often in a highly symmetrical pattern. DM20 and MBP *in situ* hybridization reveals the majority of presumptive oligodendrocytes in the ventral hindbrain (arrows). Some oligodendrocytes appear in more rostral brain regions, such as in the midbrain and the posterior commissure (asterisks). In the periphery, MBP-positive Schwann cells were found at all branches of the lateral line system and in cranial nerves (arrowheads). K,L: Same specimen taken at different focal planes. At 7 dpf (G–I) the overall distribution of myelinating cells was similar, but these cells increased in number. Scale bars = 100 μm. Figure modified from (Brösamle and Halpern 2002).
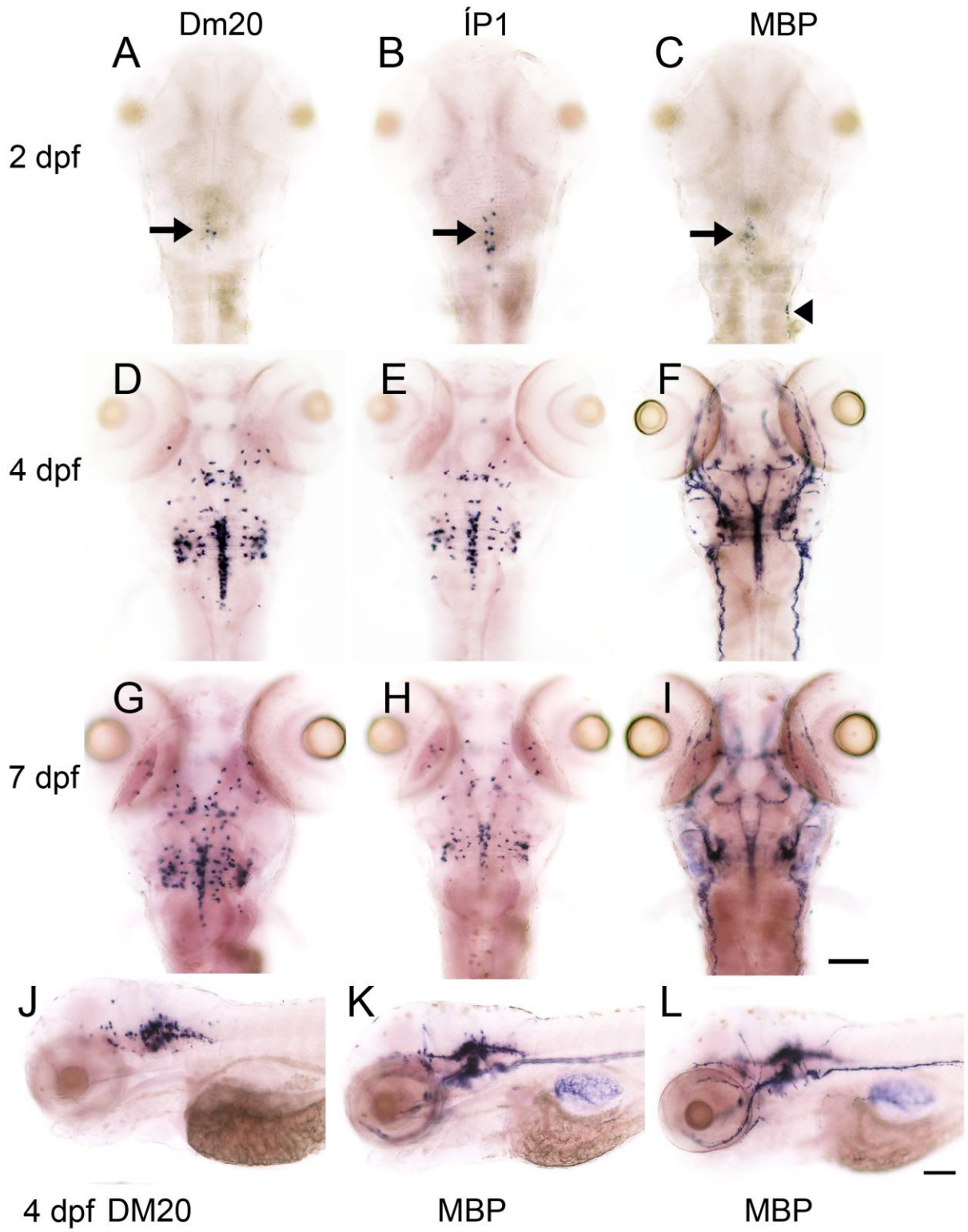
2.4 MICROARRAY EXPRESSION SCREEN TO IDENTIFY NOVEL MYELIN SPECIFIC GENES

Oligodendrocytes and Schwann cells originate from different lineages. Oligodendrocytes develop from a precursor population from the ventral neural tube, while Schwann cells are neural crest derived. Sox 10 is a SRY-box containing transcription factor, that is required for myelination in the CNS as well as in the PNS of mammals (Stolt, Rehberg et al. 2002). It is active in the neural crest and drives differentiation of the non-ectomesenchymal neural crest lineage, that gives rise to melanocytes, the enteric nervous system, components of the inner ear and Schwann cells (Herbarth et al. 1998; Southard-Smith et al. 1998). It is also important for the terminal differentiation of oligodendrocytes (Stolt, Rehberg et al. 2002). Sox 10 function is conserved in zebrafish: mutations in the *sox10* gene in mammals are associated with defects in pigmentation, ear development, the enteric nervous

_____

Figure 2.4-1: Loss of *sox10* function causes deficits in myelin gene expression and myelination.

The transcripts of the three structural proteins (A) *dm alpha2,* (C) *mbp,* and (E) *mpz* are strongly down regulated in oligodendrocytes of 4 dpf *sox10/cls^{t3}* larvae (B, D, F, respectively). Similarily, (G) *mag* and (I) *36K* mRNAs were detected at much lower levels in *sox10/cls^{t3}* larvae (H, J), while (K) *gfap* mRNA levels remained constant (L). *Mbp* expression in the PNS (C, arrows) was no longer detected in the absence of Sox10 function (D), due to the loss of Schwann cells in the *sox10/cls^{t3}* mutant larvae. At 7 dpf old large diameter axons of the posterior lateral line nerve of the PNS are ensheathed by several dense layers of Schwann cell membranes in wild type (wt) (M). In homozygous sox10/cls^{t3} mutants (N) no evidence of PNS myelin formation was found and Schwann cells were lacking completely. In the CNS, while myelin was present, it was severely reduced in the absence of Sox10 function. By 7 dpf, in the wt spinal cord large diameter axons of ventral and dorsolateral tracts (arrows) are strongly myelinated (O, Q area boxed in O). In contrast, only some of the axons in these tracts were loosely wrapped (arrowheads) by oligodendrocyte membranes in *sox10/cls^{t3}* mutant larvae (P, R area boxed in P). Similarly, reticulospinal axons in the hindbrain, that are prominently myelinated in wt larvae (S), lack most of their myelin sheath in *sox10/cls^{t3}* mutants (T). This is especially evident for the large Mauthner axon (indicated with M). Dashed line = midline, scale bars = 1 µm in M, N, Q, R; 10 µm in O, P; 3 µm in S, T. Figure modified from (Orosco, Schaefer et al. in preparation).
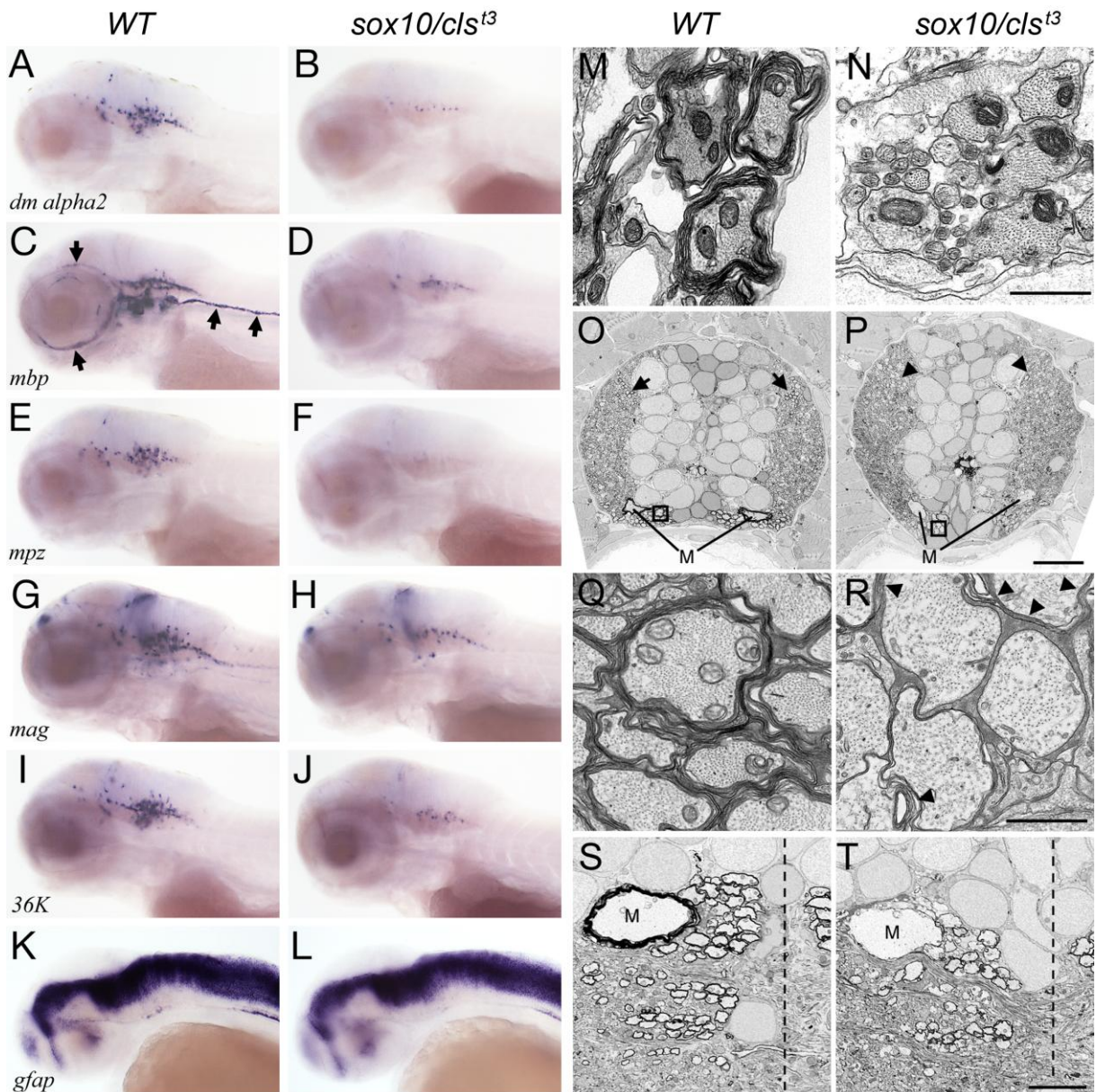
system and peripheral glia (Pingault, Bondurand et al. 1998). The zebrafish *colourless*^t3 mutant, a complete loss of function of the *sox10* gene, exhibits ear defects, loss of pigment cells and enteric nervous system, together with large reductions in sensory and sympathetic neurones and putative satellite glia and Schwann cells (Dutton, Pauliny et al. 2001). As in mammals markers of oligodendrocyte precursors are unchanged, but myelin gene expression is decreased and myelination is severely reduced in the CNS (Figure 2.4-1). In the PNS myelin gene expression is abolished and no myelin could be observed (Figure 2.4-1) (Orosco, Schaefer et al. in preparation).

Introduction

To perform a screen to identify novel myelin specific genes, RNA samples isolated from wild type (wt) and *sox10/colourless^t3^* larvae were hybridized to a microarray of synthetic oligonucleotides. These oligonucleotides were designed from 16 000 unique expressed sequence tag (EST) clusters contained in the NCBI Zebrafish Unigene database (EST sequences are typically derived from a cDNA library and their clusters generally represent expressed genes). Among the 20 transcripts, that were found to be downregulated in *sox10/colourless^t3^* larvae, were MBP, MPZ and DMalpha2, confirming the validity of the screen. Two novel transcripts, that were markedly reduced and showed an expression pattern specific for myelinating glia, were identified. The phylogenetic, biochemical and functional of these novel transcripts is the objective of this thesis.

2.5   PROMOTERS DRIVING EXPRESSION IN MYELINATING GLIA

Specific promoters are essential for a broad range of studies by regulating gene expression in a cell-specific manner. They provide a powerful tool to test gene function in heath and disease (Ingham 2009; Paquet, Bhat et al. 2009), monitor subcellular structures and target tissues for selective ablation. They can drive expression of fluorescent reporter proteins labeling specific cell types, membranes or organelles. This is useful for *in vivo* imaging of dynamic processes and has been the basis for many studies (McLean and Fetcho 2008; O'Brien, Rieger et al. 2009). Furthermore, fluorescent reporter lines enable large scale screens identifying genes with specific functions, because they allow a distinct straightforward read out rather than relying on laborious *in situ* hybridization or gross morphological phenotypes, caused by a broad range of genetic defects.

To establish zebrafish as a model to study the dynamics of glial cell behavior during myelin formation as well as during de- and remyelination in its associated diseases, promoters and transgenic lines with strong and specific expression through all stages are needed. Optimally these promoters should be easy to clone or exist in a flexible system with separate driver and responder constructs, allowing expression of any desired transcript.

Several promoters driving expression in oligodendrocytes and one promoter driving expression in Schwann cell precursor cells in zebrafish have been described (Table

2.5-1). Some have been successfully used to study differentiation, development and dynamic behavior of oligodendrocytes (Gilmour, Maischein et al. 2002; Gilmour, Knaut et al. 2004; Kirby, Takada et al. 2006; Jung, Kim et al. 2009). Yet most of them are derived from transcription factors involved in glial cell differentiation, which are downregulated after initiation of myelination and/or drive expression also in other cell populations. Some of them are contained in bacterial artificial chromosomes (BAC's) or are very large and therefore difficult to subclone. None of the identified promoters is available in a vector or transgenic line, which can be easily combined or crossed to drive expression of other desirable responders. Therefore we decided to explore the potential of the phylogenetically conserved, compact Claudin k promoter described in chapter 3.3, to drive strong and specific expression in myelinating glia through all stages.

Table 2.5-1: Overview of promoter constructs driving expression in myelinating glia

Promoter	expression	comments	ref
Nkx2.2a	gut, intestine, subset of oligodendrocytes	down reg. in mature oligodendrocytes large BAC construct	(Ng, de Jong-Curtain et al. 2005; Kirby, Takada et al. 2006)
Olig1	oligodendrocytes, cerebellum	early developmental stages analyzed	(Schebesta and Serluca 2009)
Olig 2	oligodendrocytes, retina, motorneurons, radial glia, other neurons	down reg. in mature oligodendrocytes large BAC construct	(Shin, Park et al. 2003; Park, Shin et al. 2004; Park, Shin et al. 2007)
Sox10	oligodendrocytes, Schwann cells, non-ectomesenchymal crest derivatives	early developmental stages analyzed only	(Wada, Javidan et al. 2005; Dutton, Antonellis et al. 2008)

PLP	oligodendrocytes	developmental stages until 6 dpf analyzed large BAC construct	(Wight, Duchala et al. 1993; Yoshida and Macklin 2005)
P0	oligodendrocytes	developmental stages until 5 dpf analyzed no transgenic line	(Yoshida and Macklin 2005)
zFoxD3	Schwann cell precursor cells, neural crest	precursor cells	(Gilmour, Maischein et al. 2002)
MBP	Oligodendrocytes, subset of Schwann cells	throughout all stages	(Jung, Kim et al. 2009)

3 RESULTS

3.1 ZWILLING

3.1.1 GENE STRUCTURE

Zwilling was identified by EST AW281753, the 3'-end sequence of a cDNA library from adult brain mRNA. Alignment of EST AW281753 to the genome revealed that it lies within a cluster of overlapping ESTs on Chromosome 3. Additionally we found two further non-overlapping clusters in 5' direction of this initial EST cluster (Figure 2.2-1). We established with RT-PCR, that these clusters form one transcript and defined its 5' end with RACE, resulting in a full length cDNA of 4101 bp. The gene consist of a first and a second exon of 2751 and 1350 bp, respectively with an intron of 1621 bp (GenBank accession FJ221370). A number of EST's provide evidence for alternative splicing of a shorter mRNA of 1995 bp (GenBank accession FJ360543). Analysis of existing homologues ESTs and additional sequencing support the existence of an alternatively spliced transcript of 2001 bp (GenBank accession FJ360543). The gene lies within the first exon of an orthologue of *RUN domain-containing protein 3A* (RUNDC3A syn. *rap2ip,*) - *zf RUNDC3A-1* - on the complementary strand (Figure 3.1-1, A).

Scanning the transcript for potential protein coding sequences, we found several short ORFs of up to 516 bp. To validate the candidates, we searched for the presence of a Kozak consensus sequence (Kozak 1987) and for phylogenetic conservation of the deduced amino acid sequence in other species. Surprisingly, we found two ORFs of 246 bp (Figure 3.1-1, B) in exon 1, which encode two proteins of 82 aa, that are highly homologues to each other (67% aa identity and 80% similarity). This unusual structure prompted us to name the gene '*zwilling*', the German word for twin. *Zwilling A* and *B* refer to the first and second ORF, respectively.
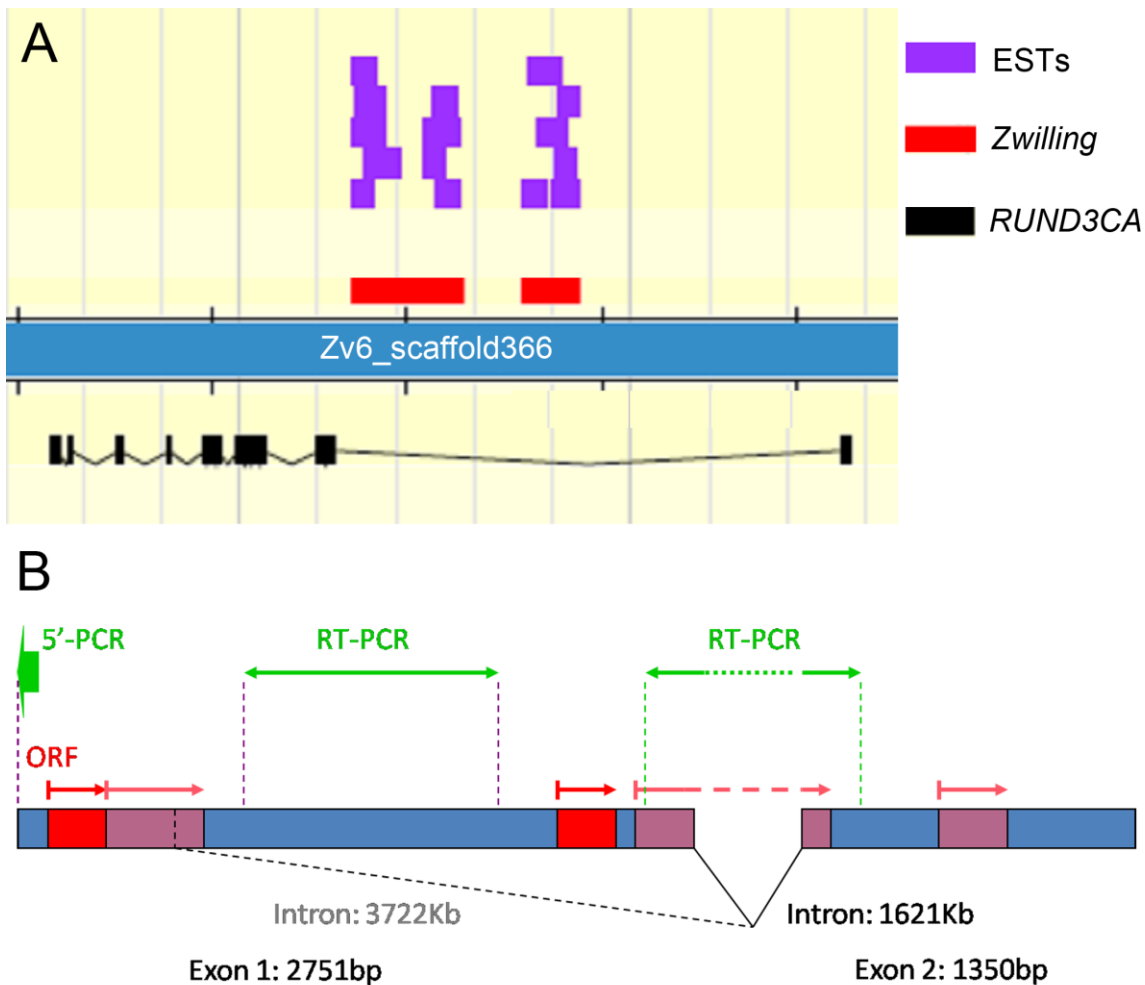
Figure 3.1-1: *Zwilling* gene locus and structure.

(A) EST AW2817533, identified in the mircoarray screen, is part of a cluster of ESTs homologous to the 3' end of the *zwilling* gene (arrow). Two more EST cluster representing the *zwilling* gene exist in close vicinity (arrowheads).The *zwilling* gene lies within the first intron of *RUNDC3A* on the opposite strand. (B) Using RT-PCR to bridge the gaps between the EST clusters and 5'RACE (green arrows), a full length mRNA of 4101 bp was reconstructed (GenBank accession FJ221370). Alternative splicing results in a shorter mRNA of 1995 bp (GenBank accession FJ360543). Several ORFs of up to 516 bp exist (dark red and light red). Two ORFs have a Kozak consensus sequence and are conserved in teleosts (dark red).

3.1.2 PHYLOGENETIC CONSERVATION OF ZWILLING-A AND -B PROTEINS AND THE ZWILLING LOCUS

Database searches using protein as well as DNA sequences of *zwilling A* and *B* identified orthologues within the teleost clade with homology ranging from 62% - 93% (identity). The phylogenetic tree of Zwilling protein alignments precisely reflects the

known phylogenetic relationship of these species. For teleosts for which significant genomic data is available – *Danio rerio, Gasterosteus aculeatus, Oryzias latipes, Fugu rubripes, Tetraodon nigroviridis* – always sequences for both *zwilling A* and *B* were found, strictly segregating in either of the two branches of the phylogenetic tree. For *Pimephales promegas zwilling A* and *B* were found, for *Gillichthys mirabilis, Oncorhynchus mykiss, Salmo salar* and *Astatotilapia burtoni* either of one of the two homologues – yet again strictly segregating in either of the branches – were found.

Not only are the protein-coding sequences of *zwilling A* and *B* conserved, but also the peculiar *zwilling* gene structure, with *zwilling A* and *B* ORFs both on one mRNA. Comparing the genomic regions, using a percent identity plot, confirms the high conservation of the *zwilling A* and *B* ORFs and shows additional conservation in the 5' untranslated region, the untranslated region between the two ORFs and in a small region of the intron (Figure 3.1-2, C).

Another strand of evidence verifying that Zwilling A and B proteins of the different species are true orthologues is the conserved synteny of the genomic region around the *zwilling* locus. All *zwilling* genes reside in the first intron of *RUNDC3A-1* and gene succession and directionality is conserved for at least 4 loci in the 5' direction. For the perciform fish, this is also true for the 3' direction while for the cyprinid *Danio rerio* syntenic conservation ends at the 5' end of *RUNDC3A*.

Comparing the corresponding paralogues of *RUNDC3A,* which excist in all species studied, shows that none of them has any gene residing in the first intron and that this first intron is always significantly shorter. This suggests that the *zwilling* gene has arisen as an insertion into the first intron after the genome duplication event at the base of the teleost radiation (Amores, Force et al. 1998; Prince, Joly et al. 1998; Hurley, Mueller et al. 2007).

Figure 3.1-2 *Zwilling* gene structure and proteins are conserved among teleosts.

In teleosts we found 8 orthologues of Zwilling A and 6 of Zwilling B shown in the alignment in (A).The phylogenetic tree in (B) clearly shows that Zwilling A and B proteins segregate in separate branches, each branch representing the known phylogenetic relationships between species. The percent identity plot (PIP) of the z*willing* locus in (C) shows, that the gene structure with two ORFs on one mRNA is conserved among teleosts. Next to the two ORFs parts of the untranslated region, a short stretch in the intronic region, and the region upstream on the 5' UTR, likely representing parts of the promoter, are conserved. *Zwilling*, nested in an intron of *RUND3CA*, lies in a syntenic cluster that extends at least for 3 genes downstream of *RUND3CA* and 3 genes upstream, except for *Danio rerio* where the cluster ends upstream of *RUND3CA*.

3.1.3 MRNA EXPRESSION

The mRNA expression pattern of *zwilling* at different developmental stages was examined using standard *in situ* hybridization (Thisse, Thisse et al. 1993). The expression of *zwilling* mRNA can be first detected at 3 dpf in the oligodendrocytes of the hindbrain. At 4 and 7 dpf in can be detected in a pattern characteristic for

oligodendrocyte and Schwann cell specific transcripts (Brösamle and Halpern 2002). The mRNA is located in the cell bodies of the myelinating glia, and not transported to the processes as seen for example for the *mbp* mRNA.
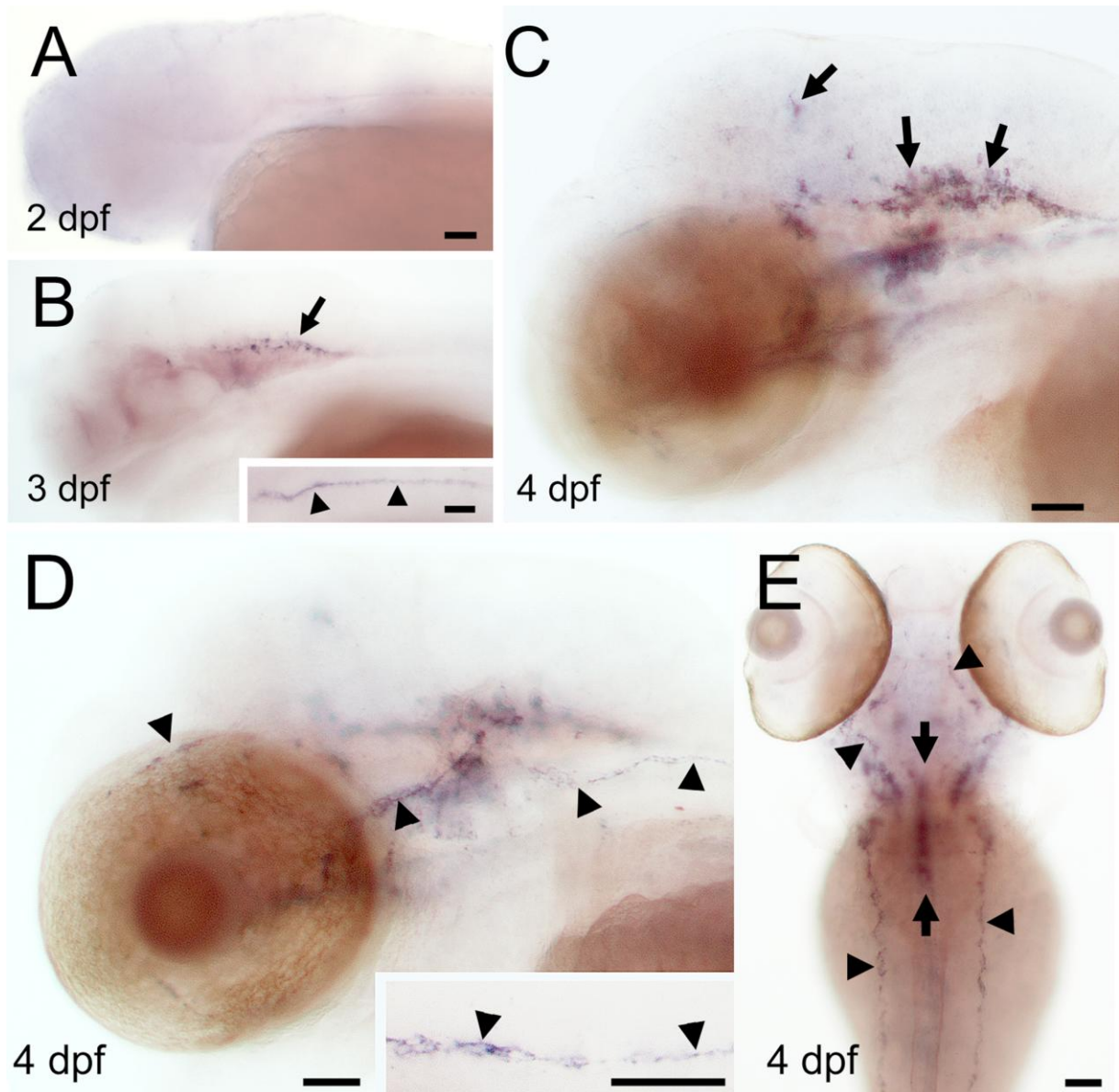
Figure 3.1-3: *Zwilling* mRNA expression pattern.

Zwilling mRNA can first be detected at 3 dpf in oligodendrocytes of the hindbrain (B, arrows) and in the Schwann cells of the posterior lateral line (PLL) nerve shown in a magnified view in the inset (B, arrowheads), while it was not detected at 2 dpf. At 4 dpf *zwilling* is expressed in the oligodendrocytes in the mid- and hindbrain and the spinal cord (C, E arrows) and in the Schwann cells of the eye muscle and ear innervation and the PLL nerve (D, E, arrowheads). Inset in (D) shows magnified view of the PLL nerve. A – D, lateral views; C and D are images taken at different focal planes; E, dorsal view; scale bars = 50 µm.

Results

3.1.4 ZWILLING PROTEIN

The Zwilling proteins A and B are very short with an approximate molecular mass of 8.6 kD. No known patterns, domains or structural motives could be found using various search algorithms. In silico prediction of secondary structures for Zwilling A and B indicated an intrinsically unstructured N-terminus, beta-sheet conformation interrupted by random coils for aa 10-70 and a certain propensity to adopt an alpha helical conformation for the C-terminus. These predictions varied though depending on the algorithms used suggesting, that Zwilling might not adopt a defined secondary structure but rather multiple conformations. Several predicted phosphorylation and myristoylation sites, some of which are conserved between species, are depicted in Figure 3.1-5. Interestingly, Zwilling A as well as Zwilling B are very basic with proteins with isoelectric points of 12.6 and 12.3, respectively.

To substantiate that the *zwilling A* and *B* ORFs are actually protein coding units, we compared the non-synonymous versus synonymous nucleotide substitution between different teleosts and calculated the Ka/Ks ratio for both *zwilling* ORFs. A Ka/Ks ratio of <1 indicates conservative evolutionary pressure on protein level (Nekrutenko, Makova et al. 2002). The very low Ka/Ks ratio of 0.062 (+/-0.037) for Zwilling A and 0.069 +/- 0.061 for Zwilling B strongly suggests the existence of the proteins.

In order to experimentally confirm the existence of the proteins *in vivo* we applied mass spectrometry. We biochemically isolated the myelin membranes from adult zebrafish brain (Morris, Willard et al. 2004), separated the obtained fraction by SDS-polyacrylamide gel electrophoresis (SDS-PAGE) and stained the proteins in the gel with Coomassie brilliant blue (Figure 3.1-4). In prominent bands of the expected molecular weight, we identified well known myelin proteins such as MBP, Myelin Protein 0 and 36K through MALDI-PMF (matrix assisted laser desorption ionization peptide mass fingerprinting) confirming the quality of the myelin preparation. Co-migrating with peptides of MBP at about 8 kD, we detected 4 peptides of Zwilling A and 3 of Zwilling B (Figure 3.1-5). For Zwilling A these peptides were confirmed by tandem mass spectrometry (LC-MS/MS).
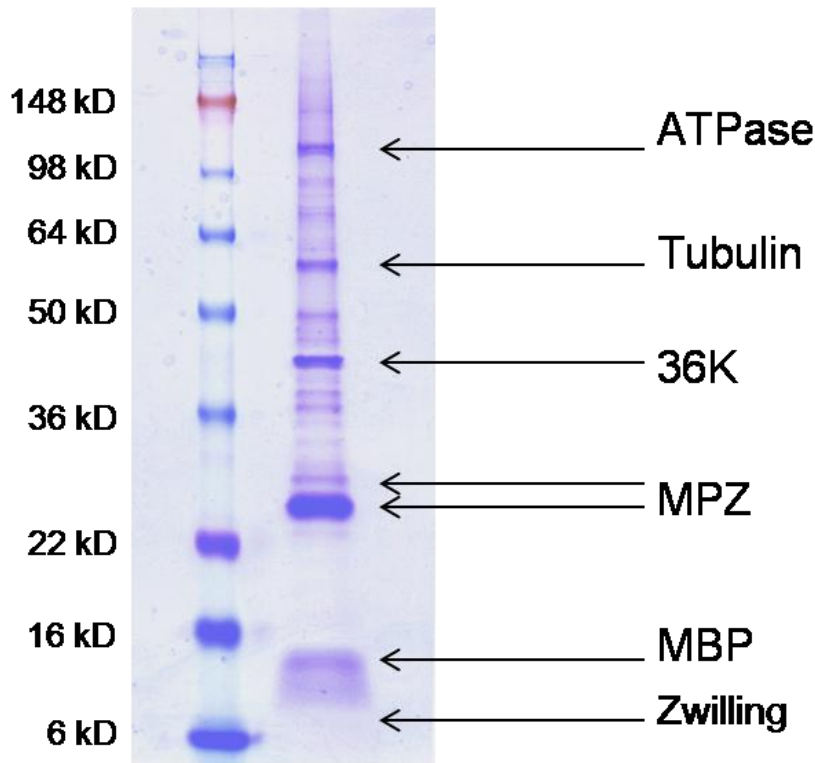
Figure 3.1-4: Myelin membrane preparation

Representative SDS-PAGE gel showing separation of a myelin membrane preparation from adult zebrafish brain. Prominent bands were identified through MALDI-PMF and include major zebrafish myelin proteins like MBP, MPZ and 36K. Zwilling A and B were found at around 8 kD co-migrating with peptides of MBP.

Figure 3.1-5: Analysis of zebrafish Zwilling proteins.

Zebrafish Zwilling A and B are highly homologous (Aa in magenta are identical and aa in purple similar) and share most of the phylogentically conserved putative phosphorylations sites (P) and a N-terminal putative myristoylation site (myr). Red bars indicate tryptic peptides in a myelin membrane preparation detected by mass spectrometry.

Results

Several approaches were taken to raise antibodies against the Zwilling proteins. We overexpressed a recombinant Zwilling A-GST (Glutathione-S-transferase) fusion protein in E-coli, affinity purified it with immobilized glutathione eluting with reduced glutathione. The fusion protein was used to immunize rats and mice to generate monoclonal antibodies. In addition three synthetic peptides were used as antigens to generate monoclonal antibodies. Furthermore, two of the synthetic peptides were used to immunize two rabbits, generating polyclonal sera. Screening was done on whole mount larvae of 4 dpf using different fixation procedures, on adult brain cryo-sections and on Western blot using larval and brain lysates. Unfortunately, no positive signal could be detected with any of the approaches.

3.2   CLAUDIN K

Claudin k, which we originally named *claudin 31* – derived from its orthology to *fugu claudin 31* (Loh, Christoffels et al. 2004) – was renamed by the zebrafish nomenclature committee according to current nomenclatures regulations. It is a teleost-specific member of the large Claudin family, is exclusively and strongly expressed in oligodendrocytes and Schwann cells and expression is severely reduced in *sox10/clst³* mutants. It localizes to the autotypic tight junctions of oligodendrocytes and Schwann cells.

3.2.1 CLAUDIN K GENE

Claudin k was represented by EST BI980908 in the microarray screen. The *claudin k* gene (Figure 3.2-1) lies on Chromosome 3 at 48,270,951-48,274,629 bp on the forward strand and consists of two exons, a short exon of 215 bp and a second exon of 1031 bp, separated by an intron of 2433bp. The whole ORF of 648 bp lies on the second exon and contains two synonymous coding SNPs (single nucleotide polymorphisms) and one non-synonymous coding SNP.
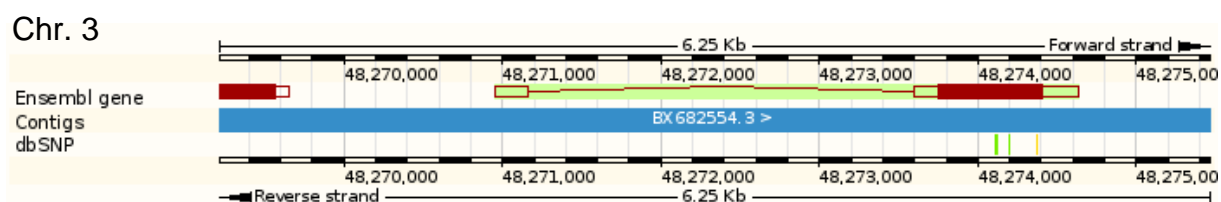
Figure 3.2-1 *Claudin k* gene.

Graphic representation of the *Claudin k* locus from the ensemble genome browser (version Zv8 56.8b). The *claudin k* gene (red with green underlay) lies on the forward strand on Chromosome 3 within the contig BX682554.3 (blue). Three SNPs are indicated and lie within the *Claudin k* ORF (solid red): two are synonymous coding (green), one is non-synonymous coding (yellow).

3.2.2 CLAUDIN K PROTEIN STRUCTURE

Teleost Claudin k is 216 aa long and has a calculated molecular weight of 22,8 kDa . Computational analysis by TMHMM 2.0 predicts the typical topology of Claudins (Figure 3.2-2), with 4 transmembrane domains, a short intracellular N-terminus and a

longer C-terminus and a long, first extracellular loop (ECL1). The length of its N- and C-terminus and its intracellular and extracellular loops, all lie within the average of classical Claudins. Significant Claudin features like the Claudin family signature ([GN]-L-W-x(2)-C-x(7,9)-[STDENQH]-C, PPsearch) with a putative disulfide bridge in ECL1 and the putative PKC phospho site (SPR, [ST]-x-[RK], Prosearch) and PDZ binding domain ([KRH]-x-Y-V, (Krause, Winkler et al. 2008)) in the N-terminus are also conserved (Figure 3.2-1). Additionally, Prosearch predicts two CK2 phospho sites ([ST]-x(2)-[DE]) at 58-62 aa (STGE) and 197-201 aa (SSDE) and another PKC phospho site at 114-116 aa (SLK). At position 214 there is a non-synonymous coding snip (single nucleotide polymorphism) resulting in a V to G ambiguity (National Center for Biotechnology Information, cluster report reference SNP: rs40911811).
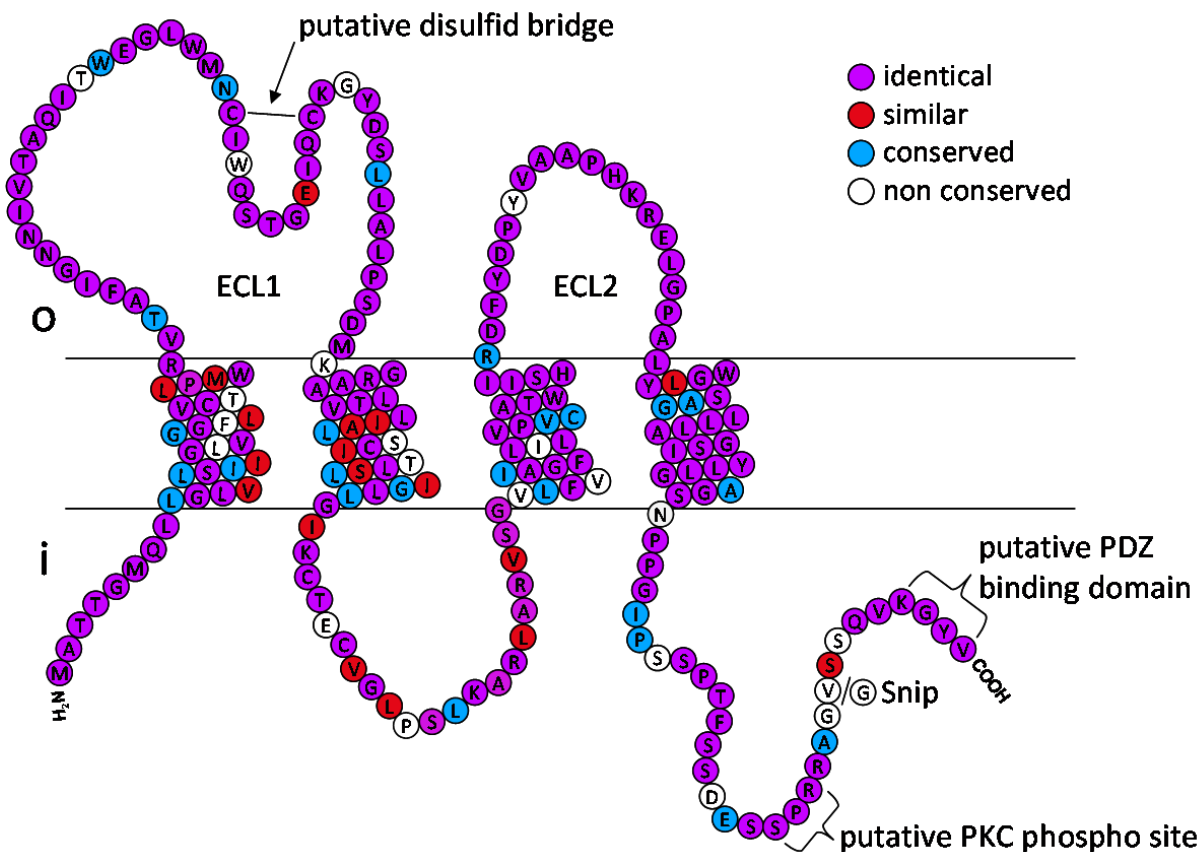
Figure 3.2-2 Claudin k protein sequence and predicted membrane topology.

The zf Claudin k sequence and its topology according to TMHMM 2.0. The color-code indicating conserved residues is based on ClustalW alignment of 9 teleost Claudin k and TeXshade 1.4. Conserved putative domains and functional sites were identified with Prosearch, PPSearch and according to Krause et al. 2008.

3.2.3 PHYLOGENY

The Claudin family is large, with so far 24 annotated members in humans (Lal-Nag and Morin 2009) and more than twice as many members in teleost – presumably the result of tandem duplications in addition to the whole genome duplication at the base of the teleost radiation (Amores, Force et al. 1998; Prince, Joly et al. 1998; Loh, Christoffels et al. 2004; Hurley, Mueller et al. 2007). Based on a Common consensus sequence, they can be divided into classical Claudins with comparably higher sequence homologue and non-classical Claudins with higher sequence divergence (Krause, Winkler et al. 2008). In the phylogenetic analysis Claudin k clearly clusters with the classical Claudins (Figure 3.2-3) and furthermore the classical-Claudin consensus sequence is conserved (data not shown). Together with fugu Claudin 31 (the fugu orthologue of zf Claudin k) zebrafish Claudin k lies on a teleost specific branch of the phylogenetic tree and clear orthologues in any other taxa than teleosts were not found. The mammalian Claudin with the highest sequence homology is Claudin 6, for example mouse Claudin 6 with 59% aa identity. Zf Claudin k also has no paralogue (e.g. no Claudin k a and b), the zebrafish Claudin with the highest homology is Claudin g (52% aa identity). Claudin 11 – also known as oligodendrocytes specific protein (OSP) – plays an important role in mammalian CNS myelin. It belongs to the non-classical Claudins and has two teleost orthologues, Claudin 11 a and b, with conserved syteny (data not shown). The phylogenetic analysis clearly shows that zf Claudin k and mouse Claudin 11 are not closely related (25% aa identity). Also mouse Claudin 19, which plays an important role in rodent PNS myelin, and Claudin k are not closely related (42% aa identity). We could find orthologs of zf Claudin k in all teleosts (Figure 3.2-4) for which significant genomic data is available: *Danio rerio* (zebrafish), *Gasterosteus aculeatus* (stickleback), *Oryzias latipes* (medaka), *Fugu rubripes* (pufferfish), *Tetraodon nigroviridis* (tetraodon) and in some species with gene expression data only (*oncorhynchus mykiss* (rainbow trout), *Salmo salar* (Antlantic Salmon), *Pimephales promegas* (fathead minnow), *Poecilia reticulata* (guppy)). The sequence homology ranges from 79% aa identity (*Poecilia reticulata*) to 92% aa identity (*Pimephales promegas*), the closest identified orthologue of zf Claudin k (Figure 3.2-4). Another strand of evidence verifying the Claudin k orthology is the conserved synteny of the respective genomic loci in teleosts (Figure 3.2-5). Conservation of gene order and gene directionality extends for several loci in both directions from the *claudin k* gene.
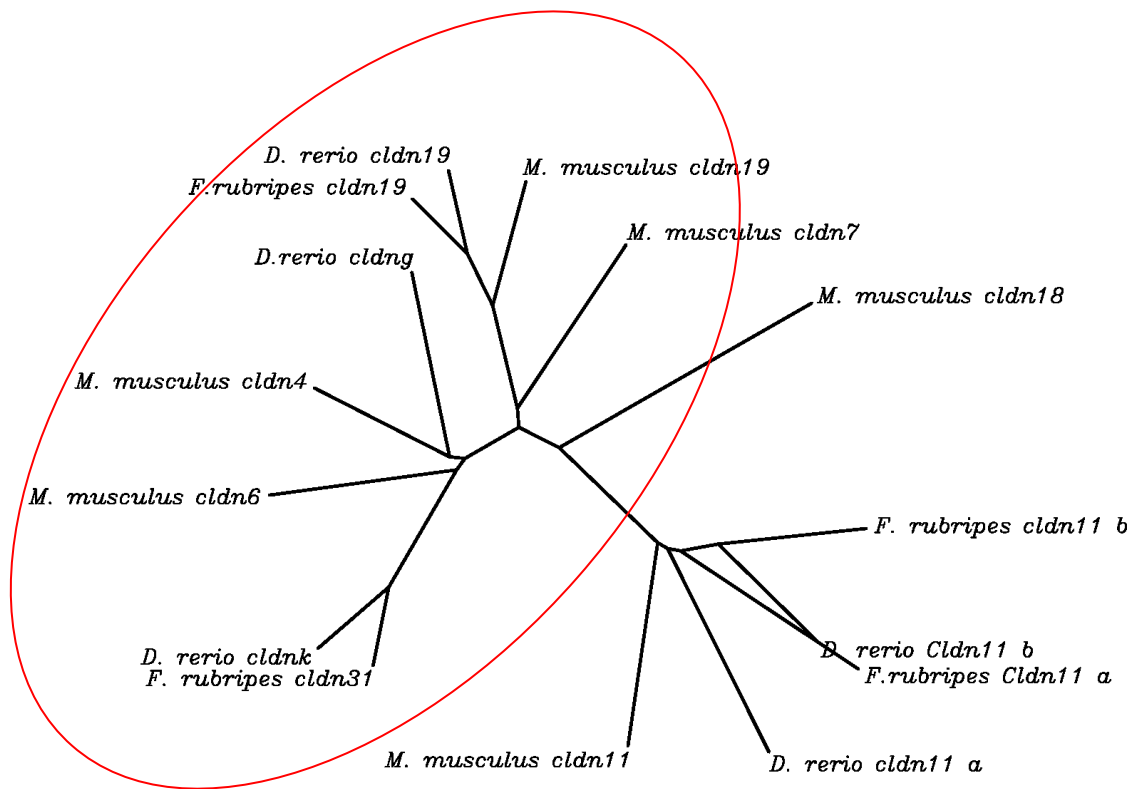
Figure 3.2-3: Unrooted phylogenetic tree of selected Claudins.

Protein alignment of 16 selected Claudins was calculated with CLUSTALW and a phylogenetic tree was built with DRAWTREE. Typical examples of classical Claudins (mouse Claudin 4, 5 and 7, 19) cluster with Claudin k while the non classical Claudins 11 and 18 lie in a more distant part of the tree (red circle indicates classical Claudins). Zebrafish Claudin k and fugu Claudin 31 are orthologues, while the closest mammalian homologue, mouse Claudin 6, lies on a different branch. Zebrafish Claudin g, the zebrafish Claudin with highest sequence homology is not a paralogue of Claudin k, it is rather the zebrafish orthologue of mammalian Claudin 4. Mammalian Claudin 19 has one orthologue in teleosts, while Claudin 11 has two orthologues in teleosts, Claudin 11 a and b.
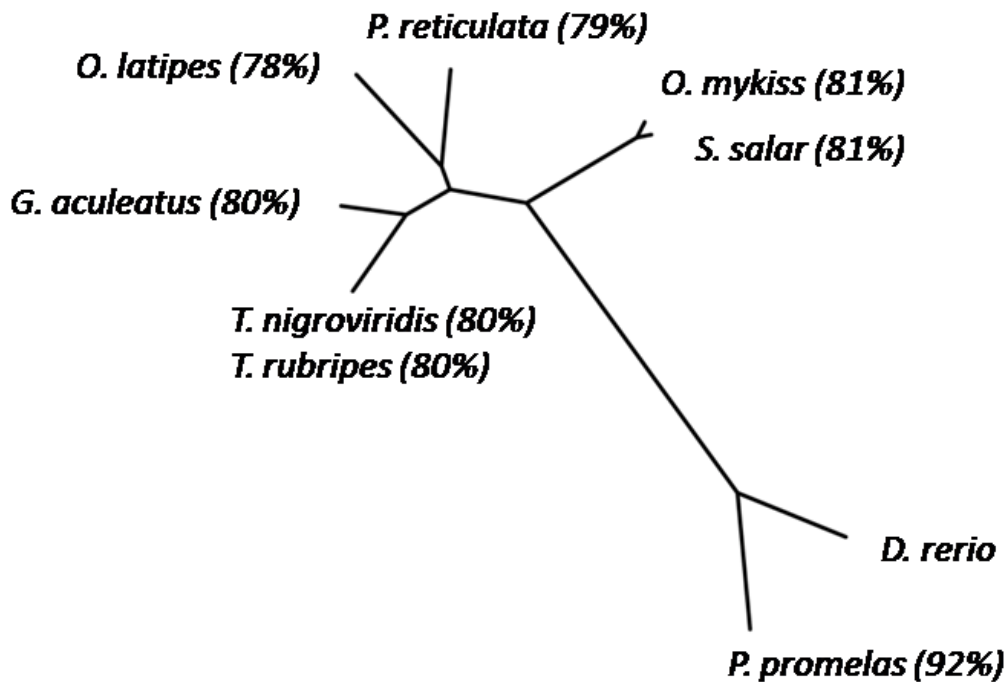
Figure 3.2-4 Phylogenetic tree of Claudin k orthologues.

Protein alignment of 9 Claudin k orthologues in teleosts was calculated with CLUSTALW and a phylogenetic tree was built with DRAWTREE. Identities are indicated in brackets and were calculated with BL2SEQ.
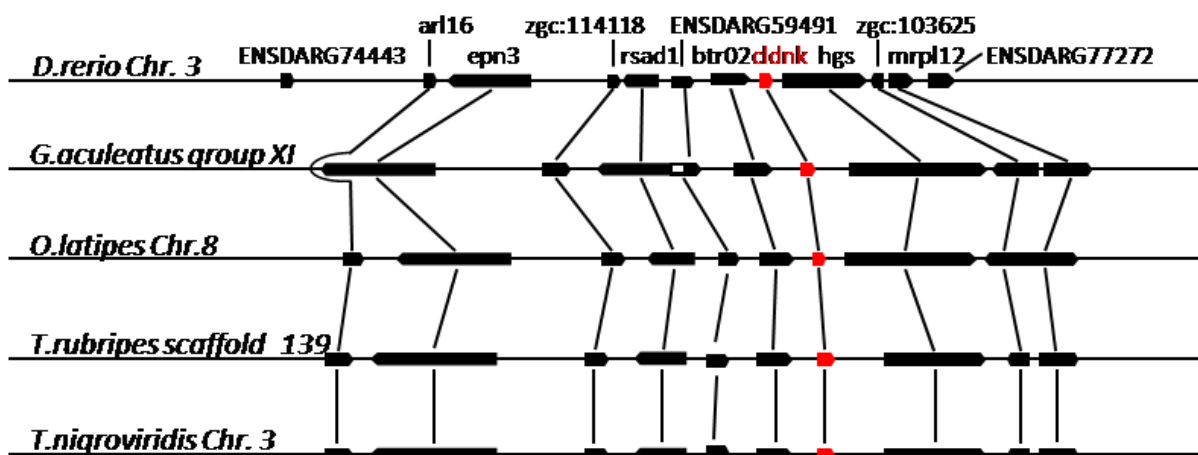
Figure 3.2-5: Synteny is conserved between Claudin k orthologue genomic loci.

The syntenic cluster extending from at least six genes downstream and 3 genes upstream of Claudin k is conserved in terms of order as well as directionality of genes in teleost. Synteny analysis is based on ensemble assembly version Zv8 56.8b.

3.2.4 MRNA EXPRESSION

The mRNA expression pattern of *claudin k* at different developmental stages was examined using standard *in situ* hybridization (Thisse, Thisse et al. 1993). The expression of *claudin k* was detected in a pattern characteristic for oligodendrocyte and Schwann cell gene expression (Brösamle and Halpern 2002). Like other myelin markers it was first detected at 2 dpf in the first oligodendrocytes of the hindbrain (Figure 3.2-6). At 3 dpf it was strongly expressed in oligodendrocytes of the hindbrain, and the ventral spinal cord and in Schwann cells of the posterior lateral line (PLL) nerve. At this stage it was also expressed in oligodendrocytes of the midbrain, the dorso-lateral spinal cord, and in Schwann cells along the nerves innervating the extraorbital muscles eyes (Figure 3.2-6). At 4 dpf expression still increased in the hindbrain, spinal cord and PLL nerve. It was detected in the midbrain and commissure and along the innervation of the ear (Figure 3.2-7). In *sox10/cls^{t3}* larvae, expression in the CNS was severely reduced, while expression in the PNS was no longer detected due to absence of Schwann cells in *sox10/cls^{t3}* larvae (Figure 3.2-7). At 2 dpf weak expression in an unknown cell population at the tip of the forehead was also detected (Figure 3.2-6). This expression domain becomes weaker at 3 dpf and disappears at 4 dpf. The *claudin k* mRNA is located in the cell bodies of the myelinating glia, and not transported to the processes, as seen for example for the *mbp* mRNA.

_____

Figure 3.2-6 *Claudin k* mRNA expression pattern at 2 and 3 dpf.

At 2 dpf (lateral (A) and dorsal (B) view, C, D higher magnification), first expression was detected in oligodendrocytes of the hindbrain (arrow) and in the spinal cord (asterisk). At 3 dpf (E- K), *claudin k* is strongly expressed in oligodendrocytes of the hindbrain, and the ventral reticulospinal tracts (lateral view in E, magnification in G and dorsal view in I) and in Schwann cells of the PLL nerve (lateral view at different focal plane in F, magnification in H and dorsal view in I, arrowheads). J: oligodendrocytes of the dorso-lateral tracts (arrows). K: Schwann cells along the nerve innervating of the extraorbital muscles of the eye. Expression in an unidentified cell population was detected at 2 dpf, getting weaker at day 3 dpf (triangle). Scale bars = 50 μm.
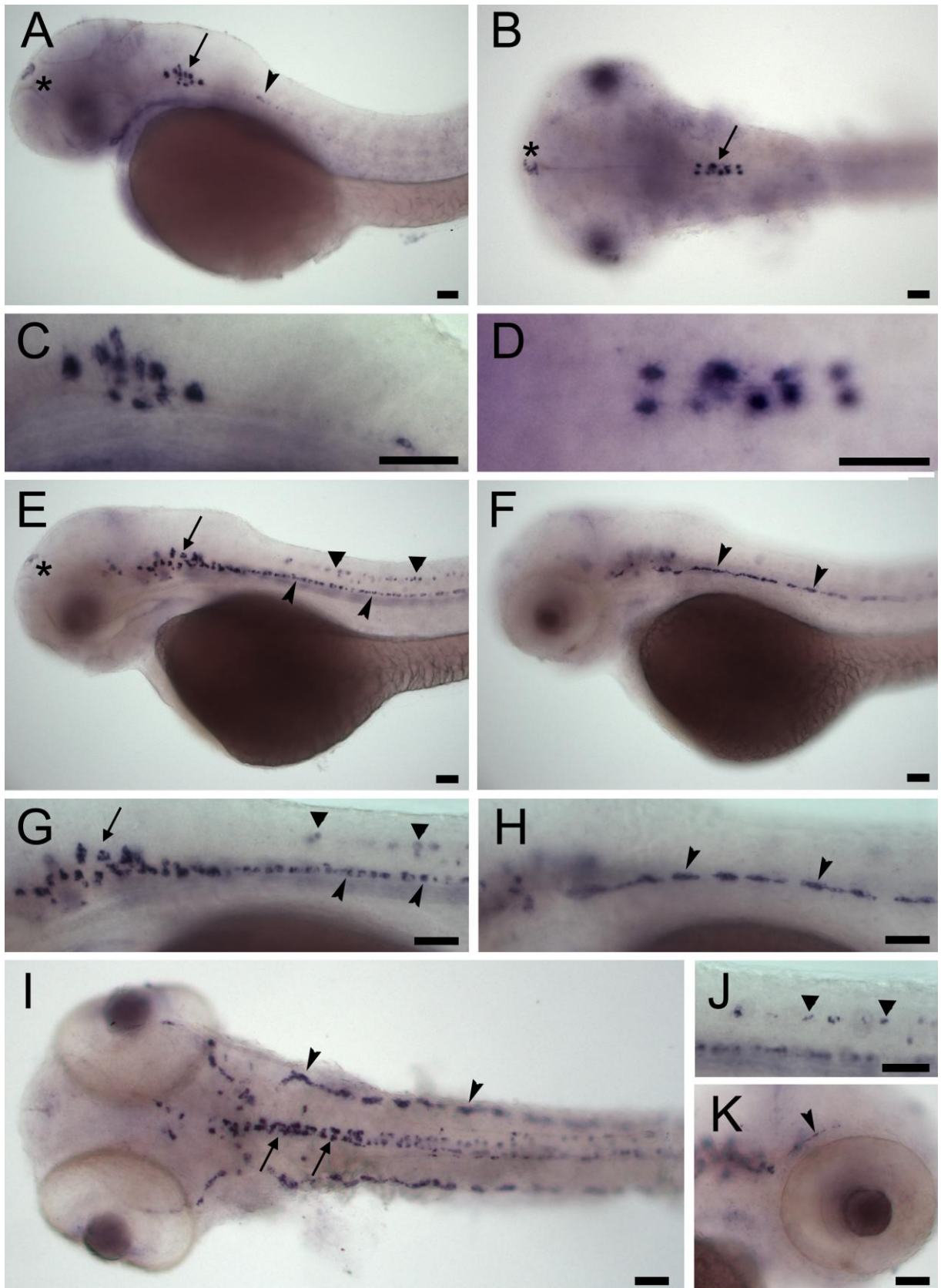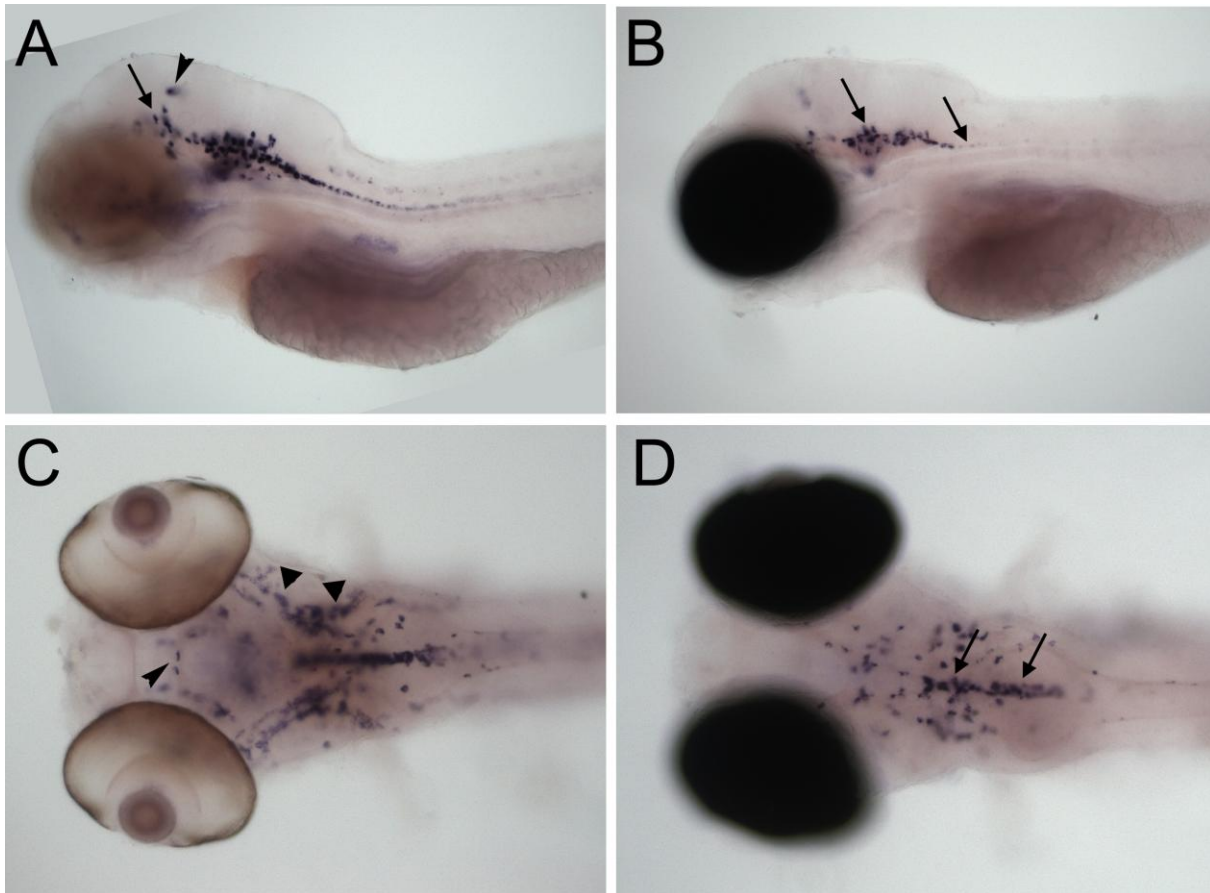
Figure 3.2-7 *Claudin k* mRNA expression at 4 dpf wt and *sox10/cls^t3* larvae.

Compared to expression at 3 dpf, expression at 4 dpf is still increasing in the hindbrain, spinal cord (A, C). It can now be additionally detected in the midbrain (A, asterisk) and commissure (F, arrows) and along the innervation of the ear (E). Expression is severely reduced in *sox10/cls^t3* larvae (B, D) compared to wt (A, C) in oligodendrocytes of the brain and spinal cord (arrows). A, B lateral view, D, C dorsal view. Reflecting the loss of Schwann cells in *sox10/cls^t3* larvae, expression of *claudin k* in the PNS can no longer be detected.

3.2.5 CLAUDIN K ANTIBODIES

An important tool to characterize a novel protein is a specific antibody. As a target to raise antibodies against we chose two peptides from the C-terminus for multiple reasons: using recombinant full-length protein as antigen is difficult, due its structure with 4 transmembrane domains and its high degree of conservation. To overexpress and purify native membrane proteins is difficult and unnatural folding reduces availability of natural epitopes. Additionally, Claudin k shows high sequence similarity to other classical Claudins, which may lead to undesirable cross-reactivity of the resulting antibodies. Because the C-terminus, exposed to the cytosol, is the most

divergent part of the Claudin family, we designed several peptides for use as antigens. Two peptides were jointly injected in two rabbits and gave rise to one positive polyclonal serum (designated α-Claudin k poly). The same peptides were subsequently used to raise monoclonal antibodies in the SFB 596 antibody facility (E. Kremmer), and an anti-Claudin k rat monoclonal antibody (clone 3H5-1-1, designated α-Claudin k mono) against the C-terminal peptide (SPRRAGVSSQVKGYV) was obtained. α-Claudin k monoclonal antibody was used as standard antibody, unless otherwise indicated.
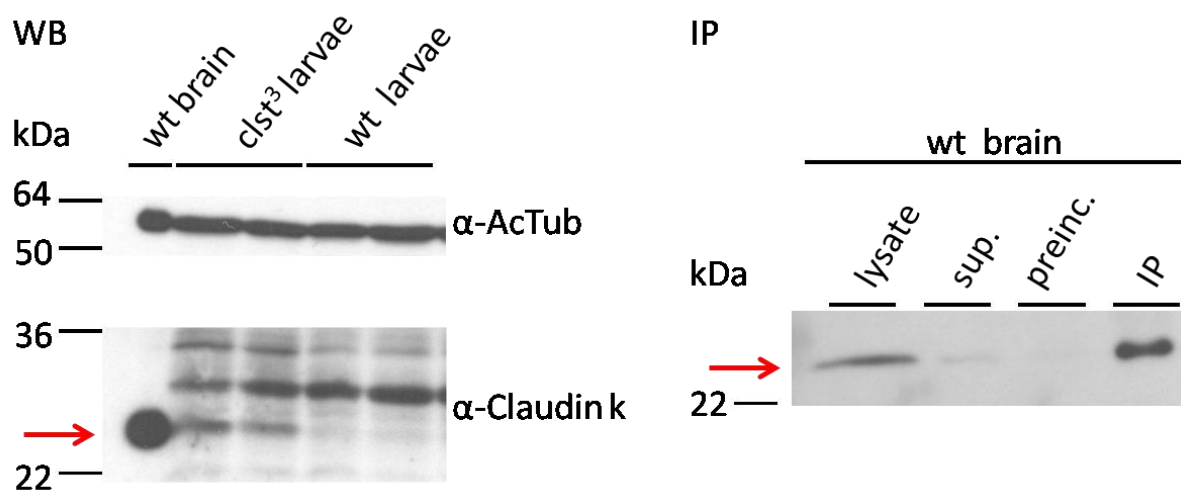
Figure 3.2-8 Analysis of Claudin k in Western blot and Immunoprecipitation.

WB: Western blot detected with Claudin k monoclonal antibody 3H5-1-1. Membrane preparations of wt adult zebrafish brain show single strong band running at expected molecular height of 23 kD. 23 kD band is present in 5 dpf membrane preparation of wt, but very weak in *sox10/cls^{t3}* larvae. Acetylated tubulin (AcTub) was used as a loading control. IP: Immunoprecipitation of Claudin k from membrane preparations of wt adult zebrafish brain was carried out using α-Claudin k poly for immunoprecipitation and α-Claudin k mono for detection. Antibody recognizes Claudin k in the lysate (lysate) and the supernatant after the IP is depleted of Claudin k protein (sup.). Claudin k does not bind unspecifically to sepharose A after preincubation of the lysate without antibody (preinc.) but Claudin k can be immunoprecipitated from the lysate using sepharose A.

To test the specificity of the antibody, we performed Western blot analysis (Figure 3.2-8). In membrane preparations of wt adult zebrafish brain, it recognizes a single strong band at the expected height of ~23 kD. The specificity of the antibody is

further demonstrated, comparing membrane preparations of wt and *sox10/cls^t3* larvae at 5 dpf. The band at 23 kD is prominent in the wt but almost gone in the preparations of mutant larvae. The Claudin k polyclonal antibody specifically immunoprecipitates Claudin k protein from adult brain membrane preparations.

3.2.6 CLAUDIN K PROTEIN EXPRESSION AND LOCALIZATION IN CELLS AND TISSUES DURING DEVELOPMENT

Protein expression of Claudin k was analyzed at different developmental stages (Figure 3.2-9). Claudin k protein was first detected at 3 dpf in the processes of Schwann cells in the PLL nerve. At 4 dpf, expression in the CNS was observed in the hindbrain and spinal cord. Also at 4 dpf, individual Schwann cells became visible, separated by small unmyelinated segments of the axon – presumptive nodes of Ranvier – and Claudin k was found along the mesaxons and at the paranodal area.

_____

Figure 3.2-9. Expression and localization of Claudin k in developing zf larvae.

Whole-mount larvae (A-I) stained with α-Claudin k monoclonal (A-D, F, H-J) or α-Claudin k poly (E, G) in green and neuronal processes stained with acetylated tubulin shown in red. At 3 dpf, the first expression was detected in processes of Schwann cells in the PLL nerve (A, B arrowheads). In the CNS, expression starts at 4 dpf (C) in the spinal cord and hindbrain (arrows). Expression in the ear and eye muscle innervation can be detected (arrowheads) and expression the PLL nerve becomes stronger. The magnification of the PLL nerve (D) shows Claudin k localizing to mesaxons (arrows) and paranodal areas (nodes are indicated by arrowheads). At 5 dpf (E lateral view, G dorsal view) two separate thick structures beginning in the midbrain, running through the hindbrain into the ventral spinal cord likely represent the myelin sheath of the Mauthner axons. In the hind- and midbrain very thin processes spread across the midline, while In the PNS ear and eye innervation becomes more pronounced. At 7 dpf (F) myelination of the nerve fibers innervating the neuromasts becomes visible. Due to difficult permeabilisation at 7 dpf staining in the CNS is not well visible. Whole mount staining at day10 dpf shows Schwann cells along the motor axons (H) and cranial nerves (I) with distinct localization of Claudin k to mesaxons and paranodal areas. (J) shows a cross section of a larva (cryosection) at 7 dpf. GFAP staining marks the spinal cord in red. Within the spinal cord Claudin k expression can be seen in two prominent areas (arrows) in the ventral spinal cord (reticulospinal tract with Mauthner axons) and in two weaker lateral areas (dorso-lateral spinal tracts). Two processes (arrowheads) project from the ventral area into lateral-ventral direction along the notochord, likely Schwann cells processes along the motor axons. Other peripheral nerves can also be seen (asterisk). Scale bars = 100 µm in A, B, E, F, G; 10 µm in C, D, H-J.
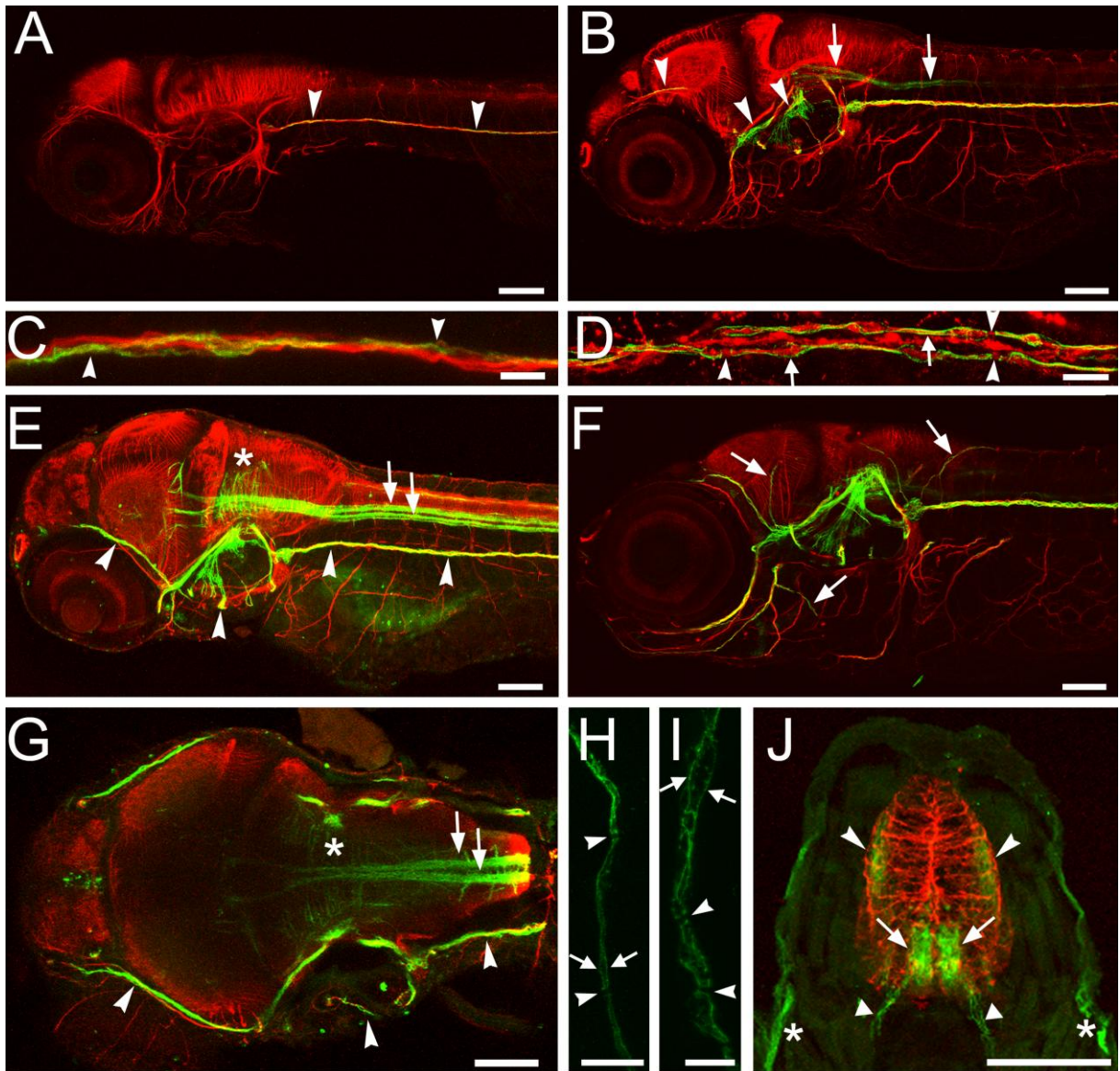
At 4,5 and 7 dpf it was detected in the hindbrain and the spinal cord, especially along the Mauthner axons in the reticulospinal tracts and the dorso-lateral tracts. It labels the Schwann cells of the cranial nerves, eye, ear and neuromast innervation, PLL nerve and the Schwann cells ensheathing the motor axons. At 10 dpf distinct localization of Claudin k to the mesaxons and paranodal area is also shown for Schwann cells along the cranial nerves and motor axons. The myelin marker MBP shows an analogous expression pattern while co-staining with GFAP, a marker for astrocytes, clearly shows that there is no overlap with the astrocytic cell population.
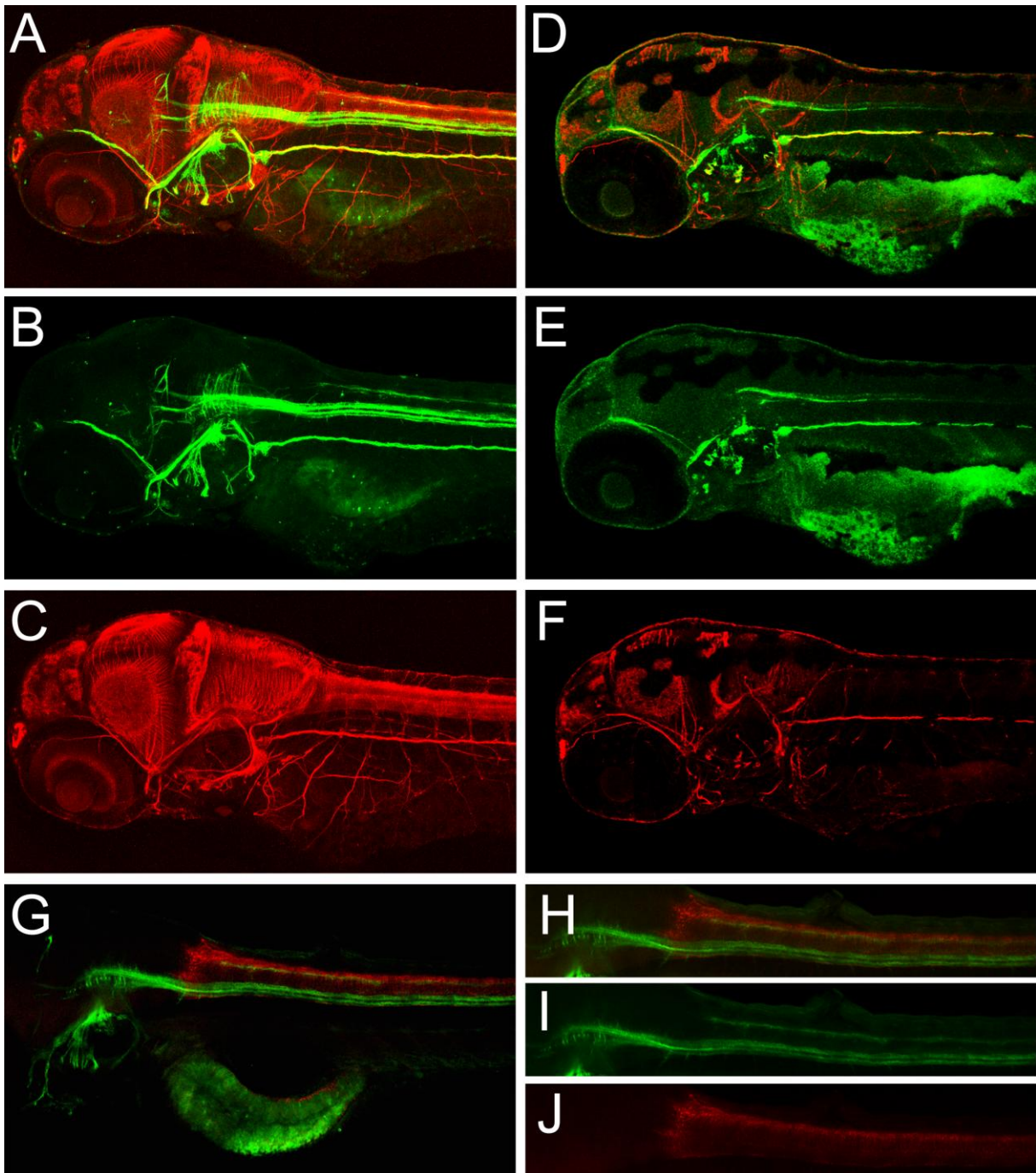
Figure 3.2-10 Claudin k expression pattern in comparison to the myelin marker MBP and the astrocytic marker GFAP.

Whole mount staining of larvae at 5 dpf with α-Claudin k poly confirm specificity of Claudin k as marker for myelinating glia in developing larvae. Claudin k and MBP are a similar expression pattern (A, B), while there is no overlap of the astrocyte marker GFAP with Claudin k staining (C).

3.2.6.1.1 Expression in the adult brain

Expression analysis of Claudin k in the adult brain reveals that Claudin k is expressed strongly in particular fiber-tracts, the commissures and along the Mauthner axons in the posterior hindbrain. It is present in thin projections in the hind- and mid-brain and in distinct layers of the optic tectum.
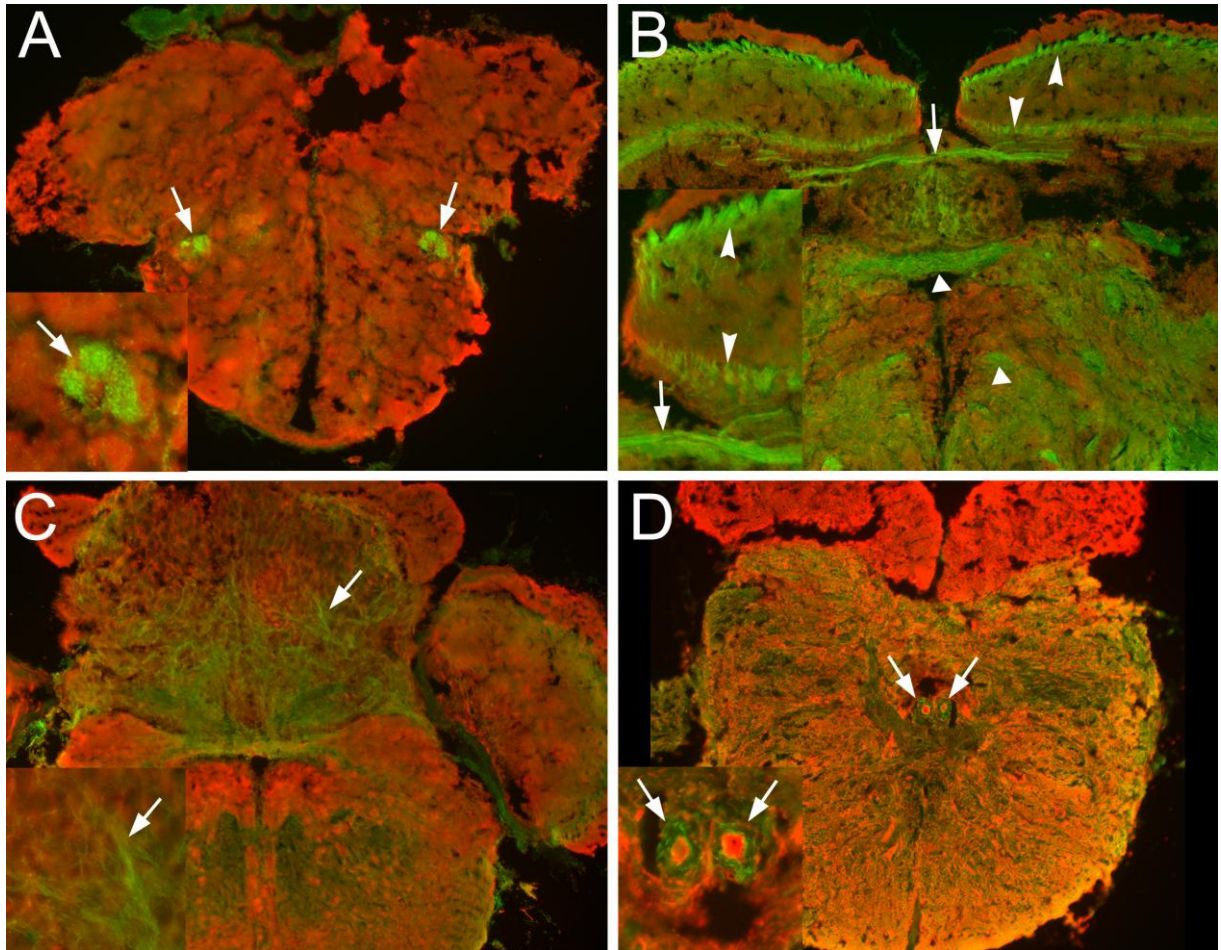
Figure 3.2-11: Claudin k is expressed in distinct areas of the adult brain.

Cross or axial cryosections of adult zebrafish brain showing Claudin k in green and acetylated tubulin in red. In the forebrain (A) there is very little Claudin k staining except for two distinct nerve bundles (inset), likely the lateral olfactory tract. In the optic tectum (B) Claudin k is seen in two distinct layers (inset) and in the commissura tecti (inset). In the midbrain (B, C) it can also be seen in the commissures (commissura horizontalis and posterior). In the cerebellum (D) it is present in thin fibers (inset). Section through crista cerebellaris and brainstem (D) shows no expression in the crista cerebellaris, while expression is strong around Mauthner axons (inset).

Results

3.2.7 CLAUDIN K PROTEIN LOCALIZATION IN CELLS

3.2.7.1.1 Cellular localization

Immunostaining of cryosections of thick peripheral nerves and teased nerves of the spinal cord showed localization around and along axons, likely the inner and outer mesaxon, in spirals in internodes, likely Schmid-Lantermann incisures, and at paranodes, likely the paranodal loops (Figure 3.2-12). The staining pattern is very similar to the observed staining patterns of mammalian Claudin 11 and 19 (Gow, Southwood et al. 1999; Miyamoto, Morita et al. 2005). In a stack of a cross section of a peripheral nerve Claudin k was found around some of the axons, likely corresponding to either paranodal loops or Schmidt-Lantermann incisures. Claudin k staining was observed very close to the axon (Figure 3.2-12, C), indicating that it localizes to the innermost layer of the myelin sheath in some areas. We hypothesize that these structures correspond to autotypic tight junctions. Claudin k also co-localizes with the tight junction marker ZO-1 in peripheral nerves (Figure 3.2-12) further supporting that the observed structures correspond to autotypic tight junctions. Co-staining of Claudin k with MBP and acetylated tubulin show that MBP surrounds the whole neuronal projection and Claudin k positive structures lie within this surrounding layer (Figure 3.2-12).

_____

Figure 3.2-12 Claudin k localizes to autotypic tight junctions in adult myelin.

Claudin k is shown in green and acetylated tubulin as a marker for neuronal processes is shown in red, except for (H). In (A) a single thick peripheral nerve fiber shows Claudin k localizing to inner and outer mesaxon (arrows) and structures similar to Schmid-Lantermann incisures (arrowheads). In B - a cross section of a peripheral nerve - Claudin k completely surrounds some axons, indicating that these fibers were cut at the level of a paranode or Schmidt-Lantermann incisure. In the cross section of the spinal cord (C), Claudin k staining can be seen very close to the Mauthner axon, supposedly at the innermost layer of the myelin sheath. (D) and (E) are two examples of single peripheral nerves, with mesaxons (arrows) and Schmidt-Lantermann incisures (arrowheads) and in (E) also a node (asterisk) with paranodal loops. Along teased single fibers of the spinal cord, Claudin k can also be detected in mesaxons (arrows), Schmidt-Lantermann incisures (arrowheads) and paranodal loops (nodes are indicated with asterisk). A bundle of thin axons accompanied by Claudin k positive structures in the optic tectum (F). Claudin k (red) co-localizes with the tight junction marker ZO-1 (green) in peripheral nerves (G). In (H) the myelin sheath was co-stained with an antibody against MBP (in blue). A-E, G, H: cryosections of adult wt fish: F, I: teased spinal cord of adult wt fish. Scale bars = 10 μm.
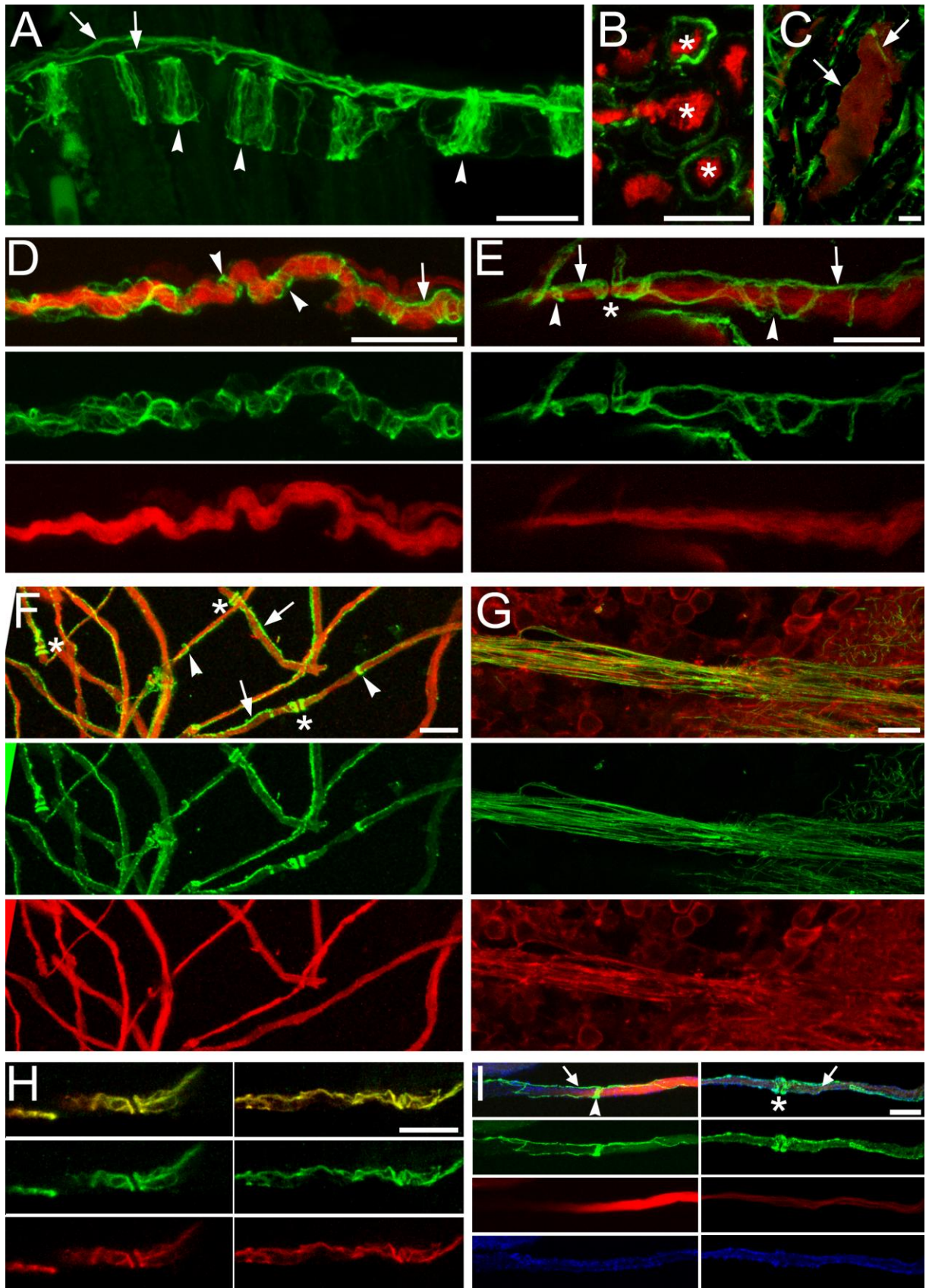
3.2.8 MORPHOLINO KNOCK DOWN

To study the function of Claudin k we designed a translation blocking anti-sense Morpholino oligonucleotide (MO), binding to the translational initiation site of the mRNA (ATG start codon). As a control, we used wt larvae and a control Morpholino, which showed no effects in previous studies. The efficiency of this approach is limited in time, since MO's are injected at the one cell stage and are then diluted and degraded over time. The knock down of Claudin k was very efficient until 5 dpf as we demonstrated by immunostaining (Figure 3.2-13). Knock down and control larvae developed morphologically normally and showed no obvious behavioral phenotype.
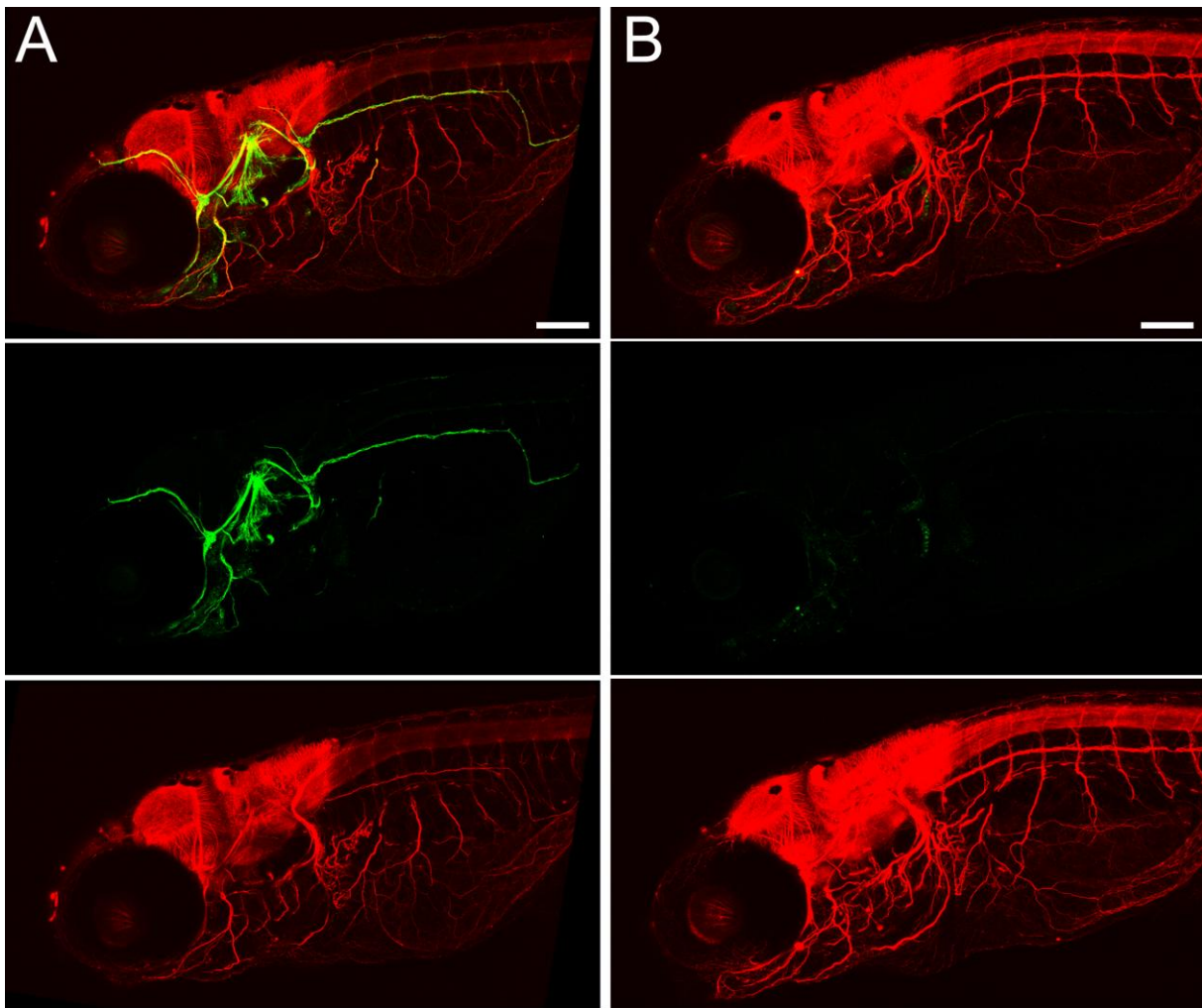
Figure 3.2-13 Knock down of Claudin k is very efficient.

Example of a 5 dpf larvae injected with control (A) and Claudin k Morpholino (B) and stained with Claudin k (in green) and acetylated tubulin (in red). Only very faint staining of Claudin k can be observed in the region of the ear. Scale bars = 100 μm.

To investigate a possible mild behavioral phenotype, we tested the startle response of the larvae in collaboration with M. Granato and R. Jain (University of Pennsylvania). The startle response in zebrafish larvae (Figure 3.2-14) consists of a "C-bend" of the body, followed by a smaller counter bend and swimming (Kimmel, Patterson et al. 1974; Liu and Fetcho 1999). It is mediated by neuronal circuits which are strongly myelinated: transfer of the stimulus from sensory organs (ear and neuromasts) via the acoustic and lateral line nerves to the brain stem, and subsequently transmission of the signal via the reticulo spinal projections to the spinal motorneurons and finally to the trunk muscles. In zebrafish, the startle response requires just three bilateral pairs of reticulospinal neurons, the Mauthner-, MiD2cm- and MiD3cm-cells (Liu and Fetcho 1999). Upon a vibrational stimulus the larvae can react in one of 3 different ways: no response, startle response with short latency C- bend (SLC), and startle response with long latency C-bend (LLC) (Figure 3.2-14). Measurement of the different parameters and kinematics (frequency and latency of C-Bend, maximal curvature of C-bend, direction and distance covered by swimming) with a high speed camera makes for a very sensitive assay.
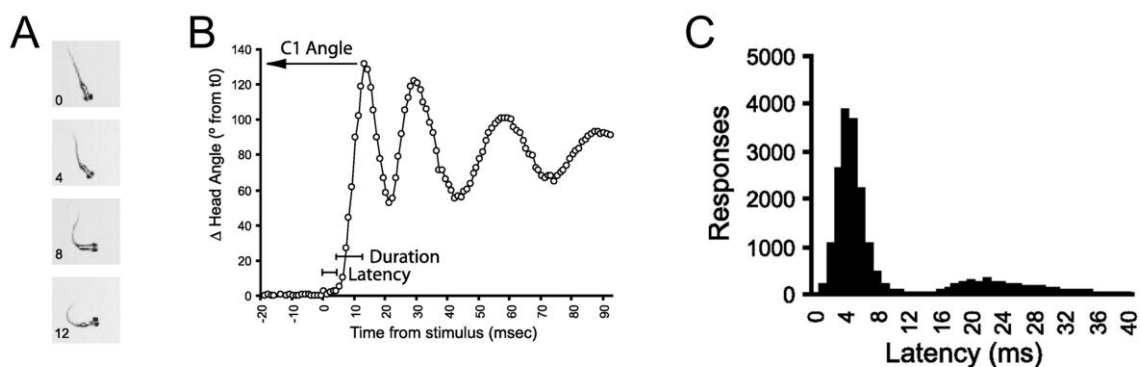
Figure 3.2-14: Measurement of startle response.

A startle response in zebrafish begins with a characteristic C-bend (A) followed by a counter bend and swimming. Latency, duration and C1 angle can be determined by plotting the head angle over time (B). There are two waves of responses which can be distinguished: the short latency and long latency startle responses (C). Diagrams from (Burgess and Granato 2007).

Results

Startle response measurements were performed twice at 5 dpf and once at 6 dpf in response to low and high intensity stimuli. The larvae were fixed and stained for control knock down efficiency and only larvae with good knock down efficiency were taken into account. We could detect no statistically relevant changes in any of the measured parameters. Selected parameters for one experiment are shown in Figure 3.2-15.
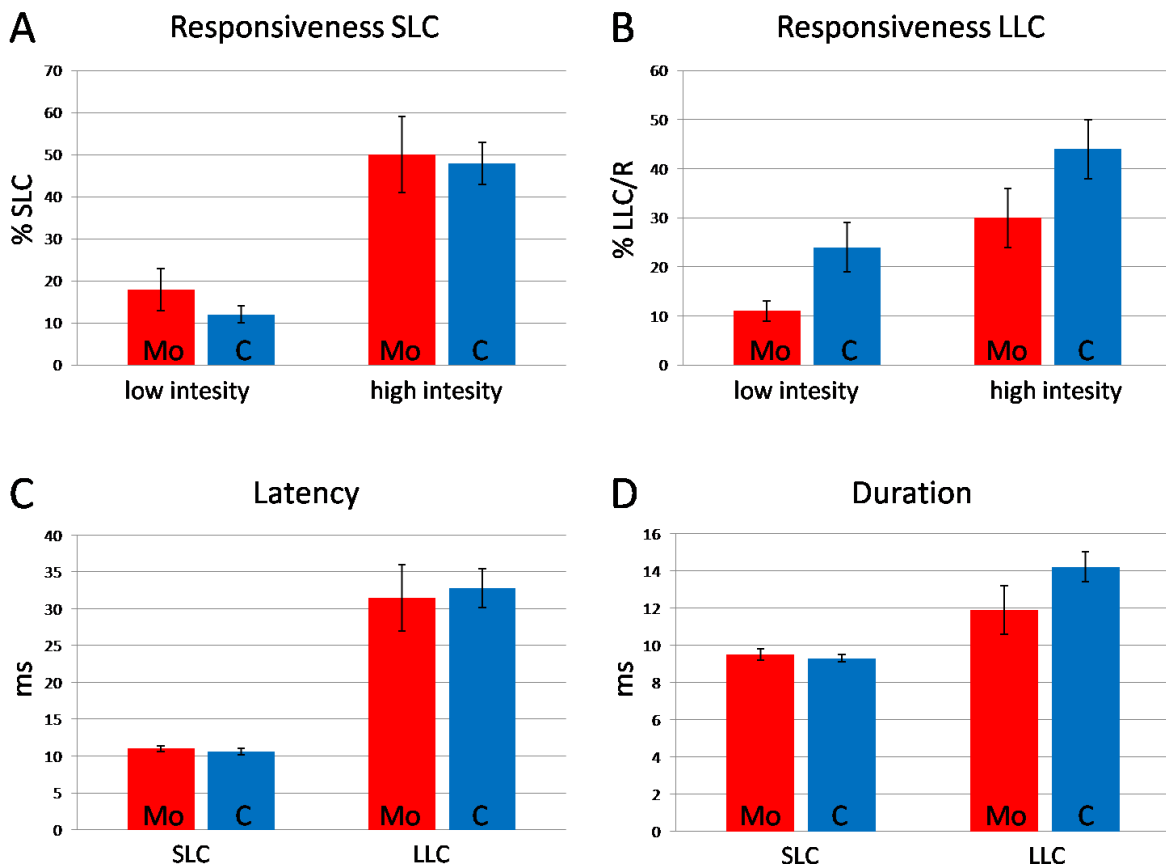
Figure 3.2-15: Claudin k knock down larvae show no impairment in their startle response behavior.

All parameters (A-D) were measured in the same experiment with 13 MO injected larvae with efficient knock down and 26 control injected larvae. Percent of larvae responding to high and low intensity stimuli with a short latency C-bend (SLC) are unchanged (A). In (B) % LLC/R is the frequency of larvae responding with a long latency C-bend (LLC), after excluding all SLC responses, since SLC responses initiate earlier, preempting the possibility of a LLC response. There is a trend towards reduced LLC responsiveness, which is not statistically relevant and did not occur in other experiments. The latency (C) and duration (D) of the SLC and LLC response are also unchanged. In (C) and (D), only the high intensity stimuli data is shown for LLC, since kinematics for LLC (but not for SLC) change depending on stimulus intensity.

3.2.9 OTHER CLAUDINS RELATED TO ZEBRAFISH MYELIN

A possible explanation, why Claudin k Morpholino knock down did not lead to a phenotype, is a potential compensation of Claudin k loss by other Claudins present in zebrafish myelin. Likely candidates are orthologues of Claudins present in mammalian myelin, Claudin 11 and Claudin 19. As described in chapter 3.2.3, teleosts genomes encode three orthologous genes, two for *claudin 11* and one for *claudin 19*. To determine whether these are expressed in myelinating glia in the zebrafish, we performed mRNA *in situ* hybridization of zebrafish embryos and larvae from 1–7 dpf.

3.2.9.1 Zebrafish Claudin 19

Zebrafish *claudin 19* mRNA was first detected at 2 dpf in a few cell populations of the brain unrelated to myelinating glia (Figure 3.2-16). At 3 dpf, expression in the myelinating glia of the oligodendrocytes of the hindbrain and Schwann cells of the PLL nerve was detected, while the expression in the other cell populations was gradually lost. At 4 dpf the typical pattern of myelinating was detected, while expression in oligodendrocytes in the *sox10/cls^{t3}* mutant larvae is strongly reduced and not detectable in Schwann cells.
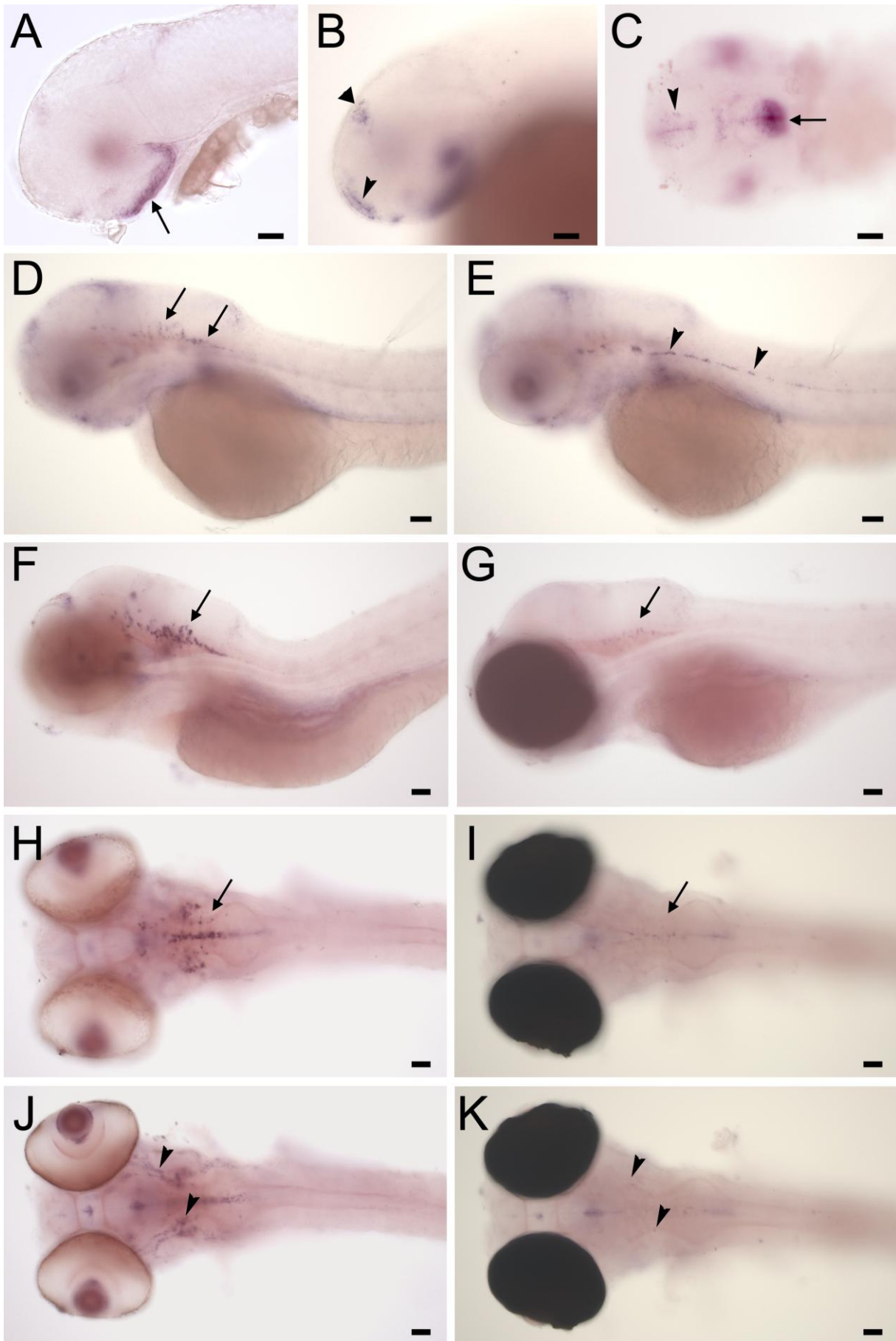
Figure 3.2-16: zebrafish Claudin 19 is expressed in the myelinating glia of the CNS and PNS.

At 2 dpf (A-C) *claudin 19* is expressed in three cell populations, likely in the hypothalamus (arrows) and at the surface of the diencephalon (triangle) and the telencephalon (arrowheads) (A, B lateral views at different focal planes, C ventral view). At 3 and 4 dpf, this expression declines, while expression in the typical pattern of myelinating glia starts. At 3 dpf, expression in oligodendrocytes (arrows) of the hindbrain (D) and Schwann cells (arrowheads) in the PLL nerve (E) is detectable and increases further at 4 dpf, (F, H, J), while expression in *sox10/cls^{t3}* (G, I, K) is strongly reduced at this stage. (D – G) lateral views; (H – K) dorsal views; (H, J) and (I, K), pictures of the same specimen taken at different focal planes. Scale bars = 50 µm.

3.2.9.2 Zebrafish Claudin 11 a and b

The *in situ* staining for *claudin 11* a as well as *11 b* was negative in embryos and larvae of 1-7 dpf. This could be due to undiscovered technical problems, lack of or low expression, or expression only at later stages. Available EST library data suggests that *claudin 11 a* is likely expressed in testis (7 ESTs), like mammalian *claudin 11*, and it might be expressed in the ovary (3 EST's) and possibly in the brain (1 EST) (19 EST's, 3 embryo, 3 adult whole body, 1 olfactory epithelium, 1 kidney), while *claudin 11 b* is likely expressed in embryo myoblasts (5 ESTs) (9 ESTs, 3 embryo, 1 adult whole body). Semiquantitative RT-PCR using adult *Fugu rubripes* tissue indicates significant expression of *claudin 11 a* in brain and heart and of *claudin 11 b* in liver (Loh et. al. 2004).

Results

3.3   *CLAUDIN K* PROMOTER

3.3.1 *CONSERVATION OF CLAUDIN PROMOTER IN TELEOST*

We analyzed the regions upstream and downstream of the first exon of the *claudin k* gene in different teleost for phylogenetic conservation. The alignment depicted in form of a percent identity plot in Figure 3.3-1 revealed that besides the conserved *claudin k* ORF, there are two conserved areas of approximately 200 bp in close proximity to the first exon, one in the 5'untranslated region and the other in the first intron. These conserved areas are not part of any known transposons or other repeats frequently found in fish genomes (data not shown), and therefore likely reflect functional parts of the *claudin k* promoter (Wasserman and Sandelin 2004; Das and Dai 2007). In order to include as many undetected regulatory elements as achievable, we cloned a 4192 bp long region, starting at the end of the next upstream gene until the ORF of *claudin k*.
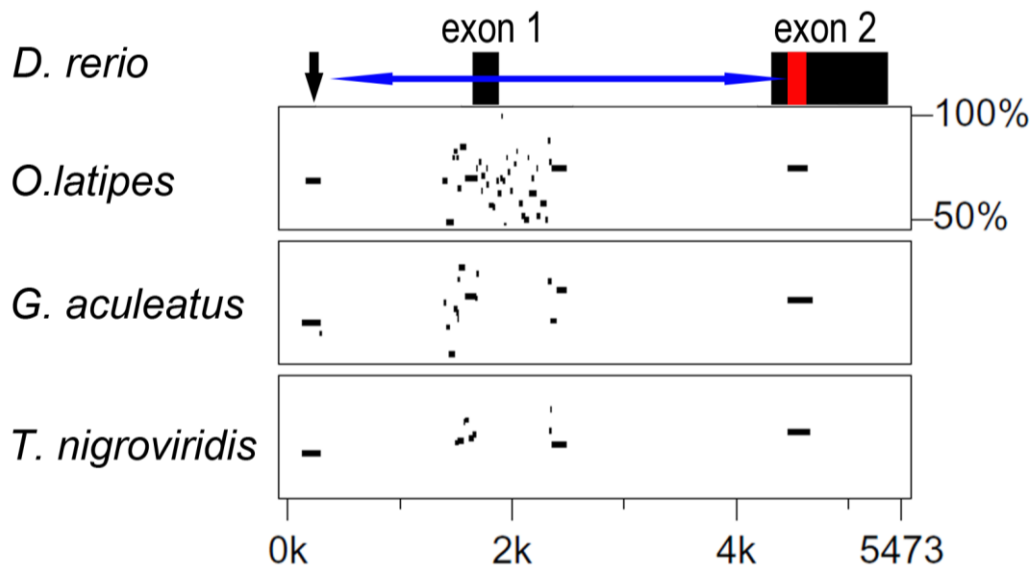
Figure 3.3-1 Conservation of the *claudin k* Promoter.

The percent identity plot, calculated with MultiPipmaker (Schwartz et al., Genome Research 10:577-586, April 2000) covers the region 5' of the *claudin k* gene. It includes the 3' end of the adjacent gene (conserved stretch at ~ 0 kb, indicated by black arrow), the first *claudin k* exon, the intron and the whole second exon. Besides the conserved *claudin k* ORF in exon 2 (indicated in red), there are two strongly conserved regions on either side of the first exon, suggesting conserved *claudin k* promoter sites. A 4192 bp long *claudin k* promoter segment (indicated in blue) was cloned to drive expression in myelinating glia.

60

3.3.2 Tol2 mediated Gal4-UAS expression system

To achieve a versatile and efficient usage of the *claudin k* promoter we decided to utilize of the Gateway compatible Tol2 mediated Gal4-UAS system (Figure 3.3.2) established by Paquet et al. (Paquet, Bhat et al. 2009). There are several advantages to this system: to accomplish efficient transgenesis it makes use of the Tol2 system, in which Tol2 sites flanking the desired transgene, allow the Tol2 transposase enzyme mediated stable integration into the genome at random positions (Kawakami 2005). High transgene expression and separation of promoter and responder construct is achieved via the Gal4-UAS system (Brand and Perrimon 1993; Scheer and Campos-Ortega 1999). The specific promoter drives expression of the Gal4 transcriptional activator, which in turn binds selectively to the UAS (upstream activating sequence) – flanked by E1b minimal promoters – activating expression of the transcript of choice (Koster and Fraser 2001). Because multiple Gal4 proteins can bind to the UAS, mRNA and thus protein expression is enhanced. Both, driver and responder constructs carry so called gateway sites for Gateway cloning, so that promoter and protein coding sequence can be efficiently inserted.
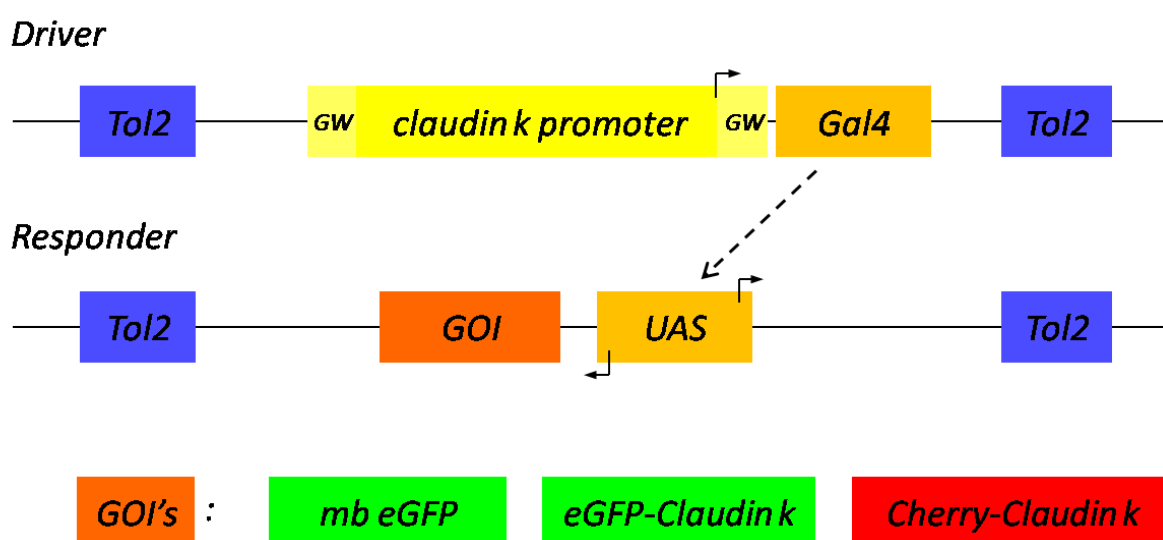
Figure 3.3-2: Tol2 mediated Gal4/UAS expression system.

Separate Driver and Responder constructs are flanked with Tol2 sites for effective trangenesis. The *claudin k* promoter (cloned via gateway sites) drives expression of the Gal4 transcriptional activator, which in turn binds to the UAS, driving the expression of the gene of interest (GOI) . GOIs are cloned via gateway sites and correspond to membrane-bound eGFP (mb eGFP), eGFP-Claudin k fusion construct and Cherry-Claudin k fusion construct.

Results

The generated constructs are depicted in Figure 3.2-1. Driver and responder constructs were injected together into the first cell of the zebrafish egg, giving rise to mosaic expression of the transgene. Injected fish were crossed to wt fish and this first filial generation was then screened for fluorescent larvae, some of which were selected to arise stable transgenic lines.

3.3.3 MB EGFP UNDER THE CONTROL OF CLAUDIN K PROMOTER SPECIFICALLY AND STRONGLY LABELS THE PROCESSES OF MYELINATING GLIA.

We decided to generate a transgenic line with the *claudin k* promoter driving membrane bound eGFP (mb eGFP) to visualize the myelin membrane in particular, herein referred to as *mb egfp*. The mb eGFP consist of a membrane anchor (CAAX box from human Harvey RAS, (Zhang and Casey 1996)) which is fused to the C-terminus of eGFP. The first filial generation (F1, Figure 3.3-3), as well as F2 (data not shown) transgenic fish, showed eGFP fluorescence according to the *Claudin k* mRNA expression profile. In Figure 3.3-3 specific and strong labeling of myelinating glia cell processes in the CNS and in the PNS is documented. Ectopic expression is only observed at in the pectoral fins. The transgenic fish line can be used as a tool to visualize and analyze myelination and remyelination *in vivo*. Furthermore it sets the basis for genetic or chemical screens to identify novel factors important for myelin formation and function.

_____

Figure 3.3-3: mb eGFP under the control of *claudin k* promoter specifically and strongly labels the processes of myelinating glia.

Lateral view of 4 dpf transgenic larvae (A) showing expression in PLL nerve and along eye and ear innervation in the PNS (arrowheads) and expression in the mid and hindbrain and the spinalcord in the CNS (arrows). Ectopic expression was only observed at the tip of the pectoral fin (asterisk). In a magnification of the caudal part of the PLL nerve (B) two myelinated nerve fibers (arrowheads) and nodes (asterisk) can be seen. In the transgenic juvenile fish (2 weeks old, C - E) myelination can still be imaged very well and expression is strong and specific. Lateral view of the head in (C), lateral view of spinal cord with myelinated Mauthner axon (arrow) and motor neurons (arrowheads) in (D). (E) shows most caudal part of the myelinated PLL nerve. Expression is still strong and specific in transgenic adult fish, as seen in myelinated fibers in the caudal fin (F). Scale bars = 100 µm in A, C; 10 µm in B, D - F.
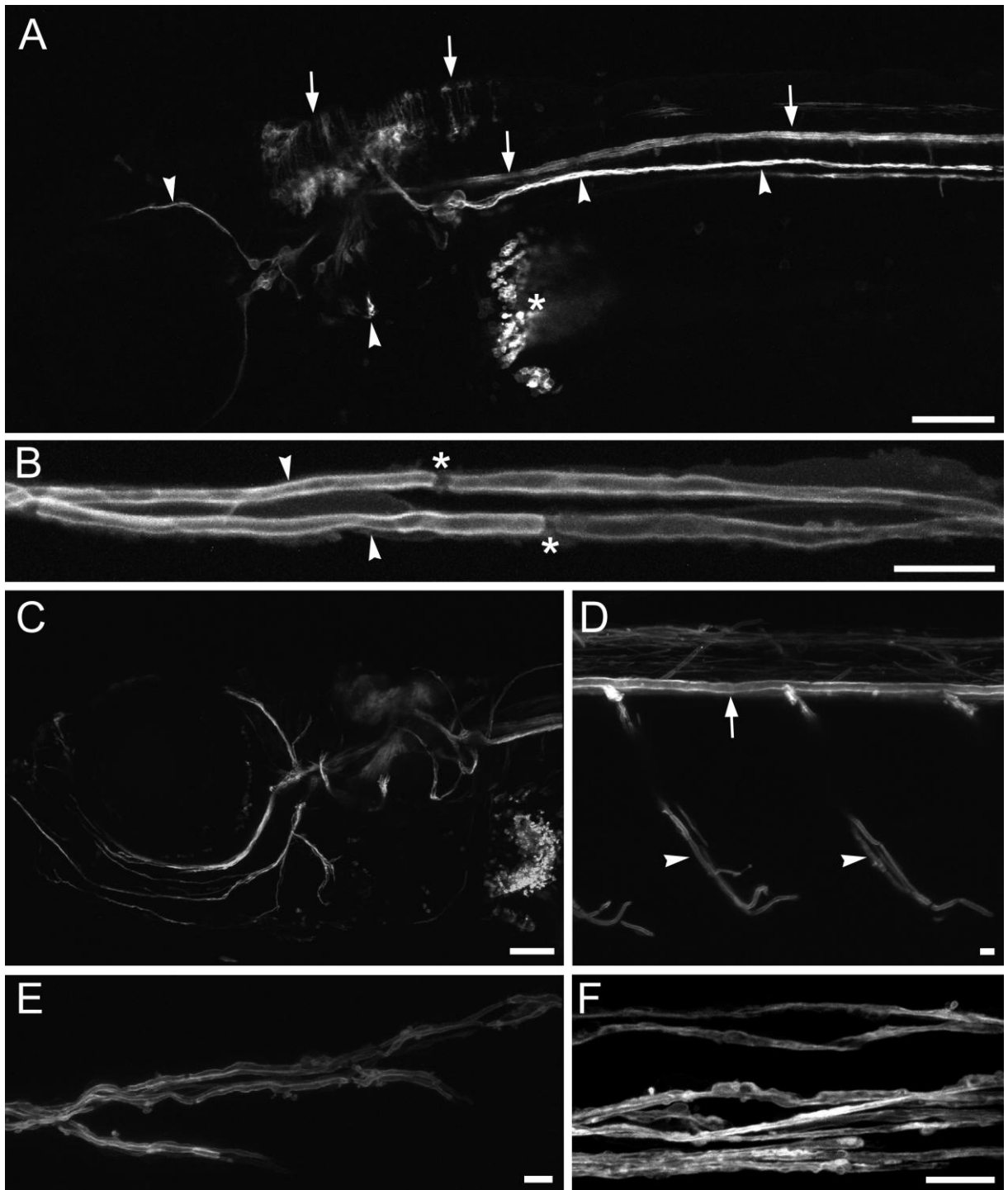
Results

3.3.4 CLAUDIN K PROMOTER DRIVING FLUORESCENTLY TAGGED CLAUDIN K

The identification of the Claudin k protein, localizing to tight junctions of the myelin, and the *claudin k* Promoter gave us the instrument to drive expression of a fluorescently tagged Claudin k to investigate tight junction formation and dynamics in myelinating glia *in vivo*. At its C-terminus Claudin k carries the PDZ binding motive conserved in most family members. The PDZ binding motif of several Claudins was shown to be important for binding to adaptor and scaffolding proteins (see introduction). We therefore fused either eGFP or Cherry to the N-terminus of Claudin k, generating two lines expressing the fusion protein under the Gal4/UAS mediated control of the Claudin k promoter, herein referred to as *egfp-cldnk* and *ch-cldnk.*

3.3.4.1 An eGFP-Claudin k fusion protein specifically labels autotypic tight junctions in myelinating glia

This *egfp-cldnk* transgenic line shows specific expression in myelinating glia and ectopic expression in pectoral fins, very similar to the transgenic *mb egfp* line. Compared with mb GFP fish, fluorescence of eGFP Claudin k fish appears less bright. Live imaging of injected mosaic and stable transgenic larvae clearly shows that eGFP-Claudin k protein localizes to autotypic tight junctions at Schmidt-Lantermann incisures, paranodal loops, and mesaxons of the developing myelin sheath. Specific characteristics of, and differences between, certain cell populations can now be easily observed: While the myelin sheath of the Mauthner axon

_____

Figure 3.3-4 EGFP-Claudin k fusion protein specifically labels autotypic tight junctions in myelinating glia.

Expression pattern of transgenic *egfp-cldnk* at 8 dpf (A) labels myelinating glia very similar to transgenic mb eGFP larvae of Figure 3.3-3. Magnification of the spinal cord (B) shows the myelin sheath of a Mauthner axon, with many Schmidt-Lantermann incisures (arrows), but, in agreement with earlier observations (Yasargil, Greeff et al. 1982; Funch, Wood et al. 1984), without classical nodal structures. The same area of the PLL nerve was imaged in 5 (C) and 6 dpf (D) injected mosaic zebrafish larvae. EGFP-Claudin k labels mesaxons (arrowheads) and paranodal loops (asterisk). The same area of the Mauthner axon was imaged in 5 and 6 dpf injected mosaic zebrafish larvae (E, F). Two examples (G, H) of individual Schwann cells in 11 dpf PLL nerve show Schmidt-Lantermann incisures (arrows) additionally to paranodal loops (asterisk) and mesaxons (arrowhead). Scale bars = 100 μm in A; 10 μm in B - H.
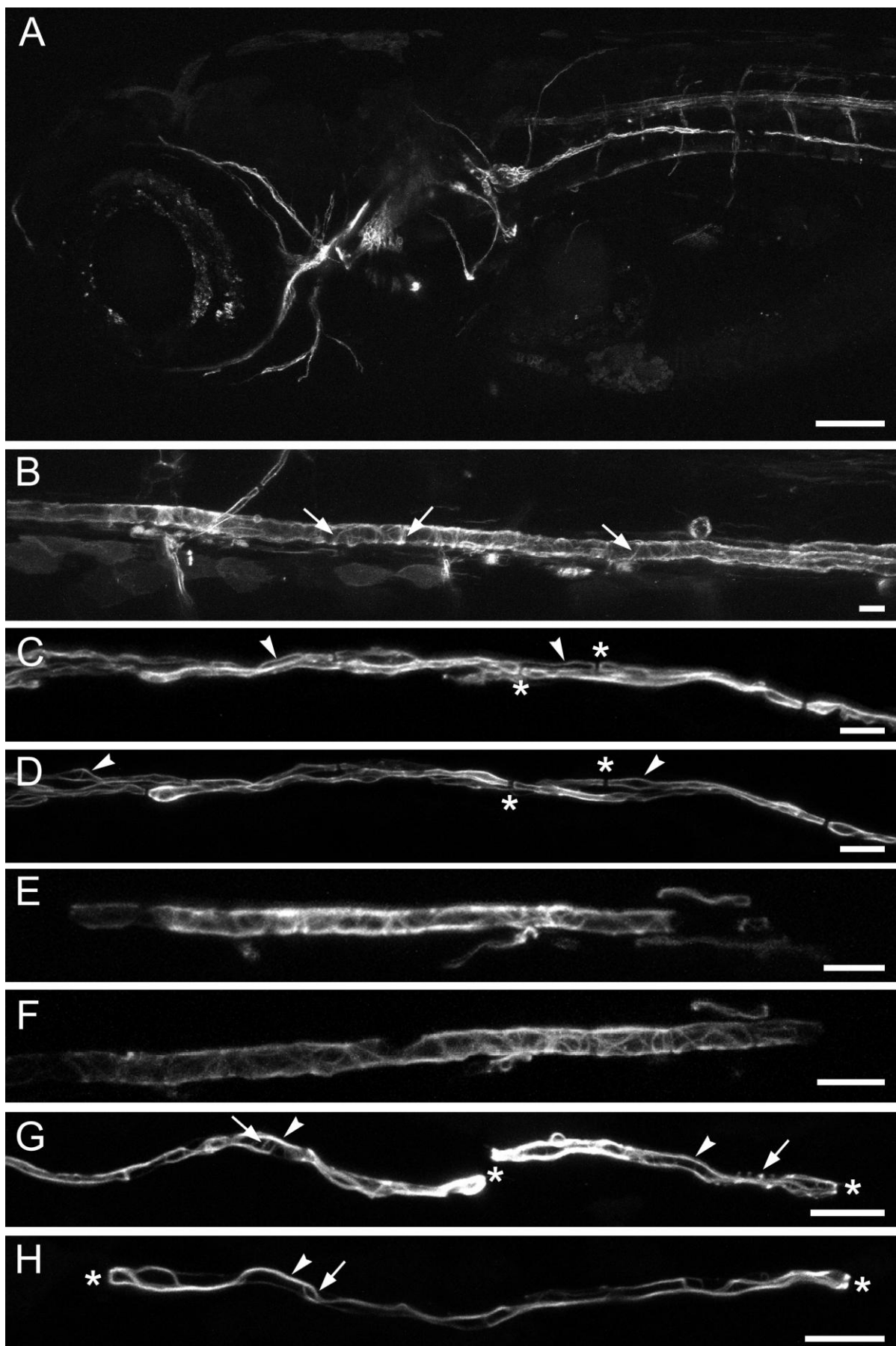
comprises a particularly dense network of Schmidt-Lantermann incisures early on and, in agreement with earlier observations (Yasargil, Greeff et al. 1982; Funch, Wood et al. 1984), no classical nodes, the Schwann cells of the PLL nerve first show mesaxons and nodal structures before Schmidt-Lantermann incisures become evident. Using the transgenics, we can visualize tight junction development also over time. Imaging the same area over multiple time points we can observe how the myelin sheath extends, when and where tight junctions form, and how dynamically these tight junction strands behave. Additionally, screens and experiments modifying or disrupting autotypic tight junctions in myelinating glia might help to understand their function in the physiology of Schwann cells and oligodendrocytes.

3.3.4.2 A Cherry-Claudin k fusion protein aggregates in myelinating glia

Live imaging of the Cherry-Claudin k fusion protein in transgenic larvae shows localization of Claudin k to the Schmid-Lantermann incisures, paranodal loops and mesaxons like eGFP-Claudin k. However, in contrast to eGFP-Claudin k, most of the protein is found in aggregates of varying sizes. This transgenic line could serve as a model for ER stress due to misfolded proteins in myelinating glia. ER stress, including the unfolded protein response, proteasomal degradation and autophagy have been implicated in myelin disorders, such as Pelizaeus-Merzbacher, vanishing white matter and Charcot-Marie-Tooth disease.
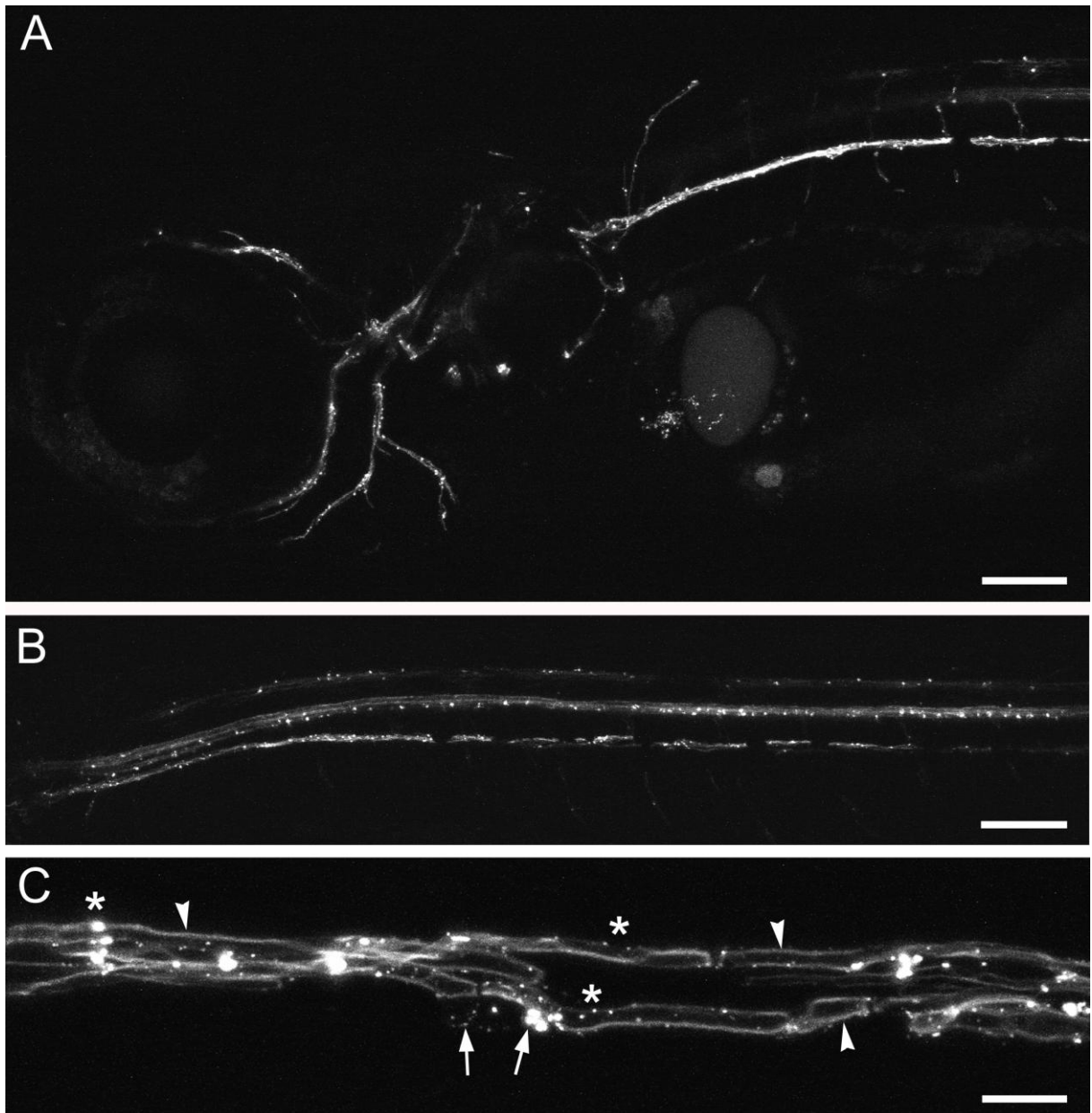
Figure 3.3-5 Cherry-Claudin k fusion protein aggregates in myelinating glia.

Lateral view head (A) and trunk (B) and magnification of PLL nerve of 7 dpf transgenic larvae (C). Cherry-Claudin k localizes partially to autotypic tight junctions (arrowheads) but mainly aggregates in the processes (asterisk) and soma (arrows) of myelinating cells. Scale bars = 100 µm in A, B; 10 µm in C.

.

4 DISCUSSION

Myelin is essential for the fast saltatory conduction of the nerve impulse and gives trophic and metabolic support to the axons it ensheathes (Simons and Trajkovic 2006; Hartline and Colman 2007; Nave and Trapp 2008). In addition, myelinating glia play a complex role in regeneration of the PNS and CNS (Maier and Schwab 2006; Jessen and Mirsky 2008; Martini, Fischer et al. 2008). Myelin related disorders, ranging from Multiple Sclerosis to rare leukodystrophies are poorly understood and no causative treatments are available. A deeper understanding of the mechanisms underlying the physiology of myelinating glia under normal and patho-physiological circumstances is essential to address critical open questions. In a screen preceding this study, two novel myelin specific proteins were identified. The aim of the present work was to analyze and characterize these new factors involved in myelination and to further establish zebrafish as a model organism to study myelination by establishing a specific promoter and fluorescent reporter lines.

4.1 ZWILLING

We identified Zwilling as a novel myelin specific protein exclusively expressed in myelinating Schwann cells and oligodendrocytes of teleosts. The microarray screen data for *zwilling* matched a cluster of EST's that were not homologues to any annotated or predicted gene. We therefore reconstructed the full length DNA and found a gene of peculiar structure: a structurally bicistronic transcript with two short ORFs, *zwilling A* and *B,* coding for two highly similar, small proteins. In the mass spectronomical analysis of a biochemical myelin membrane preparation we found evidence that both proteins are present, posing the question if the *zwilling* transcript is also functionally bicistronic. Polycistronic transcripts are common for prokaryotes and viral transcripts, but whether true functional bicistronic transcripts exists in higher eukaryotes is still under debate (Kozak 2005). Using a percent identity plot we showed, that the region 5' of the *zwilling B* ORF is phylogenetically conserved (Figure 3.1-7), indicating a potential internal ribosomal entry side, cryptic promoter or so far undetected alternative splice site (Kozak 2005; Autio, Kastaniotis et al. 2008).

The gene coding for Zwilling A and B likely originated from a common ancestor by a tandem duplication event of a small DNA segment and is present in this form in all other teleost studied. In contrast to genes of similar arrangement, such as zebrafish *wnt8* (Lekven, Thorpe et al. 2001; Ramel, Buckles et al. 2004) and Drosophila *adh/adh*r (Brogna and Ashburner 1997), we could not find a monocistronic form in other species, suggesting that *zwilling* appeared as an insertion already in its duplicated form. The occurrence of the *zwilling* gene in only one of the teleost orthologues of *RUNDC3A* and the presence of *zwilling* in species of the *Ostariophysi* (*D. rerio, P. promelas*), *Proacanthopterygii* (*S. salar, O. mykiss*), and *Acanthopterygii* (*F. rubripes, O. latipes,* and others) clades, suggests an insertional event after the genome duplication at the base of the teleost radiation (Amores, Force et al. 1998; Prince, Joly et al. 1998; Hurley, Mueller et al. 2007), but still early on in the teleost lineage. The origin of this ancestral *zwilling* gene though remains elusive.

Zwilling A and B bear no detectable homology to any known proteins and we could not identify any previously described conserved domains or motives. Nevertheless, Zwilling proteins resemble MBP in terms of their developmental expression profile and physicochemical properties, perhaps suggesting a similar function. MBP is able to adopt multiple conformations (Hill, Bates et al. 2002; Boggs 2006) and is believed to glue the cytoplasmic membrane leaflets together by binding electrostatically to negatively charged phospholipids (Mueller, Butt et al. 1999). MBP is very basic and intrinsically unstructured, similar to the Zwilling proteins (Figure 4.1-1). MBP is modified N-terminally by acylation, which contributes to membrane association, and by several protein kinases, features which are also predicted for Zwilling A and B. The Zwilling proteins might therefore contribute to and modify myelin membrane adhesion in teleosts, possibly also modulating MBP function in a direct or indirect way. Specific phosphorylation at phylogenetically conserved sites might thereby regulate zwilling membrane adhesion and protein interactions important for its physiological function. Membrane fluidity and the interactions of lipids and membrane-associated proteins are temperature dependent and effect myelin membrane adhesion and therefore proper myelin function (Hu, Doudevski et al. 2004). These additional Zwilling functions might be required, because teleost poikilothermy poses extra demands especially on a membrane as complex as the myelin sheath.

Discussion
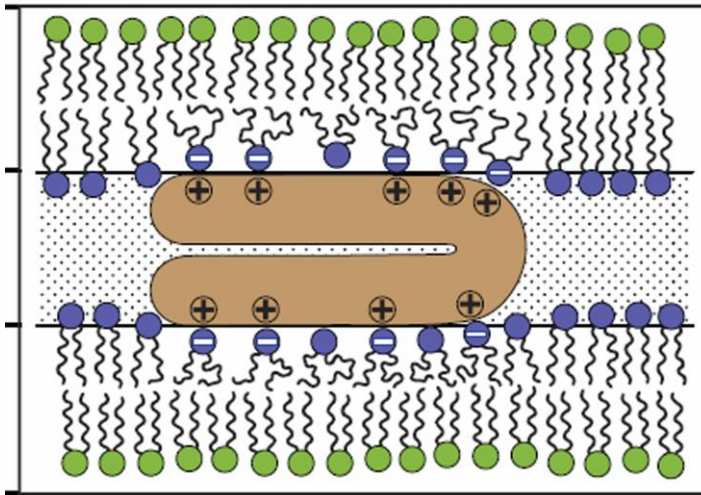
Figure 4.1-1 MBP and possibly Zwilling bind to negatively charged lipids.

Zwilling, like MBP is a flexible and positively charged protein (brown), and could play a role in myelin membrane adhesion by tightly binding to negatively charged lipids. Diagram from (Min, Kristiansen et al. 2009).

However, the role of Zwilling in teleost myelin remains unclear and further experiments to support or disprove these hypotheses are required. Unfortunately, our extensive efforts to raise antibodies against the Zwilling proteins were unsuccessful. One of the reasons may be the shortness and intrinsically unstructured nature of the Zwilling proteins leading to reduced antigenicity and a lack of stable epitopes. A common approach to track and analyze proteins, if there is no antibody available, is to overexpress a tagged version of the protein. Tagging or overexpression however, can cause misleading modifications of the protein, resulting in mislocalization, aggregation and lack of functionality. This applies especially for such small proteins as Zwilling A and B. To analyze a possible Zwilling loss-of-function phenotype, we designed and injected two Morpholino antisense nucleotides blocking the transcriptional start side of Zwilling A and B, but larvae co-injected with either or both did not show any obvious morphological or behavioral phenotype (data not shown). However, the efficiency of the knockdown could not be evaluated due to the lack of an antibody. Alternative Morpholinos, which modify pre-mRNA splicing and therefore allow efficiency to be monitored by RT-PCR, require the ORF to be contained in two or more exons. They can therefore not be used for the zwilling transcript, with both ORFs situated in the first of two exons. A *zwilling* loss-of-function-mutant could

70

circumvent these problems, but unfortunately directed generation of mutants has so far proven difficult in zebrafish. A collaborative effort by the Zebrafish TILLING Consortium to generate mutants by 'Targeting Induced Local Lesions IN Genomes' (TILLING) was started some years ago and is still ongoing (Moens, Donn et al. 2008). *Zwilling* was entered as a candidate gene, but a mutant has not been identified so far. An exceptionally exciting new approach is directed mutagenesis using zinc finger nucleases (Doyon, McCammon et al. 2008; Meng, Noyes et al. 2008; Foley, Yeh et al. 2009). In the future this might not only allow generation of specific mutants, but also the generation of 'knock-ins', which label endogenous proteins, at a reasonable time and price scale.

4.2   CLAUDIN K

The second transcript identified in the screen was Claudin k, coding for a novel myelin specific protein exclusively expressed in myelinating Schwann cells and oligodendrocytes of teleosts. Claudins are tetraspan transmembrane proteins and are generally known as components of tight junctions. In epithelial cells they form a tight barrier between adjacent cells, restricting the paracellular flux and an intramembrane barrier, restricting diffusion from the apical to the basolateral side, thus playing an important role in cell polarity. Tight junction-like structures have been observed in CNS and PNS myelin (Mugnaini and Schnapp 1974; Sandri, Van Buren et al. 1977; Tetzlaff 1978; Shinowara, Beutel et al. 1980; Gow, Southwood et al. 1999; Miyamoto, Morita et al. 2005), but whether these structures can really be regarded as a variant of classical tight junction, both structurally and functionally, is unclear due to the absence of – or lack of information on – distinctive tight junction specific cell adhesion molecules. However, in mammalian myelin, as in other tissues, the presence of tight junctions is dependent on certain tissue specific claudins. Knockout mice lacking Claudin 11 in the CNS or Claudin 19 in the PNS, also lack tight junction-like structures in their respective myelin sheaths (Gow, Southwood et al. 1999; Miyamoto, Morita et al. 2005). Apart from that, the development, ultra-structure and maintenance of the myelin sheath and nodes in these knockout mice seem to be unchanged. Both types of knockout mice show electrophysiological deficits in nerve conduction in the affected systems, indicating a Claudin function in electrical sealing of the myelin sheath. For Claudin 11 it was shown in detail, that the

effect is especially strong on medium and small diameter axons. This included an up to 60% decrease in conduction velocity, increased action potential thresholds, and an increase in potassium channel activity. These results are in accordance with the results obtained from a new computational model of nerve impulse propagation that incorporates tight junction resistance. A role of Claudin 11 in electrical sealing is further supported by the fact, that Claudin 11 containing tight junctions in the cochlea also form an electrically tight barrier (Gow, Davies et al. 2004; Kitajiri, Miyamoto et al. 2004).

In addition to these experimentally validated roles of Claudins in myelin, hypothetical functions of tight junction and claudins in myelin exist. They include the sequestering of antigens from immune surveillance (Mugnaini and Schnapp 1974), the coupling of adjacent lamella for increased mechanical strength (Tabira, Cullen et al. 1978), a role in polarized morphogenesis of myelinating glia or the compartmentalization of the myelin sheath, such as occluding the extracellular space from the compact myelin or restricting certain proteins to the adaxonal membrane. Since Claudins belong to the PMP22/Claudin superfamily, they might also serve an alternative function similar to PMP22 in the PNS, which is part of the compact myelin. However, no Claudin, which localizes to the compact myelin has been described so far.

Claudins are a large family with at least 24 members in mammals and more than twice as many in teleost. This is the result of tandem duplications in addition to the genome duplication at the base of the teleost radiation (Amores, Force et al. 1998; Prince, Joly et al. 1998; Hurley, Mueller et al. 2007). How many of the teleost Claudin family members are actually expressed and functional at protein level remains to be seen. Tissues that regulate ion electrolyte balance (gills, skin, kidney, and intestine) possibly facilitated the evolution of specialized Claudins not found in mammals. Furthermore, teleosts are poikilothermic organisms and their tissues need to adapt to varying temperatures. Membrane fluidity, protein-protein interactions and specifically also tight junction dynamics are temperature dependant (Angelow, Kim et al. 2006). In line with these considerations we show that zebrafish - in addition to Claudin k - express an orthologue of mammalian Claudin 19 in the myelinating glia of the PNS and CNS and there is evidence that also Claudin 11 is encoded in the teleost genome. The mammalian Claudin 11 has two co-orthologues - Claudin 11 a and b - in zebrafish and all other teleost with available genomic data. Expression of both

Claudin 11 a and b in zebrafish at least at an mRNA level, is supported by the existence of numerous EST's, with two Claudin 11 a EST's originating from brain specific libraries (ensemble genome browser, data not shown). Additionally RT-PCR data in *fugu* (Loh, Christoffels et al. 2004) reveal expression of Claudin 11 a especially in the brain, while Claudin b is only detected in the liver. Furthermore, Mack and Wolburg (Mack and Wolburg 2006) show Claudin 11 immunoreactivity in the myelin of the optic nerve of *Astatotilapia burtoni* using an antibody against mouse Claudin 11 (the antibody is not available). Taken together, this strongly suggests that Claudin 11 is expressed in the teleost brain, likely the Claudin 11 a orthologue.

Hence teleost express at least two, and likely three, myelin specific Claudins. This is in contrast to mammals, where so far only one CNS and one PNS specific claudin is known. This fits to the observation that tight junction-like structures seem more frequent in EM studies in teleost myelin then in mammalian myelin (Shinowara, Beutel et al. 1980). Additionally, teleost poikilothermy poses extra demands especially on the myelin membrane, as discussed above for Zwilling. The notion of a specific requirement and function rather than simple redundancy is also supported by the fact that no Claudin k orthologue exists in any other class analyzed, while Claudin k synteny and sequence is highly conserved (78% – 92% identity) among teleosts. Claudin k is strongly expressed in zebrafish CNS and PNS and localizes to the mesaxons, Schmidt-Lantermann incisures and paranodal loops, similarly to Claudin 11 and Claudin 19 in the mammalian CNS and PNS respectively (Figure 4.2-1). Claudin k co-localized with ZO-1 in the PNS, but we could not find evidence for co-localization of Claudin k with ZO-1 in the CNS (data not shown). This agrees with the observation that ZO-1 is present in mammalian tight junctions in the PNS, but not in the CNS (Gow, Southwood et al. 1999; Poliak, Matlis et al. 2002). These results led us to conclude that the Claudin k positive structures correspond to tight junctions. Since no antibodies recognizing zebrafish Claudin 19 or 11 are available, we are currently unable to determine, where in the myelin sheath they are localized.

Discussion
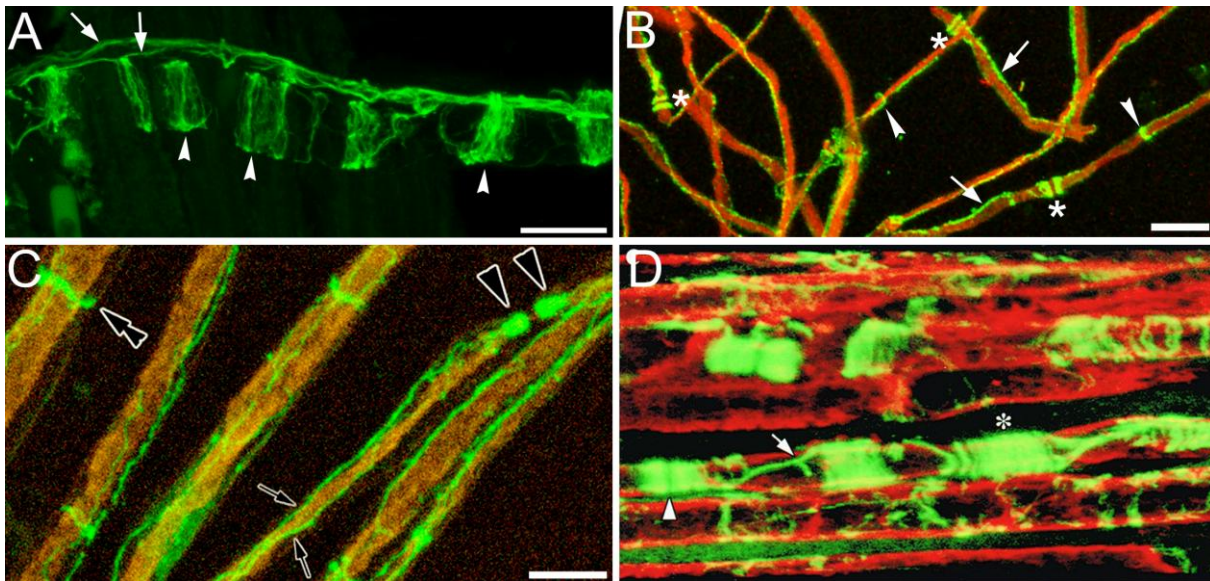
Figure 4.2-1: Localization of myelin specific Claudins.

Antibodies against Claudin k in the zebrafish PNS (A) and CNS (B), and for comparison mouse Claudin 19 in the PNS (C, (Miyamoto, Morita et al. 2005)) and Claudin 11 in the monkey CNS (D, (Gow, Southwood et al. 1999)) show similar localization to mesaxons (A-C arrows, in D arrow marks mesaxon with bifurcating channel), Schmidt-Lantermann incisures (A and B, arrowhead; C, double arrowheads; D, asterisk) and nodes with paranodal loops (B, asterisk marks node; C, arrowheads mark paranodal loops; D, arrowhead marks node). Scale bars = 10 µm in A, B; 5 µm in C.

To investigate the function of Claudin k, we designed an antisense Morpholino nucleotide, which blocks translation and injected it into zebrafish eggs. We evaluated knock down efficiency in larvae, using whole mount immunofluorescence staining for Claudin k and acetylated tubulin - marking neuronal processes as a reference. The knock down was very efficient until 5 dpf and decreased thereafter, but no obvious morphological or behavioral defects could be observed. To investigate possible mild effects – such as reduced conduction velocities or higher activation thresholds – we decided to perform startle response measurements in collaboration with R. Jain and M. Granato (University of Pennsylvania, Philadelphia, USA). The startle response relies on heavily myelinated neuronal circuits and measurements can pick up even weak specific defects. No measured parameters though, showed significant changes in knock down larvae compared to control injected larvae. This could be due to the presence of other Claudins, especially Claudin 11 and 19, which may fully or partially compensate for Claudin k. In addition, myelin is just being formed at this stage of development, with first loose membranes detected around axons at 4 dpf and first

74

compact myelin at 7 dpf (Brösamle and Halpern 2002). Later analysis of the startle response however, is in conflict with decreasing knock down efficiencies after 5 dpf.

The first problem could be addressed by double or even triple knock-downs of the corresponding Claudins. It should be taken into consideration though, that the risk of unspecific toxic effects rises with the number of injected Morpholinos. In addition, maximum efficiency and duration of Morpholinos is achieved by injecting an amount just below an unspecific toxic threshold. To stay under the toxic threshold, concentration of each individual Morpholino must be reduced, while injecting multiple Morpholinos. A Morpholino intended to affect pre-mRNA slicing of Claudin 19 was designed. The usage of a slice Morpholino was preferred over a translation blocking Morpholino, since knock down efficiency of a splice Morpholino can be examined using real-time PCR, while knock down efficiency of a splice Morpholino can only be examined using an antibody. The Morpholino was injected singly and together with the Claudin k Morpholino, both showing no obvious morphological or behavioral defects (data not shown). In the future, knock down efficiency – via real-time PCR monitoring Claudin 19 pre-mRNA slicing - should be evaluated and depending on the results further experiments could be carried out. Recently a Claudin k zebrafish mutant carrying a T to A point mutation became available (Zebrafish TILLING consortium). This mutation results in a Stop codon at aa position 166, deleting the fourth transmembrane domain and the whole C-terminus, which carries the PDZ-binding domain. The mutation potentially leads to protein instability and degradation and non-functionality. The mutant needs to be analyzed in detail for Claudin k protein presence and functionality, as well as phenotype and morphology. It might serve to investigate the function of Claudin k also in later stages of development and it could potentially be used to circumvent multiple Morpholino injections. So far tight junction strands in the myelin sheath have been observed in EM in adult electric eel, rainbow trout, goldfish and knifefish (Sandri, Van Buren et al. 1977; Bertaud 1978; Shinowara, Beutel et al. 1980). EM techniques to examine tight junctions in the myelin sheath of zebrafish larvae are currently being investigated. This approach would allow an investigation whether and how tight junctions are altered or lost in mutant or knockdown larvae.

In this study we have identified a novel myelin-specific protein, Claudin k, which is highly conserved in teleosts and localizes to autotypic tight junctions. We have also

shown that teleost, in contrast to mammals, express several myelin specific claudins. Myelinating glia are unique in terms of cell morphogenesis, cell-cell adhesion and cell motility. Therefore future studies will likely yield interesting results regarding the function of Claudins in the myelin sheath in general and with specific respect to teleosts. This will deepen our understanding of the molecular architecture and function of the myelin sheath and thus the mechanisms underlying saltatory conduction.

Taken together the identification of Claudin k and Zwilling via the microarray screen using mRNA of a myelin deficient zebrafish mutant, validate this approach as a method to identify novel myelin compounds. Further screens using alternative approaches possibly involving the established transgenic lines will likely reveal additional myelin specific transcripts giving interesting insight into myelin assembly, structure and function. Interestingly both identified proteins are teleost specific, though orthologues in lower vertebrates might be identified once substantial genomic data is available. A reason why teleost might have more myelin specific proteins, may perhaps be connected to their poikilothermy. It is intriguing to speculate about what molecular mechanisms other poikilothermic myelinating vertebrates such as cartilaginous and lobe-finned fishes, amphibia, and reptiles may have evolved to adjust to varying temperatures. With the sequencing of the genomes of more and more vertebrates of all classes, comparative evolutionary analyses may yield insights into these pathways.

4.3   *CLAUDIN K* PROMOTER

To examine changes in cellular processes, including the orientation of cell divisions, cell shape, polarity, differentiation and migration, zebrafish are especially well suited as model organism (Beis and Stainier 2006; Lieschke and Currie 2007). It provides ready access to all developmental stages, and the optical clarity of embryos and larvae allow real-time imaging of developing tissues and pathologies. Additionally straightforward techniques for the generation of transgenic lines are now available (Kawakami 2005; Foley, Yeh et al. 2009; Paquet, Bhat et al. 2009) and large scale mutagenesis screens with sophisticated read outs are possible at low costs

(Rubinstein 2003; Lieschke and Currie 2007). The zebrafish animal model therefore is very useful to address open question in the field of myelinating glia. In order to optimally utilize these advantages, tissue specific promoters are required. The identification of the *claudin k* gene and with it a phylogentically conserved *claudin k* promoter set the base for exciting new studies and transgenic lines.

Several transgenic fish lines with promoters driving expression in myelinating glia in zebrafish have been already generated and used to study differentiation, development and dynamic behavior of oligodendrocytes (Kirby, Takada et al. 2006). Most of these lines have substantial drawbacks, regarding promoter size and flexibility of use, expression in other tissues or neuronal populations and downregulation in mature oligodendrocytes. Promoters driving expression in mature Schwann cells are especially rare. So far only two lines using transcription factor promoters driving expression also in neural crest – *sox 10* and *zFoxD3* – and the *Tg(mbp:egfp)* line exist (Gilmour, Maischein et al. 2002; Wada, Javidan et al. 2005; Dutton, Antonellis et al. 2008). The *Tg(mbp:egfp)* line is the only line with evaluated expression in oligodendrocytes and Schwann cells in adult fish, although it shows expression only in a subset of Schwann cells, likely because the promoter construct is lacking important regulatory elements. The Claudin k promoter described in this study is particularly valuable, because it drives strong and specific expression in both Oligodendrocytes and Schwann cells and this expression is maintained through all stages. Moreover, the promoter with its 4200 bp is relatively compact and therefore easy to subclone into any destination vector. Additionally, it was used to generate a Gal4 driver line, allowing flexible and easy generation of combination with different UAS reporter constructs and lines, as we have shown for mb eGFP, eGFP-Claudin k and Cherry- Claudin k.

Mb eGFP under the control of the Claudin promoter, labels processes of myelinating glia and eGFP-Claudin k specifically labels tight junctions in myelinating glia. These transgenic lines open numerous possibilities: they can be utilized for *in vivo* analysis of myelination and remyelination in general and specifically with respect to the formation and dynamics of tight junctions. The *mb egfp* line has already been transferred to a collaborating group exploring regeneration in adult zebrafish, who will use them to specifically investigate aspects of myelin regeneration. These lines can also be exploited to mark myelin degeneration in other disease models, for example

Discussion

in an Alzheimer disease model introduced by Paquet et al., 2009. The *mb gfp* and *egfp-cldnk* lines can also serve as a source for large scale genetic or chemical screens to identify novel factors important for myelin formation and function and can even be used for very specific screens to identify factors involved in tight junction formation and maintenance.

The promoter itself can now be readily used for an even broader range of approaches. It will be interesting to overexpress tagged and untagged myelin related genes, such as Zwilling and other myelin genes of unknown function, to elucidate their role *in vivo*. On the other hand it can also be used for rescue experiments, and the promoter construct has already been contributed to experiments rescuing the Morpholino knockdown of a transcription factor involved in oligodendrocytes differentiation. In addition, Schwann cells and myelinating glia can be specifically ablated using toxins, like diphtheria toxin. A system to ablate astrocytes, using a driver construct with an inducible ubiquitous heat shock promoter driving Cre-recombinase, and a responder construct with a floxed stop codon and of diphtheria toxin under the control of an astrocyte specific promoter, has already been established by Stahl et al. in zebrafish in our laboratory (unpublished) and could be readily adapted to ablate myelinating glia.

Due to the excellent suitability of zebrafish to identify underlying mechanisms of disease and the possibility to perform large scale drug screens at moderate costs, the generation of zebrafish disease models is a very promising and rapidly developing field (review: (Ingham 2009)). Even though the Claudin k gene as well as any other Claudin, have not been connected to human myelin related diseases, their similarity to PMP22 make them interesting candidates. Mutations in the PMP22 gene leading to duplication, cause the most common form of Charcot Marie Tooth Type 1 disease (OMIM 118220) (Berger, Niemann et al. 2006), while a deletion leads to hereditary neuropathy with predisposition to pressure palsy (HNNP, OMIM 162500), an episodic, recurrent demyelinating neuropathy. Tight regulation of protein levels in general has been found to be important for many myelin proteins to sustain proper myelin function (Patel and Lupski 1994; Adlkofer, Martini et al. 1995; Karim, Barrie et al. 2007). Recently a range of myelinating diseases have been connected to ER stress, caused by accumulation and misfolding of various proteins (D'Antonio, Feltri et al. 2009; Lin and Popko 2009). The underlying reasoning is, that myelinating glia

78

are particularly susceptible to disturbances in protein load and processing, because they produce and maintain enormous amounts of membrane, pushing the involved cellular machinery already to its limits. Along these lines, it is not surprising that the *cherry-cldnk* line - in contrast to the *egfp-cldnk* line - displays aggregation of the fluorescently tagged Claudin k. This may be due to either higher expression levels or a higher tendency of Cherry-Claudin k to aggregate compared to eGFP-Claudin k. So far the state of the myelin sheath, Schwann cells and oligodendrocytes, has not been analyzed in detail in this transgenic line. In future experiments monitoring myelin maintenance and markers of ER stress might reveal characteristic features of demyelinating diseases. Moreover, the generation of a transgenic line overexpressing PMP22 is another promising step toward establishing a disease model for Charcot-Marie-Tooth disease. Further potential disease models involve the overexpression of native or mutant forms of MPZ for Charcot-Marie-Tooth Type 1B disease (OMIM 118200), PLP for Pelizaeus-Merzbacher disease (OMIM 312080) and α-synuclein for Multiple-System-Atrophy (OMIM 146500) – a disease in which α-synuclein positive inclusion bodies are found in oligodendrocytes (Wenning, Stefanova et al. 2008; Nakayama, Suzuki et al. 2009)

While most of the applications discussed for the promoter and transgenic lines are still to be established, they already point out the enormous potential of the *claudin k* promoter for the future examination of myelinating glia in health and disease.

5 METHODS

5.1 SEQUENCE DATA ANALYSIS

5.1.1 DATABASE SEARCHES

Protein BLAST and PSI-BLAST searches were conducted at NCBI (http://blast.ncbi.nlm.nih.gov/Blast.cgi) to identify homologous sequences.

5.1.2 MOTIVE SEARCHES

InterPro database (http://www.ebi.ac.uk/Tools/InterProScan/, European Bioinformatics Institute) was searched for conserved domains and patterns. Secondary structure prediction was carried out using the Chou-Fasman, GOR4, and PELE (which includes 7 different algorithms) prediction methods implemented on the Biology WorkBench web server (http://workbench.sdsc.edu/). Myristoylation site prediction was performed on the MYR Prediction Server (mendel.imp.ac.at/myristate; Research Institute of Molecular Pathology, Vienna) and on the Prosite database webserver (http://www.expasy.ch/prosite, Swiss Institute of Bioinformatics). Prosite was also used to detect phylogenetically conserved putative phosphorylation sites.

5.1.3 ALIGNMENTS

Protein alignments were generated using ClustalW of the PHYLIP phylogeny inference software package (Department of Genetics, University of Washington, Seattle).

5.1.4 CONSTRUCTION OF PHYLOGENETIC TREES

Phylogenetic trees constructed by DRAWTREE software, of the PHYLIP phylogeny inference software package (Department of Genetics, University of Washington, Seattle).

5.1.5 SYNTENY

Genomic sequences around the *zwilling* and *claudin k* locus were obtained from the Sanger Centre's Ensembl website and used to assess conserved synteny.

5.1.6 PERCENT IDENTITY PLOT

Genomic sequences around the *zwilling* and *claudin k* locus were obtained from the Sanger Centre's Ensembl website and used to generate percent-identity plots using MultiPIPMaker software (Penn State University Center for Comparative Genomics and Bioinformatics, http://bio.cse.psu.edu/pipmaker).

5.1.7 KS/KA VALUE

Ka/Ks values were computed with the Ka/Ks Calculation Tool of the Bergen Center for Computational Science (http://services.cbu.uib.no/tools/kaks).

5.2 MOLECULARBIOLOGAL METHODS

5.2.1 5'-RACE

5'-RACE was performed using the RLM-RACE Kit (Ambion, Foster City, CA) following instructions for 5'RLM-RACE using the standard reaction for total RNA. Total RNA was extracted from brain through phenol chloroform extraction: freshly dissected adult brain was homogenized in 1 ml Trizol per 50-100 mg tissue and incubated at room temperature (RT) for 5 min. 0,1 ml chloroform was added, gently mixed for 15 sec and incubated for 3 min at RT. Sample was centrifuged at 11.000 g for 15 min at 4 °C and aqueous phase was recovered to fresh tube. 0,5 ml isopropyl alcohol was added and incubated for 10 min at 4 °C. Supernatant was removed; the pellet washed with 1ml 75% ethanol and air dried for 10 min at RT. Pellet was dissolved in nuclease free water from the RLM-RACE Kit by incubating at 55 °C in a water bath for 10 min. Total RNA concentration was measured as described and RNA sample was stored at -80 °C.

PCR program:

temperature	time	cycles
94°C	3 min	1 x
94°C	30 sec	35 x
50°C	30 sec	

72°C	1 min	
72°C	7 min	1 x
10°C	∞	

Primers used: 5'RACE Outer Primer and Zwi-102Ro or 5'RACE Inner Primer and Zwi-102-Ri. Primer used for positive control reactions: Zwi-102Ro and Zwi-102Lc or Zwi-102-Ri and Zwi-102Lc.

10 ul PCR reaction was used for analysis with agarose gel electrophoresis and 4 µl fresh PCR reaction was used for Topo-cloning into pCR®-II-TOPO vector using TOPO® TA Cloning Kit (Invitrogen, Karlsruhe) according to manufacturer's instructions. Positive clones were analyzed via analyzing transformants by PCR as described.

5.2.2 RT-PCR

RT-PCR was performed using the Retroscript Kit (Ambion, Foster City, CA) using one step RT-PCR without heat denaturation and total RNA extracted as described for 5'RACE.

PCR program:

temperature	time	cycles
42°C	15 min	1 x
95°C	1 min	1 x
95°C	30 sec	
50°C	30 sec	40 x
68°C	2 min	
68°C	10 min	1 x
10°C	∞	

Primers used: Zwi-100L and Zwi-100R or Zwi-101L and Zwi-101R

10 µl PCR reaction was used for analysis with agarose gel electrophoresis and 4 µl fresh PCR reaction was used for Topo cloning into pCR®-II-TOPO vector using TOPO® TA Cloning Kit according to manufacturer's instructions. Positive clones were analyzed via analyzing transformants by PCR as described.

5.2.3 CLAUDIN K PROMOTER
1 µl of HUKGB735617285Q BAC preparation, prepared as described, 15 µl PCR mix, 2 ul primer mix (stock: 2 µM) and 0,5 µl Taq-polymerase were mixed on ice and PCR reaction was immediately started.

PCR program:

temperature	time	cycles
94°C	1 min	1 x
94°C	30 sec	
63°C	30 sec	28 x
72°C	2 min	

add 0,5 µl fresh Taq-polymerase

temperature	time	cycles
94°C	30 sec	
63°C	30 sec	28 x
72°C	2 min	
72°C	10 min	1 x

Primers used: Cldnk-prom-fw-bstB1 and Cldnk-prom-rev-bstB1

Methods

10 ul PCR reaction was used for analysis with agarose gel electrophoresis. 4 µl fresh PCR reaction was used for Topo cloning into pCR®8/GW vector using pCR®8/GW/TOPO® TA Cloning Kit according to manufacturer's instructions. Primer Cldnk-prom-fw and Cldnk-prom-rev carry a BSTB1 restriction site, so that the promoter can be excised from the pCR®8/GW vector via restriction enzyme digest. Positive clones were analyzed via analyzing transformants by PCR as described. The promoter was cloned into the pT2d-Dest_GW-R1-R2_Gal4VP16_pA vector by gateway cloning as described below, to yield the pT2d-EXP_Claudink _Gal4VP16_pA vector.

5.2.4 FLUORESCENTLY TAGGED CLAUDIN K

The PCR to obtain fluorescently tagged Claudin k was designed in two steps. The first PCR resulted in an amplification of the coding sequence of the fluorescent protein and Claudin k, introducing an overlap between the two. These products were mixed as template for the second PCR, which produced the full-length Cherry-Claudin k or eGFP-Claudin k fusion protein.

First PCR step:

The PCR was carried out on the cherry (pCS cherry dest) or egfp (pCSeGFP dest) template, using a forward primer introducing a Kozak sequence. The reverse primer introduced an overlap with the Claudin k coding sequence. The PCR on the Claudin k template (BI 980908) introduced an according overlap with the fluorescent protein via the forward primer.

1-2 µl plasmid (according to 200 ng), prepared as described, 45 µl PCR mix, 5 µl primer mix (stock: 2 µM) and 1 µl Taq-polymerase were mixed on ice and PCR reaction was immediately started.

PCR program 1:

temperature	time	cycles
94°C	1 min	1 x
94°C	30 sec	30 x

temperature	time	cycles
40°C	30 sec	
72°C	40 sec	
72°C	7 min	1 x
10°C	∞	

Primers used: 140-fluoro-fw and 147-fluoro-cldnk-rev on pCS cherry dest and pCSeGFP dest; 146-fluoro-cldnk-fw und 145-cldnk-rev on Claudin k template.

Second PCR step:

For preparation of template for the second PCR step, agarose gel electrophoresis was carried out and appropriate bands were isolated as described. Each 0,5 µl PCR product from step one, 15 µl PCR mix, 2 µl primer mix (stock: 2 µM) and 0,5 µl Taq-polymerase were mixed on ice and PCR reaction was immediately started.

PCR program 2:

temperature	time	cycles
94°C	1 min	1 x
94°C	30 sec	
49°C	30 sec	30 x
72°C	1 min	
72°C	7 min	1 x
10°C	∞	

Primers used: 140-fluoro-fw and 145-cldnk-rev

10 ul PCR reaction was used for analysis with agarose gel electrophoresis. 4 µl fresh PCR reaction was used for Topo cloning into pCR®8/GW vector using pCR®8/GW/TOPO® TA Cloning Kit according to manufacturer's instructions.

Positive clones were analyzed via analyzing transformants by PCR as described. The fusion protein was cloned into the pT2d-Dest_UAS_E1b_GW-R1-R2_pA vector by gateway cloning as described below to yield the pT2d-EXP_UAS_E1b_cherry-cldnk_pA and pT2d-EXP_UAS_E1b_egfp-cldnk_pA *responder* vectors.

5.2.5 AGAROSE GEL ELECTROPHORESIS

To separate DNA fragments and PCR products for analytical and preparative purposes, 1-2% (w/v) agarose gels in 1x TBE buffer and 0,2 µg/ml ethidium bromide were used depending on the expected size of the fragment. Fermentas FastRuler DNA size marker was used to define the size of the fragment. 6x loading dye was added to the DNA samples, and gels were run at 80-180 V for 15-45 min. Gels were evaluated with an Intas Geldokumetation system. DNA fragments were cut out with a clean scalpel under reduced UV intensity of the agarose gel on a UV screen and purified with the Nucleo Spin Extract II kit (Macherey-Nagel) according to the manufacturer's instructions.

5.2.6 RESTRICTION DIGESTS

Analytical digests contained 0,2-1 µg DNA and 1-5 U restriction enzyme. Respective reaction buffers and temperatures according for single or multiple enzyme digests were chosen according to the manufacturer's instructions and incubated either overnight or for 1 h at 37°. DNA fragments were purified as described above.

5.2.7 GATEWAY CLONING

Gateway Technology is a commercial cloning system offered by Invitrogen (Karlsruhe). It uses recombination of particular recombination sites mediated by the enzyme clonase instead of standard restriction digests and ligations. The sequences cloned into pCR®8/GW vector were recombined into the according destination vectors by the LR-recombination reaction, according to manufacturer's instructions.

5.2.8 TRANSFORMATION OF COMPETENT E.COLI

Competent Top10 cells were thawed on ice, mixed gently with DNA and incubated for 30 min on ice. After a heat shock in a water bath of 42°C for 90 sec, cells were incubated on ice for 5 min. 800 µl LB was added and bacteria were incubated for 30 min at 37°C with shaking. The mixture was shortly centrifuged, the pellet resuspended in 100-200 µl of LB and then plated on LB agar plates containing the respective antibiotics to select positive clones. LB agar plates were incubated at 37°C over night; single clones were analyzed as described below.

5.2.9 ANALYZING TRANSFORMANTS BY PCR

20-40 colonies were picked and resuspended in 20 µl of LB medium. 5 µl were transferred as template for the PCR reaction and mixed with 15 µl PCR mix, 2 µl M13 forward and reverse primer mix (stock: 2 µM) and 0,5 µl Taq-polymerase. Positive clones were identified by agarose gel electrophoresis. To further verify selected positive clones, an analytical digests was performed and analyzed by agarose gel electrophoresis. Positive clones were amplified using original colony suspension to inoculate LB-medium containing respective antibiotics as described below.

5.2.10 AMPLIFICATION AND PREPARATION OF PLASMIDS

Single clones were used to inoculate LB-medium containing respective antibiotics for small, medium and large scale DNA preparation (Mini, Midi and Maxi Macherey-Nagel), which was performed according to the manufacturer's instructions.

5.2.11 AMPLIFICATION AND PREPARATION OF BAC

Single clones were used to inoculate 20 ml LB-medium containing respective antibiotics over night. 40 ml culture was centrifuged and pellets were subjected to standard alkaline cell lysis with 1ml Buffer A1, A2 and A3 from the NucleoSpin Plasmid Kit (Macherey Nagel). Lysate was centrifuged at 11,000 g for 6 min. Supernatant was recovered and double the volume of ethanol was added. After 10 min at 11.000 g the occurring pellet was washed with 70% ice-cold ethanol and air dried. Pellet was dissolved in 50 µl water using a large bore pipette.

Methods

5.2.12 *MEASURING DNA AND RNA ABSORBANCE*

RNA and DNA amounts and purity were determined by measuring absorbance at 260/280 nm in a NanoPhotometer[TM] (IMPLEN, Munich).

5.2.13 *SEQUENCING*

All cDNA constructs were confirmed by sequencing by GATC Biotech AG (Konstanz, Germany).

5.3 FISH HUSBANDRY AND CARE TAKING

Zebrafish were maintained under standard conditions (Mullins, Hammerschmidt et al. 1994; Westerfield 1994) at 28.5°C. Embryos and larvae were obtained from natural matings, raised in E3 medium at 28.5°C and staged by days post-fertilization (dpf). Albino and *clst*[3] were used for *in situ* hybridization. For whole mount antibody staining larvae of the Albino strain were used.

5.4 ZEBRAFISH EGG MICROINJECTIONS

Zebrafish eggs were injected on agar-plates (1,6% in E3) with glass-capillaries using standard methods (Holley, Julich et al. 2002).

5.4.1 *ANTISENSE MORPHOLINO OLIGONUCLEOTIDE INJECTIONS*

Antisense Morpholino (MO) oligonucleotides were designed to the *claudin k* and *zwilling A* and *B* translation start site and the *claudin 19* exon 3 slice acceptoraccording to manufacturer's instructions (Gene Tools, LLC, Philomat). As control MO we used a Morpholino showing no effects in previous studies (Brösamle and Halpern 2009). All Morpholinos were resuspended in Danieau and 0.5-1.5 nl of 1 mM MO were injected into the yolk of one- to two-cell stage embryos. For startle response measurements 1.2 nl of 1 mM Claudin k ATG MO were injected.

5.4.2 INJECTIONS FOR ESTABLISHING TRANSGENIC LINES

Injection mixture was prepared shortly before injection and consisted of *Driver-* and *Responder-*vector and *Tol2-*mRNA at 25 ng/µl resolved in DEPC treated dH$_2$O containing 20 % DEPC treated phenol-red and 0.2 M KCL (Kawakami 2005). Collected zebrafish eggs were oriented on the agar-plate and injected into the first cell with ~1 nl injection solution.

5.5 STARTLE RESPONSE MEASUREMENT

Startle response measurements were done as described by (Burgess and Granato 2007) using a 1000 Hz horizontal vibrational stimulus of 3 ms/2 ms ramp up and down 0.5 ms duration and maximum acceleration of 18m/s2 (low stimuli) or 150ms (high stimuli). Each set of larvae was tested with a series of 60 stimuli - 30 high and 30 low - pseudo randomly alternating with a 15 sec interval. Each larva was scored individually, subjected to immunohistochemistry and the knockdown scored by intensity of Claudin k staining compared to acetylated tubulin. Two experiments were carried out at 5 dpf and one at 6 dpf.

5.6 IN SITU HYBRIDIZATION

Digoxigenin-labelled RNA probes were synthesized following the manufacturer's instructions (Roche Molecular Biochemicals). Probes against Claudin k, Claudin 19, and Zwilling were generated either directly from ESTs or after subcloning of the insert into pBluescript II.

RNA *in situ* hybridization was carried out as previously described (Thisse, Thisse et al. 1993). Briefly, larvae were fixed overnight in 4% paraformaldehyde (PFA) in phosphate buffered saline pH7.5 (PBS) and stored in methanol at -20 °C. After rehydration in PBS + 0.1% Tween (PBT), larvae were permeabilized by proteinase K treatment (10 µg/ml, 20 min. for larvae up to 4 days, 30 min. for older larvae), postfixed in 4% PFA and washed extensively followed by incubation in hybridization mix for 3 hrs. at 70°C. Probe hybridization was carried out overnight at 70 °C and unbound probe removed in a series of washes. Larvae were blocked for 1 hour in Pi

buffer (PBT containing 2% sheep serum and 0.2% BSA) and incubated over night at 4°C with pre-adsorbed anti-digoxigenin Fab fragments coupled to alkaline phosphatase (Roche Molecular Biochemicals). After extensive washes in PBT and AP buffer, developing solution was added to detect hybridized probe in a color reaction using nitrotetrazolium blue and bromo-chloro-indolyl phosphate as substrates. The reaction was stopped by several washes with PBT and larvae were transferred to glycerol and photographed using the Zeiss Axioplan 2 imaging compound microscope.

5.7   IMMUNOHISTOCHEMISTRY

5.7.1 GENERAL IMMUNOCYTOCHEMISTRY ANTIBODY STAINING PROCEDURE

Specimens were blocked for 1 h in 2% normal goat serum / 2% BSA in PBS, followed by incubation with the appropriate primary antibody at 4°C overnight. Specimens were washed extensively in PBT, followed by 3 h incubation in secondary antibody.

5.7.2 CRYO SECTIONS

Adult fish were killed by immersion in ice cold water (4°C). Whole adult fish heads with open neurocranium were fixed in 4% PFA overnight at 4°C and washed in PBS. Brains with adjacent tissue were dissected and transferred to 30% sucrose in PBS overnight at 4°C. Tissue was embedded in Cryo-embedding compound frozen at -20°C and cut into 18µm slices on a cryostat (Thermo Scientific, Microm HM 560). Sections were collected on glass slides and air dried for 20 min. After the staining procedure they were mounted on cover slips with Mowiol.

5.7.3 WHOLE MOUNTS

Embryos were fixed using either of the two following procedures:

in 4% PFA overnight at 4 °C, washed 3 × 5 min in PBT and transferred to methanol for storage at -20°C. After retransfer to PBT they were digested with trypsin (1%

trypsin, 1mM EDTA in PBT) for 30-40 min at 37°C, washed and digested with 5% hyaluronidase in PBT for 30-60 min at 37°C and washed in PBT.

Embryos were fixed in 2% trichloroacetic acid / 2% PFA in PBS for 10 min at room temperature, washed 3 × 5 min in PBT and transferred to methanol for storage at -20°C. After retransfer to PBT they were washed subsequently 5 min in dH_2O, 7 min in Acetone at -20°C, 5 min in dH_2O and 3 x 5 min in PBT.

After the staining procedure they were mounted in 90% glycerol in PBS on cover slips.

5.7.4 TEASED SPINAL CORD FIBERS
Adult fish were killed by immersion in ice cold water (4°C). Adult spinal cord was exposed to 4% PFA overnight at 4°C, washed in PBS, dissected and teased with fine forceps. After the staining procedure they were mounted on cover slips with Mowiol.

5.7.5 MICROSCOPY AND IMAGING
Images were taken with an LSM 510 META inverted confocal microscope using the overlay function of the Zeiss LSM software with maximum projections of z-stacks. Images comparing 2 groups of fish were done at the same time using identical settings.

5.8   MYELIN MEMBRANE PREPARATION
For biochemical analysis, zebrafish myelin membranes were prepared according to established protocols (Morris, Willard et al. 2004). 16 freshly dissected brains were homogenized in 0,5 ml of 0,9 M sucrose in 10mM HEPES, layered under 0,25 M sucrose and spun 3 h at 60,000 g. The interface containing crude myelin was collected and homogenized in 200 µl 10 mM HEPES and spun 15 min at 60000 g. The resulting pellet was homogenized in 10 mM HEPES and repelleted for 20 min at 30000 g. The pellet was homogenized in 200 µl 0,9 M sucrose in 10mM HEPES, layered under 0,24 sucrose and spun for 1 h at 60000g. The interface was homogenized in 200 µl 10 mM HEPES, spun for 20 min 60000 g. The pellet was

dissolved and diluted in HEPES and 6x SDS-sample was added. 5 µg protein was loaded on a precast 10-20% Tris-Glycin acylamid gradient gel (Novex®, Invitrogen) and run with Tris-Gycine SDS-PAGE running buffer. Gel was stained with Coomassie Brilliant Blue R-250 staining solution.

5.9   MASS SPECTROMETRY

Prominent bands and the area including proteins of approximately 5-15 kD were cut out from SDS-PAGE gel, stained with Coomassie Brilliant Blue R-250 staining solution. Tryptic peptides with masses corresponding to Zwilling-A and -B as well as other myelin protein sequences were were identified in cut-outs through MALDI-PMF; for Zwilling A these peptides were confirmed by LC-MS/MS at the SFB596 mass spectrometry facility.

5.10   PROTEIN ANALYSIS

5.10.1   *LYSIS OF EMBRYOS AND BRAIN*
For Western blot membrane preparations of larvae and brain were used. 100 larvae at 5 dpf or 2 adult brains were lysed in 1 ml ice-cold lysis buffer with protease inhibitor (Pi) mix (1:500). They were incubated 10 min on ice, centrifuged at 6000r pm for 5 min and the supernatant transferred to fresh tube. This step was repeated. Supernatant was spun 1 h at 13000 rpm. The pellet resulting from brain tissue was dissolved in 30 µl 6x SDS, then diluted 1:10 with 1x SDS. For larvae the pellet was dissolved in 50 µl 6x SDS. Just before loading probes were heated at 65°C for 5 min and spun 5 min at 6000 rpm. 5 µl of brain or 20 µl of larval membrane preparation was loaded.

5.10.2   *IMMUNOPRECIPITATION (IP)*
For IP whole brain lysate was used. 1 adult brain was homogenized in 400 µl RIPA. A probe of 40 µl was taken, designated 'lysis'. 30 µl protein A sepharose (PAS) beads were added and incubated over night at 4°C. PAS beads were separated from

the supernatant by spinning at 1000 g for 5 min at 4°C and kept as probe designated 'beads'. 3 µl α-Claudin poly and 30 µl PAS beads were added to the supernantant, incubated for 2 h at 4 °C and spun at 1000 rpm for 5 min at 4°C. PAS beads were subsequently washed with 1 ml STEN NaCl-, STEN SDS-, and STEN-buffer. 15 µl 2 x SDS was added to the PAS beads, designated as 'IP'. To the remaining 'supernatant' 100 µl 6x SDS were added. To the probe 'lysis' 10 µl 6x SDS was added and to the probe 'beads' 15 µl 2x SDS was added. Probes were heated to 65°C for 5 min and 18 µl 'lysis', 18 µl 'supernatant', 10 µl 'beads' and 10 µl 'IP' was loaded.

5.10.3 *WESTERN BLOT*

Proteins were analyzed by sodium dodecylsulphate polyacrylamide gel electrophoresis (SDS-PAGE) and Western blotting using a polyvinylidenfluorid (PVDF) membrane (Millipore). The PVDF-membranes were blocked with blocking solution containing 5% non-fat dry milk in TBS containing 0,1%Tween-20 (TBS-T) for 1 h at room temperature and then incubated with the primary antibody in blocking solution for 16 h at 4°C. After extensive washing with TBS-T, the membranes were incubated with HRP-conjugated secondary antibody. Following washing with TBS-T, the antigen was detected with the enhanced chemoluminescence (ECL) detection system (Amersham Biosciences). HRP-conjugated epitope antibodies were incubated for 16 h at 4°C, washed extensively and detected with the ECL system.

6 MATERIAL

6.1 ZEBRAFISH LINES

Wild type zebrafish (Danio rerio) of the Oregon AB strain (Fritz et al., 1996), albino zebrafish alb$^{b4/b4}$ (Chakrabarti, Streisinger et al. 1983) and *cls^{t3}/sox10* mutant stain were used. The clst^3 allele results from a transposon insertion into the second exon of the sox10 gene leading to a truncated protein, that lacks both the DNA-binding and the transactivation domain (Dutton, Pauliny et al. 2001). It is therefore assumed to be a functional null mutation.

6.2 PLASMIDS AND BACS

AW281753	RZPD distribution center (Berlin, Germany)
BC 093218	RZPD distribution center (Berlin, Germany)
BI980908	RZPD distribution center (Berlin, Germany)
pBluescript II	Stratagene
pT2d-Dest_GW-R1-R2_Gal4VP16_pA	Dominik Paquet (Paquet, Bhat et al. 2009)
HUKGB735617285Q	RZPD distribution center (Berlin, Germany)
PCS Cherry dest	Nathan Lawson
pCSeGFP dest	Nathan Lawson
pCRII-TOPO	Invitrogen

pCR8-GW-TOPO   Invitrogen

pT2d-Dest_UAS_E1b_GW-R1-   Dominik Paquet (unpublished)
R2_pA

Responder vector mb eGFP   Barbara Obirei (unpublished)

6.3 PRIMERS

All Primers were ordered from Metabion, Martinsried. Lyophilized primers were diluted in double-destilled water and stored as a 100 mM stock solution at -20°C. 2 µM primer mix (of each primer) was prepared using double-destilled water from the according stock solution.

140-fluoro-fw	GCCACCATGGTGAGCAAGGG
145-cldnk-rev	TTAAACATAACCCTTGACCTGGGAA
146-fluoro-cldnk-fw	CGGCATGGACGAGCTGTACAAGATGGCAACCACTGGCATGCAGCTCC
147-fluoro-cldnk-rev	GGAGCTGCATGCCAGTGGTTGCCATCTTGTACAGCTCGTCCATGCCG
Cldnk-prom-fw-bstB1	TCTTCGAATCTGAACAATCTGCTGCCACTACAGCTTTCACT
Cldnk-prom-rev-bstB1	TATTCGAAAGTGAATCTTTCCCAAGAATGATCACTTGGATGAGTCCAATGGAGAGCACAGACAGAACC
5' RACE Outer Primer	GCTGATGGCGATGAATGAACACTG
5 'RACE Inner Primer	CGCGGATCCGAACACTGCGTTTGCTGGCTTTGATG

Material

M13 Forward	GTAAAACGACGGCCAG
M13 Reverse	CAGGAAACAGCTATGAC
Zwi-100L	GCATTCTAAAGGGCAAAACG
Zwi-100R	GGCATTGTCACTCCCGGGCA
Zwi-101L	CACCAACAGCCAAGAAAACA
Zwi-101R	GGCATTGTCACTAAAGGGCA
Zwi-102Ro	ATTGAAGAGCCACCCACAGACA
Zwi-102-Ri	TGTGGGCTAAAGTCTTTGCATTCCA
Zwi-102Lc	GGGATTCAGATTTCTCCCAGCACA

6.4   MORPHOLINOS

All Morpholinos were ordered from Gene Tools, LLC, Eugene.

Claudin k ATG	CATGGTGAATCTTTCCCAAGAATGA
Control mismatch to the *ngr* target sequence (5 MM MO)	CTGCAGGATTAACGTCTTGATCTTT
Zwilling A ATG	CTTCCGTAAAACTGGTGTTCCCCAT
Zwilling B ATG	CCTCAGTGATACTCGTGTTACCCAT
Cldn19 exon3-slpice acceptor	GACACCTAGACCAGACAGAAATCAC

6.5 ANTIBODIES

Antibody	Species	Dilution	Company / Reference
α-Claudin k mono, 3H5-1-1	rat	IF: 1:200, WB: 1:1000	E. Kremmer
α-Claudin k poly	rabbit	WB: 1:1000	E. Kremmer
α-MBP	rabbit	IF: 1:100	W.Talbot
zrf-1 (GFAP)	mouse	IF: 1:500	ZIRC
α- acetylated tubulin, 6-11B-1	mouse	IF: 1:1000, WB: 1:2000	Sigma
α-ZO-1, ZO1-1A12	mouse	IF: 1:20	Invitrogen
α- digoxigenin		1:500	Roche Molecular Biochemicals
α-rat HRP		1:5000	Promega
α-mouse HRP		1:5000	Promega
Alexa Fluor 488 goat anti-rat IgG		1:750	Invitrogen
Alexa Fluor 488 goat anti-mouse IgG		1:750	
Alexa Fluor 488 goat anti-rabbit IgG		1:750	
Alexa Fluor 546 goat anti-rat IgG		1:500	
Alexa Fluor 546 goat anti-mouse IgG		1:500	
Alexa Fluor 647 goat anti-rabbit IgG		1:500	

Material

6.6 KITS

Geneclean	Qbiogene/MP, Heidelberg
mMessage Machine	Ambion, Darmstadt
Nucleobond AX500	Macherey Nagel, Düren
NucleoSpin Extract II	Macherey Nagel, Düren
NucleoSpin Plasmid Mini/Midi	Macherey Nagel, Düren
pCR®8/GW/TOPO® TA Cloning Kit	Invitrogen, Karlsruhe

6.7 EQUIPMENT

Mikrotom Microm HM 560	Thermo Scientific
Agarose Gelelectrophoresis chambers	Peqlab
Microwave	Bosch
Bacterial culture shaker Scientific 4518	ThermoQuest
UV detection system	Intas
PCR machine T3 Thermocycler	Biorad
Cooled benchtop microcentrifuge	Heraeus
Benchtop microcentrifuge	Eppendorf
Incubator 36 °C	Heraeus
Incubator 28,5°C	Binder
Thermomixer	Eppendorf

Film developer X-Omat	Kodak
SDS-PAGE chamber	BioRad
Blotting Chamber	BioRad
Power supply, Power Pac 300	BioRad
Gel dryer SGD 300	Savant
Nanophotometer III.4.3.0050	Implen
Injection needle puller	DMZ universal puller
Ultracentrifuge Optima TLX	Beckman Coulter
Stereomikroskop Zeiss Stemi 2000	C Carl Zeiss
Stereomikroskop Leica MZ16FA	Leica
Mikroskop Zeiss Axioplan 2 imaging	Zeiss
LSM 510 META inverted confocal microscope	Zeiss

Material

6.8 BUFFER AND MEDIA

1% agarose	1x TBE
	1% agarose (for molecular biology)
acrylamid-solution	40 % acrylamid-BIS-acrylamid 37,5:1
	in dH2O
ammoniumpersulfate (APS)	10 % ammoniumpersulfate
	in dH2O
AP buffer	5 ml 1 M Tris pH 9.5
	2.5 ml 1 M MgCl$_2$
	1 ml 5 M NaCl
	250 µl 20% Tween-20
BCIP stock	50 mg 5-bromo 4-chloro3indolyl phosphate
	1 ml anhydrous dimethyl-formamide
1x blotting buffer	20 mM Tris-Base
	150 mM glycine
	0.01% SDS
Coomassie Brilliant Blue R-250 staining solution	400 ml methanol
	100 ml acetic acid
	1,0 g Coomassie Blue R-250
	fill up with H$_2$0 to 500 ml

Danieau buffer	58 mM NaCl
	0.4 mM $MgSO_4$
	0.6 mM $Ca(NO_3)$
	5.0 mM HEPES
	pH 7.6
DEPC-dH2O	2 µl diethylpyrocarbonate
	1 l dH2O
	incubate overnight at 37°C
	autoclave 20 min at 120 °C
	stored in frozen aliquots
developing solution	5 ml AP buffer
	11.25 µl NBT (100 mg/ml)
	17.5 µl BCIP (50 mg/ml)
6x DNA-loading dye	30 % glycerol
	0,25 % bromphenol blue
	0,25 % xylene cyanol FF
	in dH2O
E3-embryo medium	5 mM NaCl
	0,17 mM KCl
	0,33 mM CaCl2
	0,33 mM MgSO4
	0,1% methylene blue

Material

50.000x ethidiumbromide	10 mg/ml in dH2O
hybridization mix	25 ml formamide 12.5 ml 20x SCC 0.5 ml heparin (5 mg/ml) 0.5 ml tRNA (50 mg/ml) 0,46 ml 1M citric acid 10,7 ml dH$_2$O 0.25 ml 20% Tween-20
LB-agar	1,5 % bacto agar 1 % bacto trypton 0,5% yeast extract 17,25 mM NaCl in dH2O
LB-medium	1 % bacto trypton 0,5% yeast extract 17,25 mM NaCl in dH2O
lysis buffer	5 mMTris pH 7,4 250 mM sucrose 5 mM EGTA

Mowiol	24 g glycerol
	9,6 g Mowiol 4-88
	24 ml dH20
	48 ml 0,2 M Tris, pH8.5
	4-6 h stirring on hot plate,
	centrifuge 15 min at 5000g
	store at -20 °C
NBT stock	Sigma, Taufkirchen
	50 mg Nitro Blue Tetraz
	0.7 ml anhydrous dimethyl-formamide
	0.3 ml dH$_2$O
PBS	140 mM NaCl
	10 mM Na2HPO4
	1,75 mM KH2PO4
	in dH2O, pH 7.4
	autoclave 20 min at 120 °C
PBST	1x PBS
	0,1 % Tween-20
PCR-Mix	200 µl 10x PCR-buffer
	each 8µl 100 mM dATP, dGTP, dTTP, dCTP
	1210 µl dH2O

Material

4% PFA for fixation	4% paraformaldehyde in PBST 2-3 h heating and mixing, then stored in frozen aliquots
PI buffer	48 ml PBT 1 ml BSA 10% 1 ml sheep serum
RIPA Buffer	20 mTris, pH 7,4 150 mM NaCl 1% NP40 0,05 % Triton X-100 0,5 % Na-deoxycholate 2,5 mM EDTA
10x running buffer for SDS-PAGE	250 mM Tris/HCl, pH 6.8 1.9 M glycine 1% SDS
6xSDS loading dye	0,35 mM Tris, pH 6.8 10,28 % SDS 36 % glycerol 0,6 M dithiothreitol 0,012% bromphenol blue

SOC-medium	2 % bacto trypton
	0,5% yeast extract
	8,6 mM NaCl
	2,5 mM KCl
	in dH2O,
	20 mM glucose
stacking gel-buffer	0,5 M Tris pH 6,8
	0,4 % SDS
	in dH2O
10 x STEN	25 ml Tris 1M pH 7,6
	15 ml NaCl 5M
	2 ml EDTA 0,5 M
	1 ml NP40 100%
	Fill up with H_2O to 500 ml
STEN NaCl	25 ml Tris 1M pH 7,6
	50 ml NaCl 5M
	2 ml EDTA 0,5 M
	1 ml NP40 100%
	Fill up with H_2O to 500 ml

Material

STEN SDS	25 ml Tris 1M pH 7,6
	15 ml NaCl 5M
	2 ml EDTA 0,5 M
	5 ml SDS 10%
	Fill up with H_2O to 500 ml
20x SSC	0.8 l dH_2O
	140.2 g sodium chloride
	65.8 g sodium citrate dihydrate, pH 7.0
running gel buffer	1,5 M Tris pH 8,8
	0,4 % SDS
	in dH2O
50x TAE Buffer for agarose gel electrophoresis	2 M Tris
	57 ml acetic acid
	50 mM Na_2EDTA x $2H_2O$, pH 8.0
	H_2O ad 1000ml
10x TBE	900 mM Tris
	900 mM boric acid
	20 mM EDTA
	in dH2O, pH 8,0

10x TBS	60,6 g Tris
	73,1 g NaCl
	Fill up with dH2O to 1l, pH 7.6
	1x TBST
	10 % 10x TBS
	0,1% Tween-20 in dH2O
TE pH 8.0	10 mM Tris pH 8.0
	1 mM EDTA pH 8.0
	in dH2O
tricaine working solution	4.2 ml tricaine stock solution
	100 ml E3-medium
tricaine anesthetic stock solution	400 mg tricaine
	97.9 ml dH2O
	~2.1ml Tris (pH 9) to adjust pH to 7

Material

MATERIALS

Agarose	Sigma, Taufkirchen
Acetone	Merck, Darmstadt
Agarose	Serva, Heidelberg
Ammonium peroxodisulfate	USB, Cleveland, USA
β-Mercaptoethanol	Merck, Darmstadt
BCIP	Roche Diagnostics, Mannheim
BSA	Sigma, Taufkirchen
Borosilicate glass capillaries	World Precision Instruments, Sarasota, USA
Bromophenol blue	Merck, Darmstadt
Chloroform	Merck, Darmstadt
Chloroform-isoamyl alcohol (24:1)	Roth, Karlsruhe
Citric acid	Merck, Darmstadt
Complete Protease-Inhibitor	Roche Diagnostics, Mannheim
Coomassie Brilliant Blue R-250	Biorad, Munich
Cryo-embedding compound (for medium and higher temperatures)	MICROM Laborgeräte, Walldorf
DEPC	Sigma, Taufkirchen
Desoxynucleoside triphosphate (dATP, dCTP, dGTP, dTTP)	Sigma, Taufkirchen
10x DIG-RNA labelling mix	Roche, Mannheim

Dimethyl sulfoxide (DMSO)	Merck, Darmstadt
DNA size marker for agarose gels	Fermentas, St. Leon-Rot
Dithiothreitol	Biomol, Hamburg
ECL detection	Ámersham, Freiburg
EDTA	Merck, Darmstadt
EGTA	Serva, Heidelberg
Ethanol	Sigma, Taufkirchen
Ethidium bromide	Sigma, Taufkirchen
Formamide	Merck, Darmstadt
Glycerol	USB, Cleveland, USA
Glycine	USB, Cleveland, USA
Heparin	Sigma, Taufkirchen
Hepes	Sigma, Taufkirchen
Hyluronidase	Sigma, Taufkirchen
Hydrochloric acid	Merck, Darmstadt
Magnesium chloride	Merck, Darmstadt
Methanol	Merck, Darmstadt
Microscope slide jar	Novoglas Labortechnik, Bern
Mowiol 4-88	Sigma, Taufkirchen
Na-deoxycholate	Sigma, Taufkirchen
Nitroblue tetrazolium chloride (NBT)	Sigma, Taufkirchen
NP40	USB, Cleveland, USA

Material

PAP pen (liquid blocker pen)	Daido Sangyo, Tokyo
Paraformaldehyde	Sigma, Taufkirchen
Phase lock gel – cups	Eppendorf, Hamburg
Polyacrylamide/bisacrylamide (29:1), 40%	Roth, Karlsruhe
Probe Quant	GE healthcare, Munich
Protease inhibitor mix	Sigma, Taufkirchen
Protein A Sepharose	Pierce, Rockford
NuPAGE Noves	Invitrogen, Karsruhe
PVDF-membrane	Millipore, Billerica, USA
1-phenyl 2-thiourea (PTU)	Sigma, Taufkirchen
Roti Phenol	Tris saturated phenol, Roth, Karlsruhe
RNAse inhibitor	Fermentas, St. Leon-Rot
Ready Red	Chloroform-isoamylalcohol (24:1), Roth, Karlsruhe
Sodium acetate	Merck, Darmstadt
Sodium ascorbic acid	Sigma, Taufkirchen
Sodium chloride	Merck, Darmstadt
Sodium citrate dihydrate	Sigma, Taufkirchen
Sodium dodecyl sulfate (SDS)	Roth, Karlsruhe
Sucrose	Sigma, Taufkirchen
Super RX film (chemiluminescence)	Fuji, Düsseldorf
Taq DNA Polymeras	Roche Diagnostics,

	Mannheim
TEMED	USB, Cleveland, OH, USA
Thioflavine S	Sigma, Taufkirchen
Trichloric acetate (TCA)	Merck, Darmstadt
tRNA	Sigma, Taufkirchen
Tris	Biomol, Hamburg
Tris saturated phenol	Appligene oncor, Heidelberg
Triton-x100	USB, Cleveland, OH, USA
Tizol	Gibco BRL, Carlsbad, USA
Typsin	Sigma, Taufkirchen
Tween-20	USB, Cleveland, OH, USA
Whatman paper	Schleicher & Schüll , Dassel
Xylene cyanol FF	Mallinckrodt Baker, Griesheim

7 APPENDIX

7.1 REFERENCES

Adlkofer, K., R. Martini, et al. (1995). "Hypermyelination and demyelinating peripheral neuropathy in Pmp22-deficient mice." Nat Genet **11**(3): 274-280.

Ainger, K., D. Avossa, et al. (1993). "Transport and localization of exogenous myelin basic protein mRNA microinjected into oligodendrocytes." J Cell Biol **123**(2): 431-441.

Amores, A., A. Force, et al. (1998). "Zebrafish hox clusters and vertebrate genome evolution." Science **282**(5394): 1711-1714.

Anderson, T. J., P. Montague, et al. (1997). "Modification of Schwann cell phenotype with Plp transgenes: evidence that the PLP and DM20 isoproteins are targeted to different cellular domains." J Neurosci Res **50**(1): 13-22.

Angelow, S., K. J. Kim, et al. (2006). "Claudin-8 modulates paracellular permeability to acidic and basic ions in MDCK II cells." J Physiol **571**(Pt 1): 15-26.

Araque, A. (2008). "Astrocytes process synaptic information." Neuron Glia Biol **4**(1): 3-10.

Arroyo, E. J. and S. S. Scherer (2000). "On the molecular architecture of myelinated fibers." Histochem Cell Biol **113**(1): 1-18.

Autio, K. J., A. J. Kastaniotis, et al. (2008). "An ancient genetic link between vertebrate mitochondrial fatty acid synthesis and RNA processing." FASEB J **22**(2): 569-578.

Avila, R. L., B. R. Tevlin, et al. (2006). "Myelin Structure and Composition in Zebrafish." Neurochem Res.

Balice-Gordon, R. J., L. J. Bone, et al. (1998). "Functional gap junctions in the schwann cell myelin sheath." J Cell Biol **142**(4): 1095-1104.

Barres, B. A. (2008). "The mystery and magic of glia: a perspective on their roles in health and disease." Neuron **60**(3): 430-440.

Bauer, J., M. Bradl, et al. (2002). "Endoplasmic reticulum stress in PLP-overexpressing transgenic rats: gray matter oligodendrocytes are more vulnerable than white matter oligodendrocytes." J Neuropathol Exp Neurol **61**(1): 12-22.

Baumann, N. and D. Pham-Dinh (2001). "Biology of oligodendrocyte and myelin in the mammalian central nervous system." Physiol Rev **81**(2): 871-927.

Beis, D. and D. Y. Stainier (2006). "In vivo cell biology: following the zebrafish trend." Trends Cell Biol **16**(2): 105-112.

Berger, P., A. Niemann, et al. (2006). "Schwann cells and the pathogenesis of inherited motor and sensory neuropathies (Charcot-Marie-Tooth disease)." Glia **54**(4): 243-257.

Bertaud, W. S. (1978). "Membrane junctions in the myelin sheath of goldfish lateral nerve." J Cell Sci **30**: 77-85.

Bhat, M. A., J. C. Rios, et al. (2001). "Axon-glia interactions and the domain organization of myelinated axons requires neurexin IV/Caspr/Paranodin." Neuron **30**(2): 369-383.

Boggs, J. M. (2006). "Myelin basic protein: a multifunctional protein." Cell Mol Life Sci **63**(17): 1945-1961.

Boison, D., H. Bussow, et al. (1995). "Adhesive properties of proteolipid protein are responsible for the compaction of CNS myelin sheaths." J Neurosci **15**(8): 5502-5513.

Boyle, M. E., E. O. Berglund, et al. (2001). "Contactin orchestrates assembly of the septate-like junctions at the paranode in myelinated peripheral nerve." Neuron **30**(2): 385-397.

Bradl, M., J. Bauer, et al. (1999). "Transgenic Lewis rats overexpressing the proteolipid protein gene: myelin degeneration and its effect on T cell-mediated experimental autoimmune encephalomyelitis." Acta Neuropathol **97**(6): 595-606.

Brand, A. H. and N. Perrimon (1993). "Targeted gene expression as a means of altering cell fates and generating dominant phenotypes." Development **118**(2): 401-415.

Brogna, S. and M. Ashburner (1997). "The Adh-related gene of Drosophila melanogaster is expressed as a functional dicistronic messenger RNA: multigenic transcription in higher organisms." Embo J **16**(8): 2023-2031.

Brösamle, C. and M. E. Halpern (2002). "Characterization of myelination in the developing zebrafish." Glia **39**(1): 47-57.

Brösamle, C. and M. E. Halpern (2009). "Nogo-Nogo receptor signalling in PNS axon outgrowth and pathfinding." Mol Cell Neurosci **40**(4): 401-409.

Bullock, T. H., J. K. Moore, et al. (1984). "Evolution of myelin sheaths: both lamprey and hagfish lack myelin." Neurosci Lett **48**(2): 145-148.

Burgess, H. A. and M. Granato (2007). "Sensorimotor gating in larval zebrafish." J Neurosci **27**(18): 4984-4994.

Chakrabarti, S., G. Streisinger, et al. (1983). "Frequency of gamma-Ray Induced Specific Locus and Recessive Lethal Mutations in Mature Germ Cells of the Zebrafish, BRACHYDANIO RERIO." Genetics **103**(1): 109-123.

Chow, E., J. Mottahedeh, et al. (2005). "Disrupted compaction of CNS myelin in an OSP/Claudin-11 and PLP/DM20 double knockout mouse." Mol Cell Neurosci **29**(3): 405-413.

Colby, J., R. Nicholson, et al. (2000). "PMP22 carrying the trembler or trembler-J mutation is intracellularly retained in myelinating Schwann cells." Neurobiol Dis **7**(6 Pt B): 561-573.

Connor, J. R. and S. L. Menzies (1996). "Relationship of iron to oligodendrocytes and myelination." Glia **17**(2): 83-93.

D'Antonio, M., M. L. Feltri, et al. (2009). "Myelin under stress." J Neurosci Res **87**(15): 3241-3249.

D'Urso, D., P. Ehrhardt, et al. (1999). "Peripheral myelin protein 22 and protein zero: a novel association in peripheral nervous system myelin." J Neurosci **19**(9): 3396-3403.

Das, M. K. and H. K. Dai (2007). "A survey of DNA motif finding algorithms." BMC Bioinformatics **8 Suppl 7**: S21.

Davis, A. D., T. M. Weatherby, et al. (1999). "Myelin-like sheaths in copepod axons." Nature **398**(6728): 571.

Devaux, J. and A. Gow (2008). "Tight junctions potentiate the insulative properties of small CNS myelinated axons." J Cell Biol **183**(5): 909-921.

Dickson, K. M., J. J. Bergeron, et al. (2002). "Association of calnexin with mutant peripheral myelin protein-22 ex vivo: a basis for "gain-of-function" ER diseases." Proc Natl Acad Sci U S A **99**(15): 9852-9857.

Doyon, Y., J. M. McCammon, et al. (2008). "Heritable targeted gene disruption in zebrafish using designed zinc-finger nucleases." Nat Biotechnol **26**(6): 702-708.

Duncan, I. D. (2005). "The PLP mutants from mouse to man." J Neurol Sci **228**(2): 204-205.

Dutton, J. R., A. Antonellis, et al. (2008). "An evolutionarily conserved intronic region controls the spatiotemporal expression of the transcription factor Sox10." BMC Dev Biol **8**: 105.

Dutton, K. A., A. Pauliny, et al. (2001). "Zebrafish colourless encodes sox10 and specifies non-ectomesenchymal neural crest fates." Development **128**(21): 4113-4125.

Edvardson, S., H. Hama, et al. (2008). "Mutations in the fatty acid 2-hydroxylase gene are associated with leukodystrophy with spastic paraparesis and dystonia." Am J Hum Genet **83**(5): 643-648.

Eichberg, J. (2002). "Myelin P0: new knowledge and new roles." Neurochem Res **27**(11): 1331-1340.

Foley, J. E., J. R. Yeh, et al. (2009). "Rapid mutation of endogenous zebrafish genes using zinc finger nucleases made by Oligomerized Pool ENgineering (OPEN)." PLoS One **4**(2): e4348.

Appendix

Funch, P. G., M. R. Wood, et al. (1984). "Localization of active sites along the myelinated goldfish Mauthner axon: morphological and pharmacological evidence for saltatory conduction." J Neurosci **4**(9): 2397-2409.

Garbern, J. Y., F. Cambi, et al. (1997). "Proteolipid protein is necessary in peripheral as well as central myelin." Neuron **19**(1): 205-218.

Gilmour, D., H. Knaut, et al. (2004). "Towing of sensory axons by their migrating target cells in vivo." Nat Neurosci **7**(5): 491-492.

Gilmour, D. T., H. M. Maischein, et al. (2002). "Migration and function of a glial subtype in the vertebrate peripheral nervous system." Neuron **34**(4): 577-588.

Givogri, M. I., E. R. Bongarzone, et al. (2001). "Expression and regulation of golli products of myelin basic protein gene during in vitro development of oligodendrocytes." J Neurosci Res **66**(4): 679-690.

Gonzalez-Mariscal, L., A. Betanzos, et al. (2003). "Tight junction proteins." Prog Biophys Mol Biol **81**(1): 1-44.

Gould, R. M., C. M. Freund, et al. (2000). "Messenger RNAs located in myelin sheath assembly sites." J Neurochem **75**(5): 1834-1844.

Gow, A., C. Davies, et al. (2004). "Deafness in Claudin 11-null mice reveals the critical contribution of basal cell tight junctions to stria vascularis function." J Neurosci **24**(32): 7051-7062.

Gow, A., C. M. Southwood, et al. (1999). "CNS myelin and sertoli cell tight junction strands are absent in Osp/claudin-11 null mice." Cell **99**(6): 649-659.

Griffiths, M. R., P. Gasque, et al. (2009). "The multiple roles of the innate immune system in the regulation of apoptosis and inflammation in the brain." J Neuropathol Exp Neurol **68**(3): 217-226.

Gunther, J. (1976). "Impulse conduction in the myelinated giant fibers of the earthworm. Structure and function of the dorsal nodes in the median giant fiber." J Comp Neurol **168**(4): 505-531.

Harauz, G., V. Ladizhansky, et al. (2009). "Structural polymorphism and multifunctionality of myelin basic protein." Biochemistry **48**(34): 8094-8104.

Harauz, G. and D. S. Libich (2009). "The classic basic protein of myelin--conserved structural motifs and the dynamic molecular barcode involved in membrane adhesion and protein-protein interactions." Curr Protein Pept Sci **10**(3): 196-215.

Harder, J. L. and B. Margolis (2008). "SnapShot: tight and adherens junction signaling." Cell **133**(6): 1118, 1118 e1111-1112.

Hartline, D. K. and D. R. Colman (2007). "Rapid conduction and the evolution of giant axons and myelinated fibers." Curr Biol **17**(1): R29-35.

Hatten, M. E. and C. A. Mason (1990). "Mechanisms of glial-guided neuronal migration in vitro and in vivo." Experientia **46**(9): 907-916.

Hayasaka, K., M. Himoro, et al. (1993). "De novo mutation of the myelin P0 gene in Dejerine-Sottas disease (hereditary motor and sensory neuropathy type III)." Nat Genet **5**(3): 266-268.

Hayashi, A., K. Nakashima, et al. (2007). "Localization of annexin II in the paranodal regions and Schmidt-Lanterman incisures in the peripheral nervous system." Glia **55**(10): 1044-1052.

Hill, C. M., I. R. Bates, et al. (2002). "Effects of the osmolyte trimethylamine-N-oxide on conformation, self-association, and two-dimensional crystallization of myelin basic protein." J Struct Biol **139**(1): 13-26.

Holley, S. A., D. Julich, et al. (2002). "her1 and the notch pathway function within the oscillator mechanism that regulates zebrafish somitogenesis." Development **129**(5): 1175-1183.

Hu, Y., I. Doudevski, et al. (2004). "Synergistic interactions of lipids and myelin basic protein." Proc Natl Acad Sci U S A **101**(37): 13466-13471.

Hurley, I. A., R. L. Mueller, et al. (2007). "A new time-scale for ray-finned fish evolution." Proc Biol Sci **274**(1609): 489-498.

Igisu, H. and K. Suzuki (1984). "Progressive accumulation of toxic metabolite in a genetic leukodystrophy." Science **224**(4650): 753-755.

Ingham, P. W. (2009). "The power of the zebrafish for disease analysis." Hum Mol Genet **18**(R1): R107-112.

Itoh, M., M. Furuse, et al. (1999). "Direct binding of three tight junction-associated MAGUKs, ZO-1, ZO-2, and ZO-3, with the COOH termini of claudins." J Cell Biol **147**(6): 1351-1363.

Jeserich, G., K. Klempahn, et al. (2008). "Features and functions of oligodendrocytes and myelin proteins of lower vertebrate species." J Mol Neurosci **35**(1): 117-126.

Jeserich, G. and T. V. Waehneldt (1986). "Characterization of antibodies against major fish CNS myelin proteins: immunoblot analysis and immunohistochemical localization of 36K and IP2 proteins in trout nerve tissue." J Neurosci Res **15**(2): 147-158.

Jessen, K. R. and R. Mirsky (2008). "Negative regulation of myelination: relevance for development, injury, and demyelinating disease." Glia **56**(14): 1552-1565.

Jung, S. H., S. Kim, et al. (2009). "Visualization of myelination in GFP-transgenic zebrafish." Dev Dyn.

Kalman, B. and T. P. Leist (2004). "Familial multiple sclerosis and other inherited disorders of the white matter." Neurologist **10**(4): 201-215.

Karim, S. A., J. A. Barrie, et al. (2007). "PLP overexpression perturbs myelin protein composition and myelination in a mouse model of Pelizaeus-Merzbacher disease." Glia **55**(4): 341-351.

Kawakami, K. (2005). "Transposon tools and methods in zebrafish." Dev Dyn **234**(2): 244-254.

Kimmel, C. B., J. Patterson, et al. (1974). "The development and behavioral characteristics of the startle response in the zebra fish." Dev Psychobiol **7**(1): 47-60.

Kirby, B. B., N. Takada, et al. (2006). "In vivo time-lapse imaging shows dynamic oligodendrocyte progenitor behavior during zebrafish development." Nat Neurosci **9**(12): 1506-1511.

Kirkpatrick, L. L., A. S. Witt, et al. (2001). "Changes in microtubule stability and density in myelin-deficient shiverer mouse CNS axons." J Neurosci **21**(7): 2288-2297.

Kirschner, D. A. and A. L. Ganser (1980). "Compact myelin exists in the absence of basic protein in the shiverer mutant mouse." Nature **283**(5743): 207-210.

Kitajiri, S., T. Miyamoto, et al. (2004). "Compartmentalization established by claudin-11-based tight junctions in stria vascularis is required for hearing through generation of endocochlear potential." J Cell Sci **117**(Pt 21): 5087-5096.

Koster, R. W. and S. E. Fraser (2001). "Tracing transgene expression in living zebrafish embryos." Dev Biol **233**(2): 329-346.

Kozak, M. (1987). "An analysis of 5'-noncoding sequences from 699 vertebrate messenger RNAs." Nucleic Acids Res **15**(20): 8125-8148.

Kozak, M. (2005). "A second look at cellular mRNA sequences said to function as internal ribosome entry sites." Nucleic Acids Res **33**(20): 6593-6602.

Krause, G., L. Winkler, et al. (2008). "Structure and function of claudins." Biochim Biophys Acta **1778**(3): 631-645.

Krause, G., L. Winkler, et al. (2009). "Structure and function of extracellular claudin domains." Ann N Y Acad Sci **1165**: 34-43.

Lal-Nag, M. and P. J. Morin (2009). "The claudins." Genome Biol **10**(8): 235.

Lassmann, H. (2009). "Axonal and neuronal pathology in multiple sclerosis: What have we learnt from animal models." Exp Neurol.

Lekven, A. C., C. J. Thorpe, et al. (2001). "Zebrafish wnt8 encodes two wnt8 proteins on a bicistronic transcript and is required for mesoderm and neurectoderm patterning." Dev Cell **1**(1): 103-114.

Lieschke, G. J. and P. D. Currie (2007). "Animal models of human disease: zebrafish swim into view." Nat Rev Genet **8**(5): 353-367.

Lin, W. and B. Popko (2009). "Endoplasmic reticulum stress in disorders of myelinating cells." Nat Neurosci **12**(4): 379-385.

Appendix

Liu, K. S. and J. R. Fetcho (1999). "Laser ablations reveal functional relationships of segmental hindbrain neurons in zebrafish." Neuron **23**(2): 325-335.

Lodish, H. F. (2000). Molecular cell biology. New York, Scientific American Books.

Loh, Y. H., A. Christoffels, et al. (2004). "Extensive expansion of the claudin gene family in the teleost fish, Fugu rubripes." Genome Res **14**(7): 1248-1257.

Mack, A. F. and H. Wolburg (2006). "Growing axons in fish optic nerve are accompanied by astrocytes interconnected by tight junctions." Brain Res **1103**(1): 25-31.

Maier, I. C. and M. E. Schwab (2006). "Sprouting, regeneration and circuit formation in the injured spinal cord: factors and activity." Philos Trans R Soc Lond B Biol Sci **361**(1473): 1611-1634.

Martini, R., S. Fischer, et al. (2008). "Interactions between Schwann cells and macrophages in injury and inherited demyelinating disease." Glia **56**(14): 1566-1577.

Martini, R., M. H. Mohajeri, et al. (1995). "Mice doubly deficient in the genes for P0 and myelin basic protein show that both proteins contribute to the formation of the major dense line in peripheral nerve myelin." J Neurosci **15**(6): 4488-4495.

Marty, M. C., F. Alliot, et al. (2002). "The myelin basic protein gene is expressed in differentiated blood cell lineages and in hemopoietic progenitors." Proc Natl Acad Sci U S A **99**(13): 8856-8861.

McLean, D. L. and J. R. Fetcho (2008). "Using imaging and genetics in zebrafish to study developing spinal circuits in vivo." Dev Neurobiol **68**(6): 817-834.

McTigue, D. M. and R. B. Tripathi (2008). "The life, death, and replacement of oligodendrocytes in the adult CNS." J Neurochem **107**(1): 1-19.

Meng, X., M. B. Noyes, et al. (2008). "Targeted gene inactivation in zebrafish using engineered zinc-finger nucleases." Nat Biotechnol **26**(6): 695-701.

Min, Y., K. Kristiansen, et al. (2009). "Interaction forces and adhesion of supported myelin lipid bilayers modulated by myelin basic protein." Proc Natl Acad Sci U S A **106**(9): 3154-3159.

Miyamoto, T., K. Morita, et al. (2005). "Tight junctions in Schwann cells of peripheral myelinated axons: a lesson from claudin-19-deficient mice." J Cell Biol **169**(3): 527-538.

Mobius, W., J. Patzig, et al. (2008). "Phylogeny of proteolipid proteins: divergence, constraints, and the evolution of novel functions in myelination and neuroprotection." Neuron Glia Biol **4**(2): 111-127.

Moens, C. B., T. M. Donn, et al. (2008). "Reverse genetics in zebrafish by TILLING." Brief Funct Genomic Proteomic **7**(6): 454-459.

Morris, J. K., B. B. Willard, et al. (2004). "The 36K protein of zebrafish CNS myelin is a short-chain dehydrogenase." Glia **45**(4): 378-391.

Mueller, H., H. J. Butt, et al. (1999). "Force measurements on myelin basic protein adsorbed to mica and lipid bilayer surfaces done with the atomic force microscope." Biophys J **76**(2): 1072-1079.

Mugnaini, E. and B. Schnapp (1974). "Possible role of zonula occludens of the myelin sheath in demyelinating conditions." Nature **251**(5477): 725-727.

Mullins, M. C., M. Hammerschmidt, et al. (1994). "Large-scale mutagenesis in the zebrafish: in search of genes controlling development in a vertebrate." Curr Biol **4**(3): 189-202.

Nakayama, K., Y. Suzuki, et al. (2009). "Microtubule depolymerization suppresses alpha-synuclein accumulation in a mouse model of multiple system atrophy." Am J Pathol **174**(4): 1471-1480.

Nave, K. A. and B. D. Trapp (2008). "Axon-glial signaling and the glial support of axon function." Annu Rev Neurosci **31**: 535-561.

Nekrutenko, A., K. D. Makova, et al. (2002). "The K(A)/K(S) ratio test for assessing the protein-coding potential of genomic regions: an empirical and simulation study." Genome Res **12**(1): 198-202.

Neurophysiology (North Dakota State University). http://www.psych.ndsu.nodak.edu/mccourt/Psy460/Neurophysiology%20of%20vision/myelin.JPG: 09.12.2009.

116

Ng, A. N., T. A. de Jong-Curtain, et al. (2005). "Formation of the digestive system in zebrafish: III. Intestinal epithelium morphogenesis." Dev Biol **286**(1): 114-135.

O'Brien, G. S., S. Rieger, et al. (2009). "Two-photon axotomy and time-lapse confocal imaging in live zebrafish embryos." J Vis Exp(24).

OMIM® (Johns Hopkins University). "Online Mendelian Inheritance in Man." http://www.ncbi.nlm.nih.gov/Omim/mimstats.html: 09.12.2009.

Orosco, L., K. Schaefer, et al. (in preparation). "Gene expression screen reveals target of *Sox 10* regulation in neural crest and myelinating glia."

Paquet, D., R. Bhat, et al. (2009). "A zebrafish model of tauopathy allows in vivo imaging of neuronal cell death and drug evaluation." J Clin Invest **119**(5): 1382-1395.

Park, H. C., J. Shin, et al. (2004). "Spatial and temporal regulation of ventral spinal cord precursor specification by Hedgehog signaling." Development **131**(23): 5959-5969.

Park, H. C., J. Shin, et al. (2007). "An olig2 reporter gene marks oligodendrocyte precursors in the postembryonic spinal cord of zebrafish." Dev Dyn **236**(12): 3402-3407.

Patel, P. I. and J. R. Lupski (1994). "Charcot-Marie-Tooth disease: a new paradigm for the mechanism of inherited disease." Trends Genet **10**(4): 128-133.

Pedraza, L., L. Fidler, et al. (1997). "The active transport of myelin basic protein into the nucleus suggests a regulatory role in myelination." Neuron **18**(4): 579-589.

Perea, G., M. Navarrete, et al. (2009). "Tripartite synapses: astrocytes process and control synaptic information." Trends Neurosci **32**(8): 421-431.

Pfeiffer, S. E., A. E. Warrington, et al. (1993). "The oligodendrocyte and its many cellular processes." Trends Cell Biol **3**(6): 191-197.

Pingault, V., N. Bondurand, et al. (1998). "SOX10 mutations in patients with Waardenburg-Hirschsprung disease." Nat Genet **18**(2): 171-173.

Plotkowski, M. L., S. Kim, et al. (2007). "Transmembrane domain of myelin protein zero can form dimers: possible implications for myelin construction." Biochemistry **46**(43): 12164-12173.

Poliak, S., S. Matlis, et al. (2002). "Distinct claudins and associated PDZ proteins form different autotypic tight junctions in myelinating Schwann cells." J Cell Biol **159**(2): 361-372.

Poliak, S. and E. Peles (2003). "The local differentiation of myelinated axons at nodes of Ranvier." Nat Rev Neurosci **4**(12): 968-980.

Prince, V. E., L. Joly, et al. (1998). "Zebrafish hox genes: genomic organization and modified colinear expression patterns in the trunk." Development **125**(3): 407-420.

Queiroz, L. S. and R. A. Paes (State University of Campinas). http://anatpat.unicamp.br/nervnormal.html: 09.12.2009.

Raine, C. S. and A. H. Cross (1989). "Axonal dystrophy as a consequence of long-term demyelination." Lab Invest **60**(5): 714-725.

Rakic, P. (1972). "Mode of cell migration to the superficial layers of fetal monkey neocortex." J Comp Neurol **145**(1): 61-83.

Ramel, M. C., G. R. Buckles, et al. (2004). "Conservation of structure and functional divergence of duplicated Wnt8s in pufferfish." Dev Dyn **231**(2): 441-448.

Rubinstein, A. L. (2003). "Zebrafish: from disease modeling to drug discovery." Curr Opin Drug Discov Devel **6**(2): 218-223.

Salzer, J. L. (2003). "Polarized domains of myelinated axons." Neuron **40**(2): 297-318.

Salzer, J. L., P. J. Brophy, et al. (2008). "Molecular domains of myelinated axons in the peripheral nervous system." Glia **56**(14): 1532-1540.

Sandri, C., J. M. Van Buren, et al. (1977). "Membrane morphology of the vertebrate nervous system. A study with freeze-etch technique." Prog Brain Res **46**: 1-384.

Schebesta, M. and F. C. Serluca (2009). "olig1 Expression identifies developing oligodendrocytes in zebrafish and requires hedgehog and notch signaling." Dev Dyn **238**(4): 887-898.

Scheer, N. and J. A. Campos-Ortega (1999). "Use of the Gal4-UAS technique for targeted gene expression in the zebrafish." Mech Dev **80**(2): 153-158.

Appendix

Scheiermann, C., P. Meda, et al. (2007). "Expression and function of junctional adhesion molecule-C in myelinated peripheral nerves." Science **318**(5855): 1472-1475.

Schweigreiter, R., B. I. Roots, et al. (2006). "Understanding myelination through studying its evolution." Int Rev Neurobiol **73**: 219-273.

Shapiro, L., J. P. Doyle, et al. (1996). "Crystal structure of the extracellular domain from P0, the major structural protein of peripheral nerve myelin." Neuron **17**(3): 435-449.

Sherwood, C. C., C. D. Stimpson, et al. (2006). "Evolution of increased glia-neuron ratios in the human frontal cortex." Proc Natl Acad Sci U S A **103**(37): 13606-13611.

Shin, J., H. C. Park, et al. (2003). "Neural cell fate analysis in zebrafish using olig2 BAC transgenics." Methods Cell Sci **25**(1-2): 7-14.

Shinowara, N. L., W. B. Beutel, et al. (1980). "Comparative analysis of junctions in the myelin sheath of central and peripheral axons of fish, amphibians and mammals: a freeze-fracture study using complementary replicas." J Neurocytol **9**(1): 15-38.

Simons, M. and K. Trajkovic (2006). "Neuron-glia communication in the control of oligodendrocyte function and myelin biogenesis." J Cell Sci **119**(Pt 21): 4381-4389.

Southwood, C. M., J. Garbern, et al. (2002). "The unfolded protein response modulates disease severity in Pelizaeus-Merzbacher disease." Neuron **36**(4): 585-596.

Staehelin, L. A. (1973). "Further observations on the fine structure of freeze-cleaved tight junctions." J Cell Sci **13**(3): 763-786.

Stolt, C. C., S. Rehberg, et al. (2002). "Terminal differentiation of myelin-forming oligodendrocytes depends on the transcription factor Sox10." Genes Dev **16**(2): 165-170.

Susuki, K. and M. N. Rasband (2008). "Molecular mechanisms of node of Ranvier formation." Curr Opin Cell Biol **20**(6): 616-623.

Tabira, T., M. J. Cullen, et al. (1978). "An experimental analysis of interlamellar tight junctions in amphibian and mammalian C.N.S. myelin." J Neurocytol **7**(4): 489-503.

Tambuyzer, B. R., P. Ponsaerts, et al. (2009). "Microglia: gatekeepers of central nervous system immunology." J Leukoc Biol **85**(3): 352-370.

Tetzlaff, W. (1978). "The development of a zonula occludens in peripheral myelin of the chick embryo. A freeze-fracture study." Cell Tissue Res **189**(2): 187-201.

Thisse, C., B. Thisse, et al. (1993). "Structure of the zebrafish snail1 gene and its expression in wild-type, spadetail and no tail mutant embryos." Development **119**(4): 1203-1215.

Trapp, B. D., J. Peterson, et al. (1998). "Axonal transection in the lesions of multiple sclerosis." N Engl J Med **338**(5): 278-285.

Tsukita, S., M. Furuse, et al. (2001). "Multifunctional strands in tight junctions." Nat Rev Mol Cell Biol **2**(4): 285-293.

Wada, N., Y. Javidan, et al. (2005). "Hedgehog signaling is required for cranial neural crest morphogenesis and chondrogenesis at the midline in the zebrafish skull." Development **132**(17): 3977-3988.

Waehneldt, T. V., S. Stoklas, et al. (1986). "Central nervous system myelin of teleosts: comparative electrophoretic analysis of its proteins by staining and immunoblotting." Comp Biochem Physiol B **84**(3): 273-278.

Wagner, C. and E. Hossler (University of Delaware). http://www.udel.edu/biology/Wags/histopage/empage/ebv/ebv6.gif: 9.12.2009.

Warner, L. E., M. J. Hilz, et al. (1996). "Clinical phenotypes of different MPZ (P0) mutations may include Charcot-Marie-Tooth type 1B, Dejerine-Sottas, and congenital hypomyelination." Neuron **17**(3): 451-460.

Wasserman, W. W. and A. Sandelin (2004). "Applied bioinformatics for the identification of regulatory elements." Nat Rev Genet **5**(4): 276-287.

Wenning, G. K., N. Stefanova, et al. (2008). "Multiple system atrophy: a primary oligodendrogliopathy." Ann Neurol **64**(3): 239-246.

Westerfield, M. (1994). The zebrafish book. Eugene, OR, University of Oregon Press.

Wight, P. A., C. S. Duchala, et al. (1993). "A myelin proteolipid protein-LacZ fusion protein is developmentally regulated and targeted to the myelin membrane in transgenic mice." J Cell Biol **123**(2): 443-454.

Will, C., M. Fromm, et al. (2008). "Claudin tight junction proteins: novel aspects in paracellular transport." <u>Perit Dial Int</u> **28**(6): 577-584.

Windebank, A. J., P. Wood, et al. (1985). "Myelination determines the caliber of dorsal root ganglion neurons in culture." <u>J Neurosci</u> **5**(6): 1563-1569.

Woodward, K. J. (2008). "The molecular and cellular defects underlying Pelizaeus-Merzbacher disease." <u>Expert Rev Mol Med</u> **10**: e14.

Xu, K. and S. Terakawa (1999). "Fenestration nodes and the wide submyelinic space form the basis for the unusually fast impulse conduction of shrimp myelinated axons." <u>J Exp Biol</u> **202**(Pt 15): 1979-1989.

Xu, X. and P. Shrager (2005). "Dependence of axon initial segment formation on Na+ channel expression." <u>J Neurosci Res</u> **79**(4): 428-441.

Yasargil, G. M., N. G. Greeff, et al. (1982). "The structural correlate of saltatory conduction along the Mauthner axon in the tench (Tinca tinca L.): identification of nodal equivalents at the axon collaterals." <u>J Comp Neurol</u> **212**(4): 417-424.

Yin, X., R. C. Baek, et al. (2006). "Evolution of a neuroprotective function of central nervous system myelin." <u>J Cell Biol</u> **172**(3): 469-478.

Yin, X., G. J. Kidd, et al. (2008). "P0 protein is required for and can induce formation of schmidt-lantermann incisures in myelin internodes." <u>J Neurosci</u> **28**(28): 7068-7073.

Yoshida, M. and W. B. Macklin (2005). "Oligodendrocyte development and myelination in GFP-transgenic zebrafish." <u>J Neurosci Res</u> **81**(1): 1-8.

Zalc, B. (2006). "The acquisition of myelin: a success story." <u>Novartis Found Symp</u> **276**: 15-21; discussion 21-15, 54-17, 275-281.

Zalc, B., D. Goujet, et al. (2008). "The origin of the myelination program in vertebrates." <u>Curr Biol</u> **18**(12): R511-512.

Zhang, F. L. and P. J. Casey (1996). "Protein prenylation: molecular mechanisms and functional consequences." <u>Annu Rev Biochem</u> **65**: 241-269.

Appendix

7.2 INDEX OF FIGURES

8 ACKNOWLEDGMENTS

Firstly, I would like to thank Dr. Christian Brösamle for opening the door to the zebrafish community for me through a fascinating and insightful project. I greatly valued his support, not only for my lab work and thesis, but also in attending conferences and additional courses and trainings, which helped me to gain a broader knowledge for my current and future work. I would like to especially mention, how much I appreciated his support and positive attitude towards and during my motherhood.

I'm especially thankful to PD Dr. Konstanze Winklhofer for being my PhD advisor and for the fruitful discussions, support and always open door. I would like to thank Prof. Dr. Christian Haass for being my second referee, for his generous support and scientific input, and for the good working atmosphere in the Laboratory of Neurodegenerative Disease Research. Further thanks are due to Prof. Dr. Martin Biel, Prof. Dr. Klaus Förstemann, Prof. Dr. Dietmar Martin and Prof. Dr. Christian Wahl-Schott, the members of my thesis committee, for taking the time to review and examine my work.

Thanks also to PD Dr. Regina Fluhrer for valuable discussions and evaluation of my work as a member of my PhD committee. Thanks very much also to Dr. Bettina Schmidt and her group for excellent management of the fish facility and for technical advice and support. To Dr. Elisabeth Kremmer, Dr. Axel Imhof, Dr. Roshan Jain, Prof. Dr. Michael Granato and their colleagues special thanks for successful collaboration. I would especially like to mention the great working atmosphere at the institute – thanks to everyone! Especially thanks to Katharina Stahl and my former colleagues Daniele Franc and Barbara Obirei, to my desk neighbors Alex Hruscha and Matthias Teucke and to Frauke van Bebber and Dominik Paquet. To Dominik special thanks for the constructs and technical support. Additional thanks are due to Katharina for sharing the ups and downs of working towards a doctoral degree and giving valuable feedback on my work.

I owe my deepest thanks to my family and friends for support and distraction, but also listening in times of frustration. To Andrew, for his love, dedication and commitment to our family and to my wonderful son who puts things into perspective and can spread good mood like no one else.

9 CURRICULUM VITAE

Personal details

Name	Karin Schaefer
Date and place of birth	9.9.1980, Nordenham
Nationality	German
Marital status	Married

Education

05/2006 - present	PhD at the Laboratory for Neurodegenerative Disease Research, Neurobiochemistry, Ludwig-Maximilians-University Munich
	Project: 'Characterization of two novel Myelin proteins' Supervisor: Dr. Brösamle, Chair: Prof. Dr. Haass
10/2000 - 03/2006	Diploma in Chemistry, Ludwig-Maximilians-University Munich, grade 1,2
09/2005 - 03/2006	Diploma thesis at the Gene Center, Faculty of Chemistry and Pharmacy, Ludwig-Maximilians-University Munich
	Project: 'Immunohistochemical investigation of potential interaction partners of Miranda, a multi adaptor protein in asymmetric cell division in Drosophila Neuroblasts' Supervisor: Dr. Petritsch, Chair: Prof. Dr. Jansen
1991 - 2000	Abitur at the Friedrich-Schiller-Gymnasium Marbach a. N., grade 1,5

Publications und Poster

Orosco L., <u>Schaefer K.</u>, Halpern M. and Brösamle C. Gene expression screen reveals target of *Sox 10* regulation in neural crest and myelinating glia. In preparation

<u>Schaefer K.</u> and Brösamle C. Zwilling-A and -B, two related myelin proteins of teleosts, which originate from a single, bicistronic transcript. Mol Biol Evol. 2009 Mar;26(3):495-9

Harcourt RD., <u>Schaefer K</u>., and Coote ML. Some comments on valence bond representations for the radical exchange reaction X*+R:Y-->X:R+Y*. J Phys Chem A. 2007 Dec 20;111(50):13278-82

<u>Schaefer K</u>. and Brösamle C. Myelin-specific Claudins in zebrafish: evolutionary and functional characterization. Poster at the 6th European Zebrafish Genetics and Development Meeting 2009, Rome, Italy

<u>Schaefer K</u>. Myelin specific Claudins in Teleosts: redundancy or specialization? Poster at the Interact PhD symposium 2009, life science community Munich

<u>Schaefer K</u>. Characterization of novel factors involved in myelination. Poster at the Interact PhD symposium 2007, life science community Munich

<u>Schaefer K</u>. and Brösamle C. Characterization of novel factors involved in myelination. Poster at the 5th European Zebrafish Genetics and Development Meeting 2007, Amsterdam, Netherlands.